Design, Synthesis, and Biological Evaluation of PROTACs Targeting G9a/GLP Methyltransferase

2025

Anirban Mukherjee

Abstract

Histone methylation plays an important role in chromatin structure and epigenetic gene expression. G9a and G9a like protein (GLP) are histone methyltransferases that facilitate the mono- and di-methylation of histone H3 at lysine 9 (H3K9). Aberrant expression of G9a/GLP has been associated with numerous pathological conditions, including cancer, neurodegenerative diseases, and other disorders. Therefore, G9a/GLP inhibition is expected as an effective therapeutic strategy. However, conventional G9a/GLP inhibitors that inhibit only the catalytic function of G9a/GLP do not achieve the complete eradication of cancer. In this context, novel G9a modulators that are distinct from the conventional G9a inhibitors are expected to be applied as alternative therapeutic strategies.

In recent years, targeted protein degradation by proteolysis targeting chimeras (PROTACs) has emerged as a promising therapeutic approach in medicinal chemistry. PROTACs consist of two components: a ligand for the protein of interest (POI) and a ligand for ubiquitin ligase (E3). Because PROTACs induce ubiquitination and the subsequent proteasomal degradation of the POI, they effectively inhibit all functions of the POI. Focusing on the features of PROTACs, in this study, I attempted to identify G9a/GLP PROTACs. In other words, it is expected that the G9a/GLP PROTACs should exhibit the desired therapeutic effects because they should not only inhibit the catalytic activity but also disrupt interactions of G9a/GLP with other proteins.

Two distinct classes of PROTAC candidates were designed and synthesized using UNC0638 or RK-701 as G9a/GLP-binding ligand. Biological evaluation revealed that UNC0638-based class I PROTAC candidates were unable to induce the degradation of G9a. However, some candidates of this class exhibited antiproliferative effects against MCF-7 cells, suggesting potential off-target interactions that may contribute to their anticancer activity

independent of G9a degradation. To overcome this challenge, several class II PROTACs were designed using a highly selective norleucine-based inhibitor RK-701. Among these, AMB-03-378

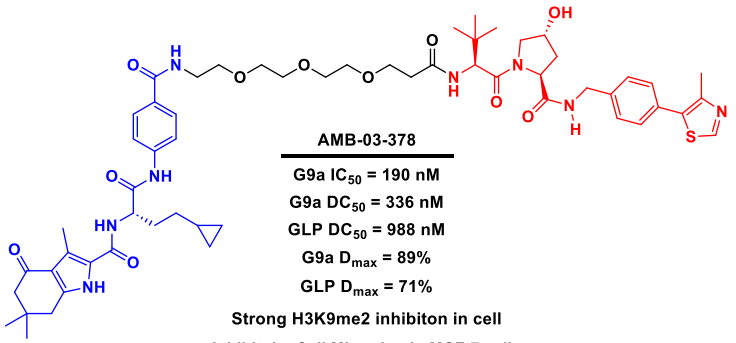

was identified as the most potent PROTAC degrader, demonstrating a dose- and time-dependent degradation of G9a and GLP via the ubiquitin-proteasome system (UPS). As a result of G9a/GLP degradation, AMB-03-378 strongly decreased the levels of di-methylated H3K9 (H3K9me2) in MCF-7 cells. Additionally, AMB-03-378 demonstrated the ability to downregulate the expression of HP1γ, shedding light on the scaffolding role of G9a/GLP. Notably, it promoted neurite outgrowth in the mouse neural crest-derived cell line N2a, highlighting its potential in neural development and repair. Although AMB-03-378 inhibited the migration of MCF-7 breast cancer cells, it had no significant impact on their proliferation, suggesting a need to reevaluate the role of G9a/GLP in breast cancer development. In this context, AMB-03-378 may serve as an important pharmacological probe.

Contents

General Introduction

1. Epigenetics

The term ‘epigenetics’ was coined by Conrad Waddington in 1942 to describe inheritable changes in gene activity that occur without modifications to the DNA sequence, resulting in alterations in biological phenotypes.[1] In molecular biology, the ‘central dogma’ states that DNA is the primary source of genetic information. In 2003, the human genome was fully sequenced, revealing all three billion base pairs of deoxyribonucleic acid (DNA) in humans.[2] According to the central dogma, understanding DNA should therefore theoretically explain all life phenomena. However, this is not the case in reality. For instance, different cell types in the body, such as nerve cells, skin cells, and immune T cells, all originate from the single fertilized egg cell and share an identical DNA sequence. Yet, these cells differ significantly in structure and function. Why is that? Protein synthesis in the body involves two processes: ‘transcription’, where genetic information from DNA is copied into mRNA, and ‘translation’, where proteins are synthesized from mRNA. The transcription process likely determines which genes are expressed and which remain dormant in each cell. Thus, ‘epigenetics’ derived from the Greek ‘epi’, meaning ‘later born’ or ‘beyond’—refers to mechanisms that regulate gene expression patterns without altering the underlying DNA sequence.

2. Epigenetic Mechanisms

One key mechanism in epigenetics involves histones, proteins around which DNA is wrapped. Histones play a dynamic role in regulating gene expression. They contain lysine, an amino acid whose chemical modifications such as methylation and acetylation serve as markers for gene activity.[3] These modifications, where methyl or acetyl groups are added to or removed from lysine, influence whether specific genes are expressed or silenced. Another mechanism involves DNA methylation (Figure 1), which adds methyl groups to DNA, typically leading to gene silencing by inhibiting transcription. Demethylation, the removal of these groups, can

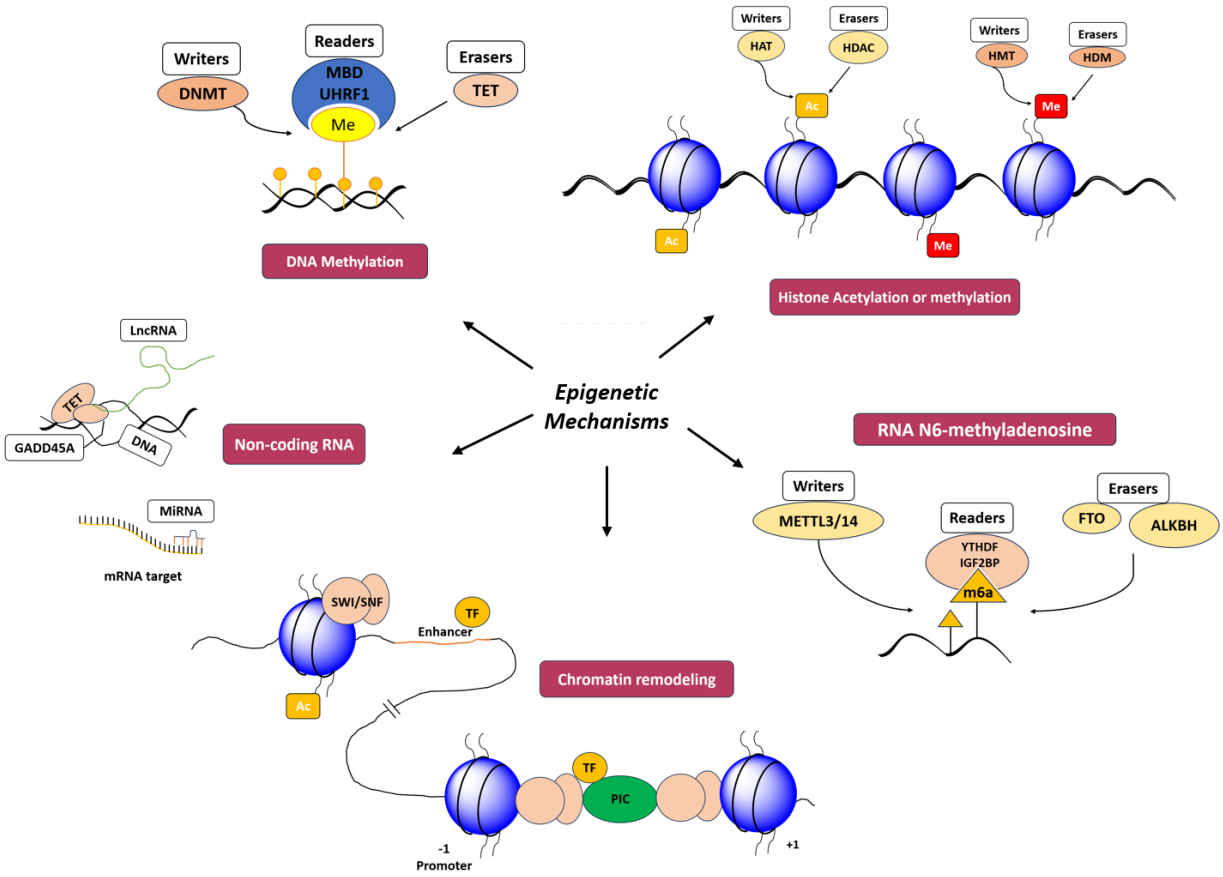

Figure 1. Overview of the epigenetic mechanism and the enzymes that regulate gene expression.[5]

reactivate genes.[4] Other mechanisms involved RNA modifications, chromatin remodeling, and non-coding RNA (ncRNA) regulation (Figure 1).[5] Together, these processes regulate gene

expression, without altering the underlying DNA sequence. Epigenetic modifications are regulated by a set of enzymes with specialized functions, categorized as 'writers', 'erasers', 'readers', and 'remodelers'.[6-8] Writers, such as DNA methyltransferases (DNMTs), add modifications like methyl groups to DNA, forming 5-methylcytosine (m5C).[9] Histone methyltransferases (HMTs) catalyze the methylation of lysine residues on histone proteins.[10] Erasers such as Ten-Eleven Translocation (TET) enzymes remove methylation marks by oxidizing 5-methylcytosine (5mC) into several intermediates, including 5-hydroxymethylcytosine (5hmC) as the initial oxidation product, followed by 5-formylcytosine (5fC) as the second product, and finally 5-carboxylcytosine (5caC) as the third product.[11] Histone deacetylases (HDACs) regulate gene expression by catalyzing the lysine deacetylation of histones.[12] Readers are proteins that recognize and bind to these modifications, influencing gene expression by modifying chromatin structure.[13] Remodelers impact chromatin accessibility by shifting nucleosomes.[14] Additionally, non-coding RNAs (ncRNAs) function as separate regulators of gene expression, interacting with specific RNA or DNA regions, and playing crucial roles in cellular functions and disease mechanisms.[15]

3. Histone Methylation

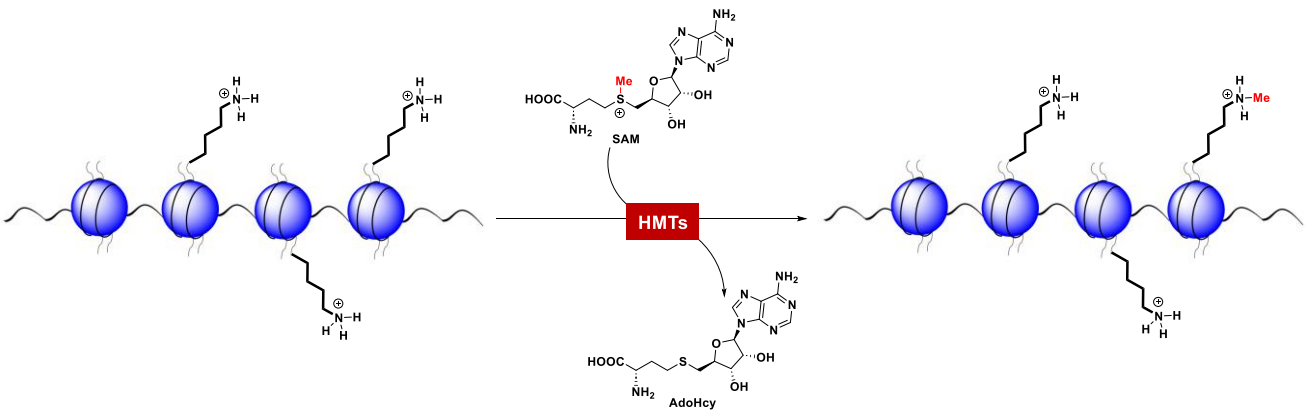

Figure 2. Schematic of the catalytic activity of HMTs showing the transfer of methyl group from SAM to histone.

As mentioned above histone methylation plays an important role in chromatin structure and epigenetic gene expression. Since their discovery in 2000, histone methyltransferases (HMTs) have been recognized for catalyzing the methylation of both histone and non-histone proteins.[16] These enzymes are broadly categorized into two major families: lysine methyltransferases (KMTs) and arginine methyltransferases (PRMTs). KMTs are further classified into two groups based on structural domains: the SET domain-containing KMTs, named after the Su(var), E(z), and Trithorax proteins, and the non-SET domain KMTs, with DOT1L being the sole representative of the latter. The SET domain KMTs are organized into five main families based on sequence similarity: SUV (Suppressor of Variegation), SET1, SET2, EZ (Enhancer of Zeste), and RIZ (Retinoblastoma protein-Interacting Zinc finger protein).[17] HMTs facilitate the methylation of lysine or arginine residues on histones H3 and H4 by utilizing *S*-adenosyl-L-methionine (SAM) as a cofactor, which is converted to *S*-adenosyl-L-homocysteine (AdoHcy) during the reaction (Figure 3). Dysregulation of histone methylation has been implicated in various diseases, including cancer, prompting significant interest in understanding the roles of HMTs and exploring their therapeutic potential. This has sparked extensive research into small-molecule modulators of HMTs, driving their use as essential tools for investigating enzyme functions and as promising leads for developing new therapeutic drugs.[18]

4. Histone Methyltransferase G9a/GLP

G9a and G9a-like protein (GLP), also known as EHMT2 and EHMT1, are key histone lysine methyltransferases (KMTs) critical for epigenetic regulation. These enzymes predominantly catalyze the mono- and di-methylation of histone H3 lysine 9 (H3K9) and H3K27, using SAM as a cofactor.[19-21] Acting as corepressors, they play a significant role in

gene silencing, chromatin condensation, and regulating cellular processes such as pluripotency, genomic imprinting, and embryonic development.[20,22] G9a and GLP form heteromeric or homomeric complexes via their SET domains, which enhance their methyltransferase activity. The SET domains of G9a and GLP, sharing approximately 80% sequence similarity, play a critical role in facilitating the formation of functional complexes between these enzymes.[20] Additionally, the ankyrin repeat domain of G9a is essential for its nuclear localization and protein–protein interactions, enabling selective binding to H3K9me1/2 while excluding H3K9me3. This specificity explains why H3K9 trimethylation is primarily carried out by other histone methyltransferases. The catalytic SET domain is indispensable for G9a's activity, as even inactive variants mimic the effects of complete gene knockout, emphasizing its pivotal role in epigenetic regulation.[20] Beyond its canonical histone targets, G9a also modifies nonhistone proteins, hinting at its involvement in a wide array of cellular functions. However, the biological significance of these nonhistone modifications remains poorly understood due to the complexity of G9a's regulatory network.[22,23] A key aspect of its function is its interaction with DNA methyltransferase 1 (DNMT1), particularly in heterochromatic regions of chromosomes. This interaction promotes the coordinated methylation of both DNA and histones, resulting in stable gene silencing. Disruption of G9a or GLP significantly reduces DNA methylation levels, while depletion of DNMT1 decreases H3K9me2 levels and G9a/GLP expression.[24] These findings reveal a reciprocal regulatory relationship between histone and DNA methylation, emphasizing the intricate nature of epigenetic regulation.

Overexpression of G9a and GLP is strongly associated with increased proliferation and metastasis in various cancers, including breast cancer, hepatocellular carcinoma, brain tumors, esophageal squamous cell carcinoma, aggressive ovarian carcinoma, and multiple myeloma.[25,26] Through transcriptional repression of tumor suppressor genes such as E-cadherin (CDH1) and p53, as well as activation of oncogenic pathways like the hypoxia response, G9a

plays a central role in promoting carcinogenesis.[27-31] Additionally, G9a facilitates transforming growth factor (TGF)-β-induced epithelial-to-mesenchymal transition (EMT) in head and neck squamous cell carcinoma and enhances invasion and metastasis in lung cancer by modulating epithelial adhesion molecules, although the precise pathways in lung cancer remain unclear.[32,33]

Beyond cancer, G9a dysregulation is implicated in several human disorders, including fibrosis, Prader–Willi syndrome, foot-and-mouth disease, sarcomere assembly defects, and chronic pain.[34-39] G9a also plays a role in globin disorders such as sickle cell disease (SCD), where its inhibition activates fetal γ-globin and represses adult β-globin expression in hematopoietic precursor cells.[40] Moreover, studies have shown that blocking G9a activity can reduce neurodegeneration and cognitive decline, highlighting its potential therapeutic application in treating Alzheimer's disease (AD).[41,42] Further research into the diverse functions and regulatory mechanisms of G9a could provide deeper insights into its role in epigenetic regulation and its broader impact on cellular physiology and disease progression.

5. Epigenetic Modulators

For instance, if lysine, which is normally acetylated, fails to undergo acetylation and vice versa due to disruptions in genetic information processing, it can lead to diseases such as cancer, neurodegenerative disorders, and diabetes. Modulating the addition or removal of acetyl and methyl groups on lysine could offer a potential approach to develop treatments for these diseases. The process of modifying lysine is mediated by enzymes, and if the activity of such enzyme is inhibited, the methylation, demethylation, acetylation, and deacetylation of lysine can be controlled. This insight led to the development of chemical inhibitors for these enzymes, resulting in the identification of several powerful epigenetic modulators, a field known as 'chemical epigenetics'.[43] Hence, targeting epigenetic enzymes that regulate gene

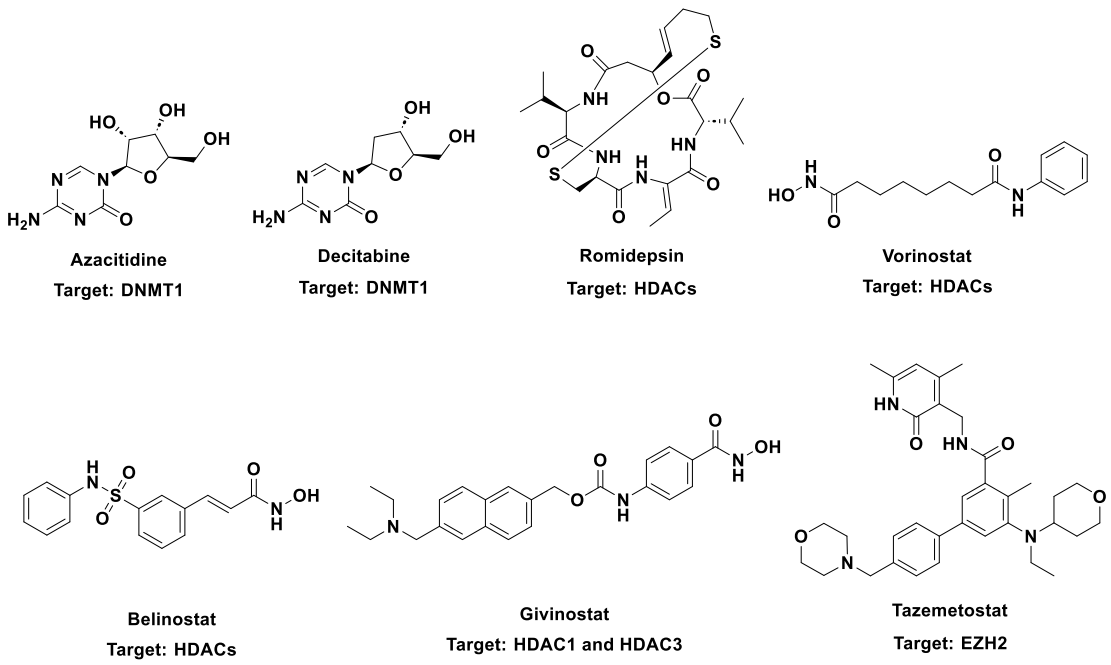

Figure 3. Epigenetic drugs approved by the FDA.

expression, offer a powerful approach for treating diseases, particularly cancer. Unlike traditional treatments that either kill or inhibit the proliferation of cancer cells, epigenetic therapies target abnormal gene expression patterns in tumor cells.[44] These drugs aim to restore normal cellular function, offering a more precise and often less toxic alternative.[45] Epigenetic agents have the unique ability to bypass some of the limitations of conventional therapies, such as chemotherapy or radiotherapy, which can be harsh and lead to drug resistance. Epigenetic drugs, including DNMT inhibitors, HDAC inhibitors, and EZH2 inhibitors, are already being explored in clinical settings, showing promise in cancer treatment. Several epigenetic-targeting drugs are approved for clinical use by Food and Drug Administration (FDA) (Figure 3), representing a breakthrough in cancer care with potential for broader applications.[5] Azacitidine is a nucleoside analog that inhibits DNA methyltransferases, leading to hypomethylation of DNA and reactivation of tumor suppressor genes. It is used primarily in the treatment of

myelodysplastic syndromes (MDS) and acute myeloid leukemia (AML).[46] Decitabine is another DNA methyltransferase inhibitor that induces DNA hypomethylation, promoting gene expression that may have been silenced in cancers. It is used to treat MDS and AML, particularly in older patients unable to undergo intensive chemotherapy.[47] Romidepsin is a histone deacetylase inhibitor (HDACi) that restores tumor suppressor gene expression by acetylating histones and relaxing chromatin. It is approved for the treatment of cutaneous T-cell lymphoma (CTCL) and peripheral T-cell lymphoma (PTCL).[48] Vorinostat is a pan-HDAC inhibitor that works by increasing the acetylation of histones, thereby reactivating silenced genes. It is FDA-approved for treating cutaneous T-cell lymphoma and is being explored for other cancers.[49] Belinostat is an HDAC inhibitor that enhances the acetylation of histones and other proteins, leading to gene re-expression and cell cycle arrest. It is used to treat patients with relapsed or refractory peripheral T-cell lymphoma (PTCL).[50] Givinostat is an HDAC1/3 inhibitor that has shown potential in treating inflammatory and hematological diseases. It is under investigation for use in diseases like Duchenne muscular dystrophy and various cancers.[51] Tazemetostat is an EZH2 inhibitor that targets and inhibits the enzymatic activity of EZH2, a histone methyltransferase involved in gene silencing. It is used to treat patients with relapsed or refractory EZH2-mutated follicular lymphoma and other cancers.[52]

6. G9a/GLP Inhibitors

Small molecule inhibitors of G9a and GLP have attracted considerable attention in the fields of medicinal chemistry and chemical biology. Beyond their potential as therapeutic agents for treating various diseases, these inhibitors serve as valuable research tools for exploring the functional roles of G9a and GLP. By targeting these enzymes, researchers can uncover their enzymatic and regulatory activities in different cellular and pathological settings,

providing essential insights into their involvement in disease mechanisms and progression. The catalytic activity of the G9a/GLP enzyme is governed by its SET domain, which contains distinct binding sites for the SAM cofactor and the protein substrate. These pockets are attractive targets for small-molecule inhibitors, offering potential therapeutic strategies to disrupt G9a/GLP-mediated methylation.

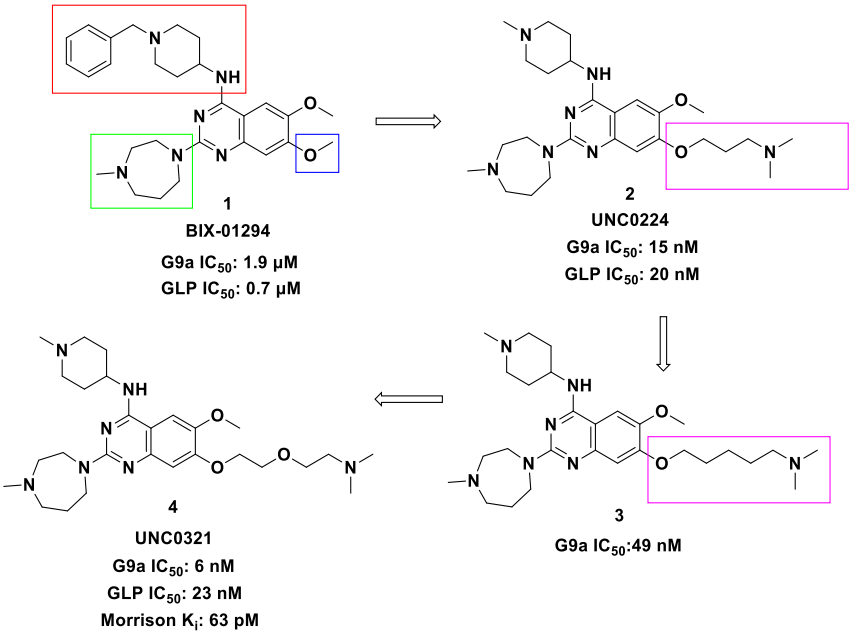

Figure 4. Chemical structures and inhibitory activity of compounds **1**, **2**, **3**, and **4**.

BIX-01294 (**1**, Figure 4) is the first synthetic inhibitor of G9a/GLP, identified through high-throughput screening.[53] It exhibits selective inhibition of G9a and GLP, with IC_{50} values of 1.7 and 38 μM, respectively. Under linear reaction conditions, it shows stronger inhibition of GLP (IC_{50} = 0.7 μM) than G9a (IC_{50} = 1.9 μM).[54] BIX-01294 reduces H3K9me2 levels at G9a target genes like *magea2*, *Bmi1*, and *Serac1*, with effects reversible upon discontinuation. The crystal structure of the catalytic SET domain of GLP in the complex formed by **1** and *S*-adenosyl-L-homocysteine (AdoHcy) reveals its binding at the substrate peptide groove of GLP,

mimicking histone H3, and inhibiting methyltransferase activity.[55] The inhibitor has therapeutic potential across diseases. In cancer, it decreases oncogenicity in breast cancer cells, including under hypoxic conditions, and inhibits migration and invasion of MDA-MB-231 cells.[56] In leukemia, it regulates proliferation, apoptosis, and differentiation in HL-60 and NB4 cells.[57, 58] Additionally, it enhances TRAIL sensitivity in breast cancer, promoting apoptosis via mitochondrial pathways.[59-61] Beyond cancer, BIX-01294 mitigates peritoneal fibrosis in mice and promotes differentiation of goat adipose-derived stem cells. Nevertheless, at concentrations exceeding 4.1 μM, compound 1 exhibits cytotoxicity, restricting its potential as a viable chemical probe for targeting G9a.

To address the limitations of BIX-01294 (**1**), the structure–activity relationship (SAR) of a quinazoline scaffold was explored to improve potency and selectivity.[62] Analysis of the GLP–1 complex revealed that the benzyl group in 1 did not contribute significantly to binding. Modifications to the 4-amino moiety identified that retaining an alkylated nitrogen, specifically 1-methylpiperidin-4-ylamino, was crucial for maintaining potency. Similarly, optimizing the 2-amino region with methylpiperazine or piperidine resulted in enhanced activity, while chlorine substitution diminished efficacy. A 7-aminoalkoxy side chain was added to the quinazoline scaffold to engage the lysine-binding channel, leading to the development of UNC0224 (**2**, Figure 4), a potent G9a inhibitor with an IC_{50} of 15 nM. High-resolution X-ray crystallography revealed that the 7-dimethylaminopropoxy side chain of **2** interacts with Tyr1154 and Leu1086, strengthening binding. Further interactions of the 4-amino and diazepane groups with Asp residues contributed to its superior potency compared to **1**. These modifications also improved both selectivity and inhibitory efficiency. The crystal structure of the G9a–**2** complex showed available space in the lysine-binding channel, suggesting the potential for longer or bulkier aminoalkoxy chains. Subsequent SAR studies revealed that G9a could accommodate a 5-carbon aminoalkoxy chain, resulting in the synthesis of **3** (Figure 4).

Substituting various amino capping groups, such as pyrrolidine and piperidine, either maintained or enhanced potency. A basic nitrogen in the side chain was essential for activity, with its removal leading to reduced inhibition. The addition of an ethoxyethyl chain produced UNC0321 (**4**, Figure 4), a highly potent G9a inhibitor (IC_{50} = 6–9 nM) with a Morrison Ki of 63 pM, approximately 40-fold stronger than **2** and 250-fold stronger than **1**.[63]

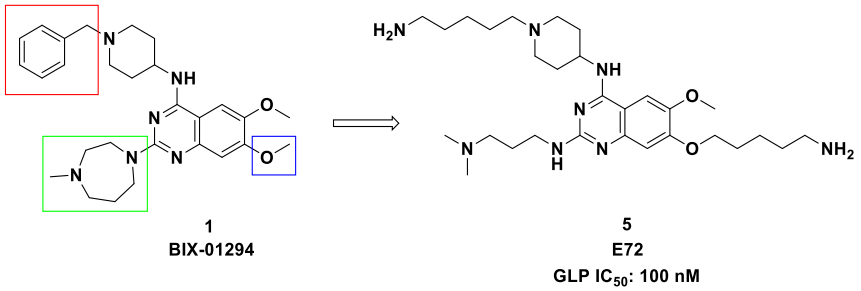

Figure 5. Chemical structures and inhibitory activity of compounds **1** and **5**.

The design of E72 (**5**, Figure 5), a derivative of **1**, enhanced its binding affinity and inhibitory potency against G9a and GLP.[64] Key modifications included replacing the 7-methoxy group with a 5-aminopentyloxy group to mimic lysine, substituting the diazepane and benzyl groups to improve interactions, and optimizing binding to the GLP lysine-binding channel and peptide-binding groove. E72 exhibited low toxicity, effectively reversing K-ras-mediated silencing of the proapoptotic Fas gene in NIH 3T3 cells, though it showed reduced cell-based potency compared to **1**.

UNC0638 (**6a**, Figure 6) was developed to address the low cellular potency of earlier G9a inhibitors by increasing lipophilicity while maintaining high in vitro activity.[65] **6a** is a potent, selective inhibitor of G9a (IC_{50} < 15 nM) and GLP (IC_{50} = 19 nM), with minimal off-target effects. It occupies the substrate-binding groove without interacting with the SAM-

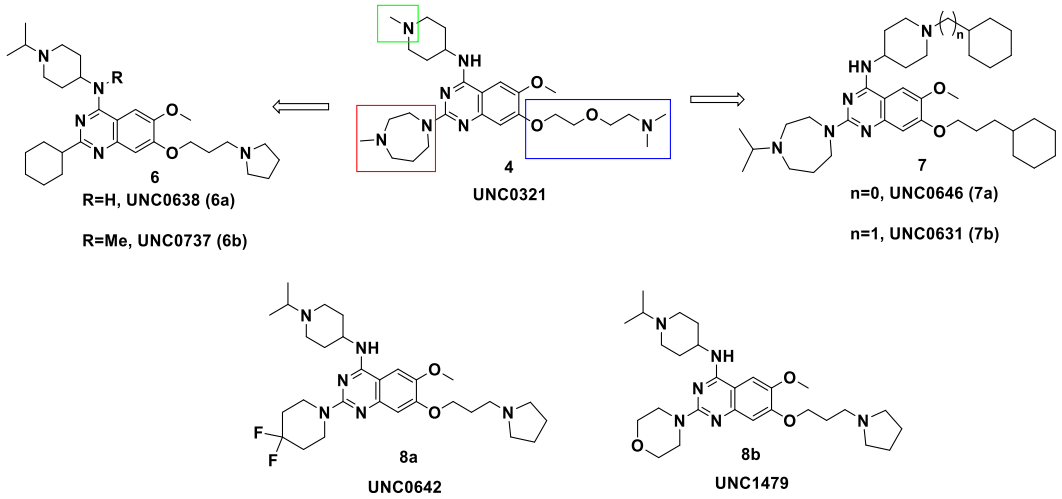

	4	6a	6b	7a	7b	8a	8b
G9a IC_{50}:	<15 nM	<15 nM	5 μM	6 nM	4 nM	<2.5 nM	<2.5 nM
GLP IC_{50}:	15 nM	19 nM	>10 μM	<15 nM	–	<2.5 nM	–

Figure 6. Chemical structures and inhibitory activity of **4**, **6a**, **6b**, **7a**, **7b**, **8a** and **8b**.

binding pocket and effectively reduces H3K9me2 levels by 60–80% at 250 nM across various cell lines, comparable to G9a/GLP knockdown. However, **6a** exhibits low systemic exposure and rapid clearance, limiting its suitability for in vivo studies. Despite its high structural similarity to **6a**, the N-methyl analog UNC0737 (**6b**, Figure 6) is significantly less potent, serving as a negative control. **6a** selectively inhibits G9a/GLP-mediated dimethylation of p53 K373 in cellular assays without affecting protein levels, demonstrating its capability to block G9a/GLP methyltransferase activity in cells, though its pharmacokinetics constrain its therapeutic potential. The identification of 6a as an active G9a/GLP probe in cell-based assays prompted further development of G9a/GLP inhibitors for cellular applications. Modifications at the 2-, 4-, and 7-positions of the quinazoline scaffold of **4** led to the creation of UNC0646 (**7a**) and UNC0631 (**7b**) (Figure 6).[66] These inhibitors effectively reduced H3K9me2 levels across various cell lines, including MDA-MB-231, PC3, and MCF-7, while exhibiting minimal

toxicity. Notably, **7a** displayed an excellent toxicity:function ratio, particularly in MCF-7 (470) and 22Rv1 (510) cells, positioning it as a valuable tool for investigating G9a biology. The poor metabolic stability of G9a/GLP inhibitor **6a** was addressed by modifying its 2-cyclohexyl group, leading to the development of UNC0642 (**8a**, Figure 6), a potent and selective inhibitor.[67] **8a** exhibited high in vitro potency (IC_{50} < 2.5 nM), excellent metabolic stability, and enhanced pharmacokinetics in mice, including >10-fold higher plasma concentration and AUC than **6a**. It demonstrated moderate brain penetration, potent activity against pancreatic cancer cells (PANC-1, IC_{50} = 40 nM), and reduced clonogenicity. In mouse models, **8a** improved survival in Prader–Willi syndrome and cognitive function in Alzheimer's disease by reducing H3K9me2, β-amyloid plaques, and enhancing neuronal markers. Another inhibitor of this series UNC1479 (**8b**, Figure 6) demonstrated improved penetration into the central nervous system, achieving a brain-to-plasma ratio of 0.68.[67]

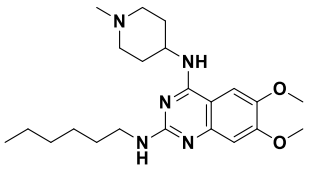

9
MS012
G9a IC_{50}: 992 nM
GLP IC_{50}: 7 nM

Figure 7. Chemical structures, inhibitory activity of **9**.

Compound **1** was found to exhibit 3–5 times greater selectivity for GLP than for G9a. Motivated by this finding, a novel GLP inhibitor, MS012 (**9**, Figure 7), was developed.[54] **9** is a highly selective inhibitor for GLP, with more than 140-fold greater selectivity (IC_{50} = 7 nM) for GLP over G9a (IC_{50} = 992 nM). It inhibits the peptide substrate competitively, while acting noncompetitively against SAM. Although its binding mode shares similarities with both GLP

and G9a, the precise structural basis for its selectivity remains elusive. Despite its selectivity for various methyltransferases, MS012 exhibited poor membrane permeability and a high efflux ratio, limiting its potential for use in cellular assays. X-ray crystallography (Figure 6b) highlighted critical hydrogen bonds and unique orientations of the 2-hexylamino group, which contribute to its specificity for GLP.

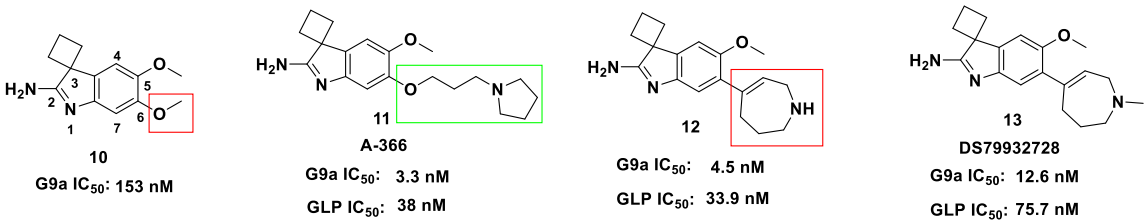

Figure 8. Chemical structures, inhibitory activity, and PK properties of **10** ,**11**, **12**, and **13**.

Chemically distinct G9a inhibitor **10** (IC_{50} = 153 nM) was identified through a peptide-based assay, exhibiting high binding efficiency (Figure 8). Structural optimization produced A-366 (**11**, Figure 8), with enhanced potency (IC_{50} = 3.3 nM).[68] **11** was found to be competitive for the peptide substrate and noncompetitive for SAM and demonstrated high selectivity against 21 methyltransferases, retaining activity against GLP (IC_{50} = 38 nM). In PC3 cells, 3 μM of **11** reduced H3K9me2 levels by 50% without affecting other histone marks. X-ray analysis revealed strong hydrophobic and electrostatic interactions in the G9a substrate-binding site. *In vivo,* A-366 achieved 45% tumor growth inhibition in an AML xenograft model. Inspired by the prior study[69] a tetrahydroazepine moiety was introduced at the 6-position of indole-based G9a inhibitor **11** to form compound **12**, which led to the synthesis of the orally available G9a/GLP inhibitor DS79932728 (**13**, Figure 8).[70] The X-ray cocrystal structure of **13** with G9a revealed a binding pattern similar to **11**, with hydrogen bonds stabilizing the interaction. **13** showed favorable pharmacokinetics, including high solubility, metabolic stability, and 96%

oral bioavailability. *In vivo*, **13** induced γ-globin production in a cynomolgus monkey model, suggesting its potential for treating β-thalassemia and sickle cell disease by stimulating fetal hemoglobin production.

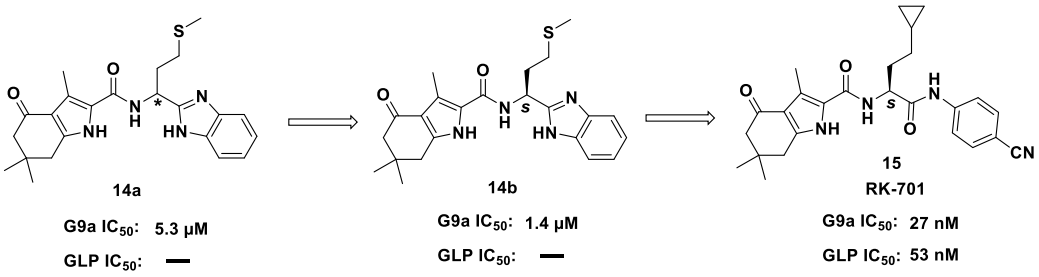

Figure 9. Chemical structures, inhibitory activity, and PK properties of **14** and **15**.

Through high-throughput screening (HTS), a novel G9a inhibitor, **14a** (IC_{50} = 5.3 μM), was identified.[71] The optically active *S*-enantiomer, **14b** (Figure 9), exhibited approximately four times greater potency (IC_{50} = 1.4 μM) than **14a**. Compound **14b** contains a tetrahydroindole ring on the left, a benzimidazole ring on the right, and an S-methionine side chain at the center, giving it distinctive peptidomimetic properties. Kinetic studies revealed that **14b** acts as a competitive inhibitor against the H3K9 substrate peptide and as a noncompetitive inhibitor of SAM. Further structure-activity relationship (SAR) analysis led to the development of RK-701 (**15**, Figure 9), a highly potent and selective G9a inhibitor with an IC_{50} of 27 nM, which shows superior activity compared to related histone methyltransferases (HMTs). At a concentration of 100 nM, compound **15** exhibited a dose-dependent reduction in H3K9me2 levels in a cell-based assay using the MOLT-4 human T lymphoblast cell line, alongside significant inhibition of cell growth. Additionally, **15** promoted the expression of fetal hemoglobin (HbF) by disrupting γ-globin repressor complexes at the BGLT3 locus,[72] showing

promise as a novel therapeutic for epigenetic modulation and potential treatment for sickle cell disease. Although both **6a** and **15** target the substrate binding pocket of G9a, they interact with distinct regions within that site.

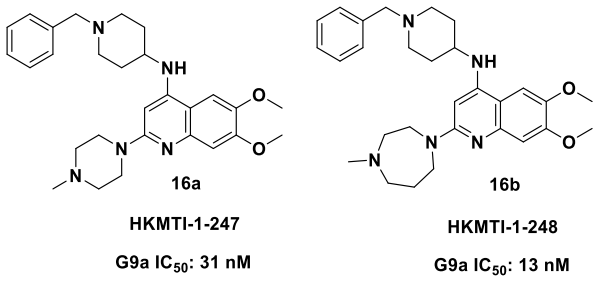

Figure 10. Chemical structures and inhibitory activity of **16a** and **16b**.

X-ray crystallography of the **6a**–G9a complex revealed that the *N*-3 nitrogen of the quinazoline ring may not be essential for binding to G9a. Based on this observation, modifications were made to the pharmacophoric elements of quinazoline-based G9a/GLP inhibitors, focusing on optimizing the central heterocyclic scaffold while maintaining key interactions within the enzyme's substrate pocket. As a result, quinoline-based compounds HKMTI-1-247 (**16a**) and HKMTI-1-248 (**16b**) were developed, exhibiting potency five times greater than the parent compound **1** (Figure 10).[73]

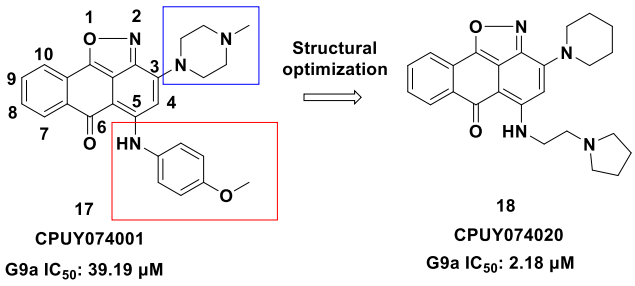

Figure 11. Chemical structures, inhibitory activity, and PK profiles of **17** and **18**.

Ligand-based virtual screening using OMEGA/ROCS identified novel G9a inhibitors by analyzing 3D shape similarity to **6a**. An isoxazole-based compound, CPUY074001 (**17**, Figure 8), showed 39.34% inhibition (IC_{50} = 39.19 μM) by occupying G9a's histone peptide–binding site and forming hydrogen bonds with Asp1088 and Asp1078.[74] Optimization yielded CPUY074020 (**18**, Figure 11), with 91.52% inhibition (IC_{50} = 2.18 μM) and improved antiproliferative effects on HCT116 and MCF-7 cells. Compound **18** reduced H3K9 methylation levels and exhibited favorable pharmacokinetics, including 55.5% oral bioavailability. Its binding included electrostatic interactions via flexible side chains, highlighting the potential of tailored isoxazole scaffolds for G9a inhibition and anticancer therapy.

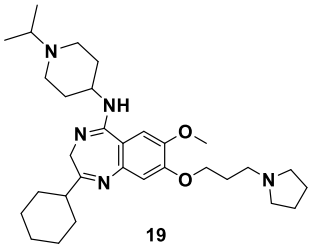

Figure 12. Chemical structures, inhibitory activity of **19**.

A scaffold-hopping strategy replaced the quinazoline core of G9a/GLP inhibitor **6a** with a benzodiazepine framework, yielding EML741 (**19**, Figure 12) (IC_{50} = 23 nM).[75] Compound **19** demonstrated high stability (72 h in PBS), low turnover in human microsomes (2.25% vs. 2.93% for **6a**), and strong permeability (P_{app} = 4.8 ×10^{-7} cm s^{-1}), with effective blood-brain barrier penetration (P_{app} = 2.3 × 10^{-7} cm s^{-1}). When treated with compound **19** at concentrations up to 5 μM, neither MDA-MB-231 nor U-343 cells showed a reduction in metabolically active cell numbers after 72 hours, compared to the vehicle control. In contrast, MCF-7 cells exhibited a similar initial response at 24 hours, but toxicity gradually increased at 48 and 72 hours.

Despite the lack of significant impact on cell viability, compound **19** effectively reduced H3K9me2 levels in a dose- and time-dependent manner.

A molecular docking-based virtual screening was performed using the G9a binding pocket complexed with **6a**, aiming to evaluate a range of small molecules and select the most promising candidates for subsequent in vitro testing.[76] Among the 125 compounds assessed, the piperidine derivative DCG066 (**20**, Figure 13) emerged as a promising inhibitor, exhibiting activity comparable to compound 1. Compound **20** selectively reduced H3K9me2 levels without influencing H3K27me3. It displayed substantial growth inhibition across multiple cell lines, with IC50 values ranging from 1.7 to 6.6 μM, showing the greatest potency in K562 cells (IC_{50} = 1.7 μM), which was 2.3 times more potent than **1**.

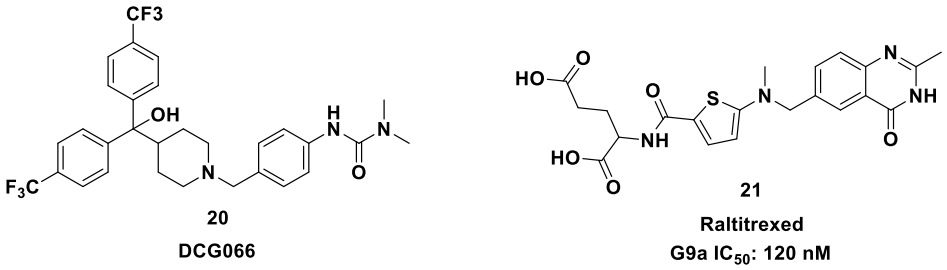

Figure 13. Chemical structure of DCG066 (**20**) and Raltitrexed (**21**).

Through 3D QSAR screening of a compound database comprising 400,000 molecules, raltitrexed (**21**, Figure 13) was identified as a substrate-competitive inhibitor of G9a, with an IC_{50} of 120 nM.[77] Compound **21** effectively reduced H3K9me2 levels in *Caenorhabditis elegans* CL2006, a strain known for its elevated H3K9me2 expression and its utility in Aβ-mediated neurodegeneration studies. Additionally, **21** demonstrated no toxicity in *C. elegans* CL2006, and its potential efficacy against Alzheimer's disease (AD) was further explored. Treatment with **21** resulted in a dose-dependent improvement in locomotive function, alongside a significant reduction in Aβ aggregates, up to 47%.

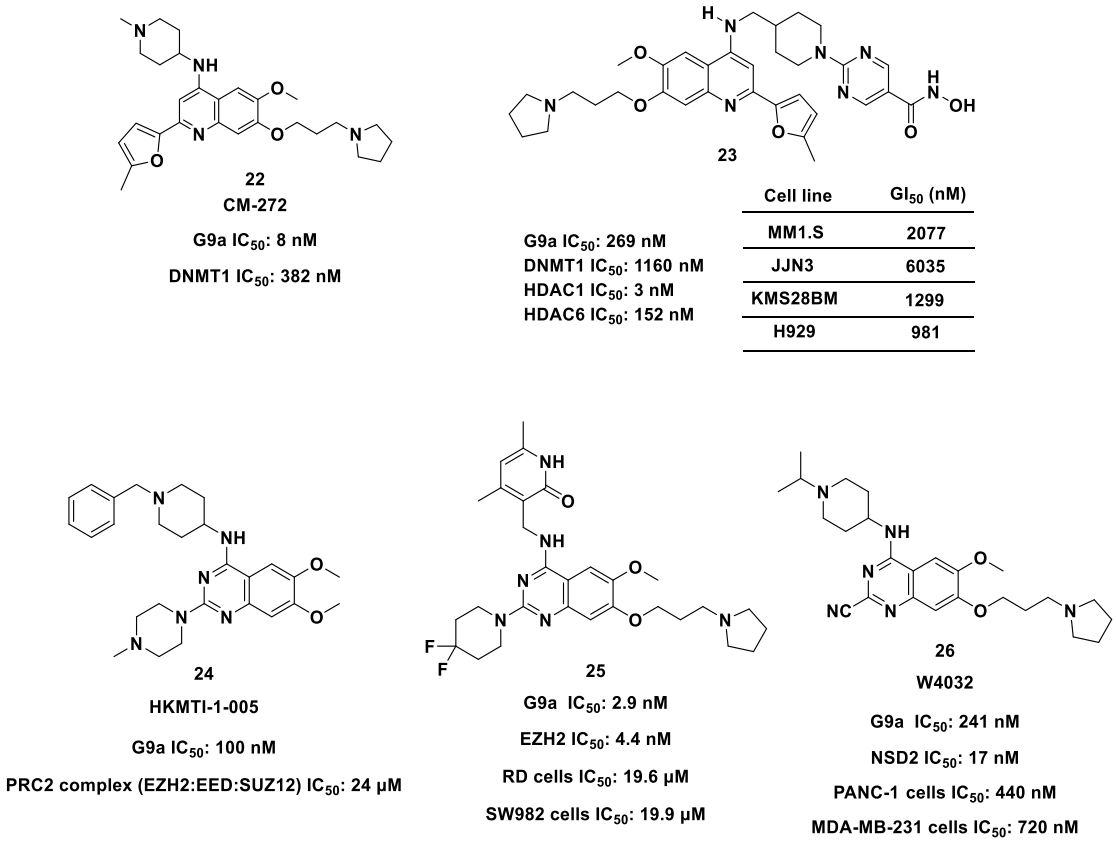

Figure 14. Chemical structure and inhibitory activity of **22**, **23**, **24**, **25** and **26**.

A promising approach for cancer therapy was identified by the simultaneous inhibition of crucial epigenetic pathways responsible for silencing tumor suppressor genes. Recent studies have advanced dual inhibitors targeting G9a and associated enzymes like DNMT1, EZH2, and NSD2. As shown in Figure 14, quinoline-based **22** improved G9a inhibition (IC_{50} = 8 nM) compared to **6a** and showed substantial activity against DNMT1 (IC_{50} = 382 nM).[78] **22** exhibited potent antiproliferative effects (GI_{50} = 218–455 nM) and robust pharmacokinetics, achieving 70% tumor growth inhibition (TGI) in AML xenografts. **23**, a multitarget inhibitor of G9a, DNMT1, and HDACs, demonstrated efficacy in vitro but was toxic *in vivo*.[79] Dual G9a-EZH2 inhibitors like **24** and **25** showed superior selectivity and reduced tumor progression

in various models, with **25** exhibiting high bioavailability and 86.6% TGI in rhabdomyosarcoma xenografts.[80, 81] For G9a-NSD2 dual inhibition, W4032 (**26**) selectively targeted both enzymes, reducing H3K36me2 levels and suppressing NSD2-regulated genes in PANC-1 cells.[82] In xenograft models, **26** demonstrated moderate efficacy (47.4% TGI) with low toxicity. These advances highlight the therapeutic potential of dual and multitarget inhibitors in addressing cancer-associated epigenetic dysregulation.

BIX-01338 (**27**) (Figure 15) was identified in the same screening as compound **1**, exhibiting broad inhibition across all tested enzymes.[53] Kinetic analysis revealed that **27** acts as a competitive inhibitor of SAM, making it the first reported SAM-competitive G9a inhibitor (IC_{50} = 4.7 μM). However, despite its inhibitory activity in enzyme assays, compound **27** did not affect cellular H3K9 methylation or inhibit the growth of cancer cells.

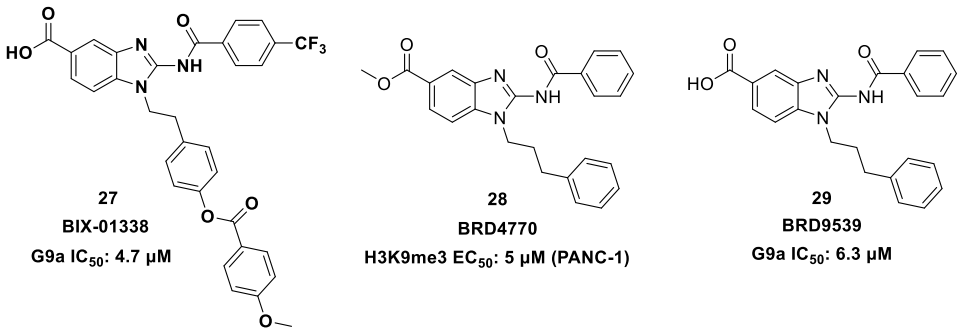

Figure 15. Chemical structure and inhibitory activity of **27**, **28** and **29**.

A focused library of SAM mimetics was screened to identify compounds that inhibit G9a, leading to the discovery of five promising hits across both biochemical and phenotypic assays.[83] Among these, BRD4770 (**28**, Figure 15) was identified as a lead compound, demonstrating a 23% reduction in H3K9 trimethylation in PANC-1 cells at 5 μM, without affecting other histone marks. BRD9539 (**29**, Figure 15), a carboxylic acid derivative of **28**,

showed strong biochemical inhibition of G9a but lacked cellular activity. The IC_{50} of **28** increased with higher SAM concentrations, confirming its role as a competitive SAM inhibitor. It is possible that **28** is converted to the less cell-permeable **29** inside cells, as methyl esters like **28** are typically hydrolyzed to their carboxylic acid forms in cells, acting as prodrugs. Notably, **28** did not induce caspase activation, suggesting that its effects on apoptosis are independent of G9a inhibition. Instead, it reduced cell proliferation, triggered G2/M arrest, and activated ataxia telangiectasia mutated (ATM) kinase without causing DNA damage. These findings suggest that 28 could serve as a valuable tool for investigating G9a-related biological pathways.

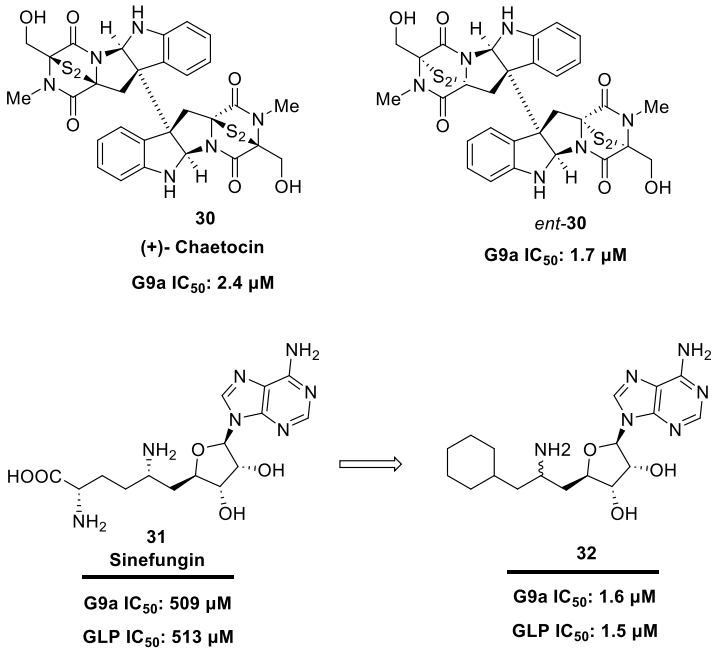

Figure 16. Chemical structure and inhibitory activity of **30**, *ent*-**30**, **31** and **32**.

Chaetocin (**30**, Figure 16), a SAM-competitive inhibitor initially isolated from *Chaetronium minutum*, weakly inhibits G9a (IC_{50} = 2.5 μM) and was the first reported G9a inhibitor.[84] Its activity is attributed to its sulfur moiety, as sulfur-deficient analogs were inactive. **30** and its enantiomer (*ent*-**30**) exhibited similar inhibition (IC_{50} = 1.7 μM), indicating its 3D

structure is non-essential. Sinefungin (**31**, Figure 16), a nucleoside analog from *Streptomyces* cultures, showed weak G9a (IC_{50} = 509 μM) or GLP (IC_{50} = 513 μM) inhibition.[85] Structural optimization led to **32**, significantly enhancing inhibition of G9a (IC_{50} = 1.6 μM) and GLP (IC_{50} = 1.5 μM) while maintaining selectivity. **32** exhibited weak activity against DNMT1 (IC_{50} = 179 μM) and no significant inhibition of PRMT1 or SET7/9, highlighting its potential as a targeted SAM-competitive inhibitor for epigenetic research.

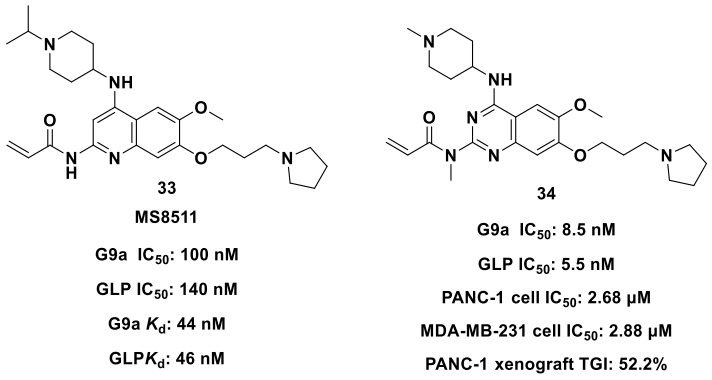

Figure 17. Chemical structure and inhibitory activity of **33** and **34**.

X-ray cocrystal structure analysis of G9a and GLP bound to **6a** identified cysteine residues (Cys1098 in G9a, Cys1186 in GLP) as targets for covalent inhibitor design. Compound **33** (Figure 17), a covalent inhibitor targeting these residues, demonstrated time-dependent inhibition of G9a and GLP, with stronger effects on G9a. Covalent modifications stabilized binding and offset differences in the binding pocket sizes.[86] **33** selectively inhibited G9a/GLP without affecting 21 other methyltransferases and reduced H3K9me2 levels in MDA-MB-231 and K562 cells, showing antiproliferative effects. Another identified covalent inhibitor **34** (Figure 17) showed selective inhibition against G9a/GLP and 52.2% tumor growth inhibition (TGI) in vivo at a dose of 2 mg/kg for 22 days without toxicity.[87] Covalent binding of **34** was confirmed via crystal structures, with nearly identical binding modes in G9a and GLP.

G9a/GLP has emerged as a crucial epigenetic target due to its involvement in cancer and neurodegenerative diseases. The catalytic SET domain of G9a/GLP offers two binding pockets—for the SAM cofactor and the protein substrate—making it amenable to small-molecule inhibition. Over the past 17 years, substantial progress has been made in designing selective inhibitors for G9a/GLP, distinguishing them from other methyltransferases and even between G9a and GLP, despite their 80% sequence similarity. Computational techniques, including X-ray crystallography and virtual screening, have been instrumental in identifying and optimizing inhibitors. These efforts have yielded both covalent and non-covalent inhibitors, with some demonstrating efficacy in reducing histone methylation, alleviating neurodegeneration, and inhibiting cancer growth. However, no G9a/GLP inhibitors have advanced to clinical trials, primarily due to toxicity concerns associated with compounds like those featuring quinazoline cores.

Future research would therefore be expected on addressing these limitations. Efforts to design inhibitors targeting the underexplored SAM binding pocket could open new therapeutic avenues. Additionally, macrocyclic inhibitors and allosteric modulators may enhance selectivity and efficacy. Traditional G9a/GLP inhibitors focus solely on blocking their catalytic activity. As an alternative approach, modulators that can disrupt the entire range of G9a/GLP functions—such as their catalytic roles, protein interactions, and involvement in signal transduction—may offer a promising strategy for treating diseases linked to G9a/GLP overexpression. Beyond inhibition, degraders represent a promising approach,[88] as they not only inhibit catalytic activity but also disrupt the overall function, which is vital for its protein-complex interactions. The choice between G9a inhibitors and degraders hinges on the pathology involved. Bridging medicinal chemistry with molecular biology will be essential to tailor therapeutic strategies, paving the way for safer and more effective drugs targeting G9a/GLP and other epigenetic regulators.

7. Proteolysis Targeting Chimera (PROTAC)

The genomic revolution has led to the discovery of many novel protein targets associated with diseases. However, traditional strategies for developing small molecule inhibitors often face challenges due to the homology between target proteins, particularly in conserved functional domains. A more recent and promising approach is targeting proteins for post-translational degradation, rather than mere inhibition, which offers a novel solution to these therapeutic limitations. Most proteins are degraded through the ubiquitin-proteasome system (UPS), a process that begins with the attachment of ubiquitin to the target protein. As presented in Figure 18a, this process occurs in three steps. First, an E1 ubiquitin-activating enzyme activates ubiquitin using ATP, producing an activated ubiquitin–adenylate that forms a thioester intermediate with the catalytic cysteine of the E1 enzyme. In the second step, ubiquitin is transferred to the catalytic cysteine of an E2 ubiquitin-conjugating enzyme via transthioesterification. Finally, in the third step, ubiquitin is transferred to the substrate protein through a ternary complex formed by the E2 enzyme, an E3 ubiquitin ligase, and the substrate, creating an isopeptide bond between ubiquitin and a lysine residue on the target protein. This process can be repeated to form a poly-ubiquitin chain, which is recognized and degraded by the 26S proteasome. Proteolysis-targeting chimera (PROTAC) technology leverages this UPS mechanism by linking a ligand that binds the target protein of interest (POI) with another ligand that recruits an E3 ubiquitin ligase.[88-91] This induces a chemically mediated proximity between the POI and the E3 ligase, leading to the ubiquitination and subsequent degradation of the POI via the UPS (Figure 18a). Hence, the overall function of the POI is inhibited. Furthermore, PROTAC technology relies solely on the binding of a ligand to the protein of interest (POI), where even weak interactions can trigger the degradation of the target. This feature makes PROTACs particularly advantageous for targeting proteins that are otherwise considered undruggable. The structures of several active PROTAC molecules are presented in Figure 18b.

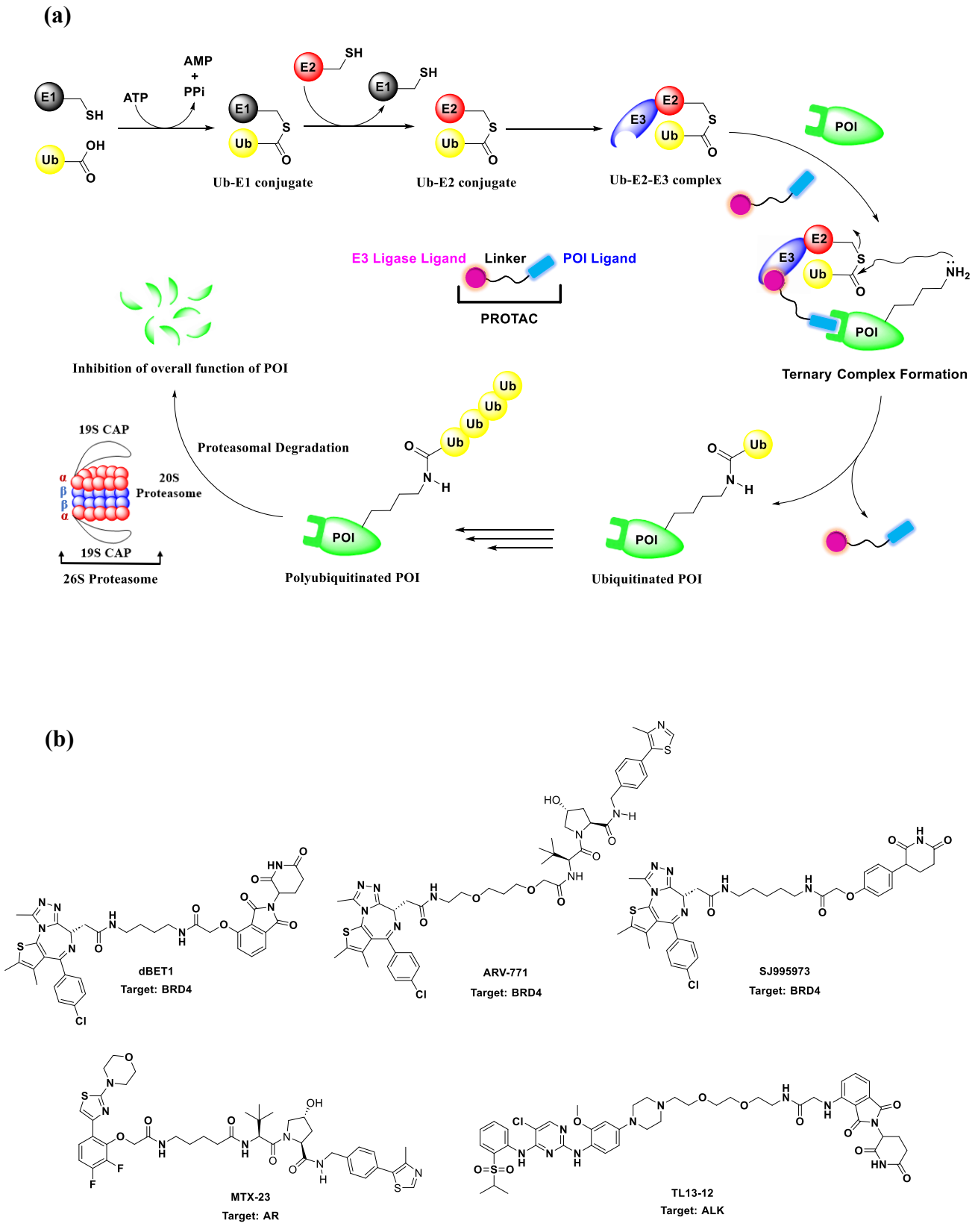

Figure 18. (a) Mechanism of PROTAC induced degradation. (b) Example of PROTAC degraders.

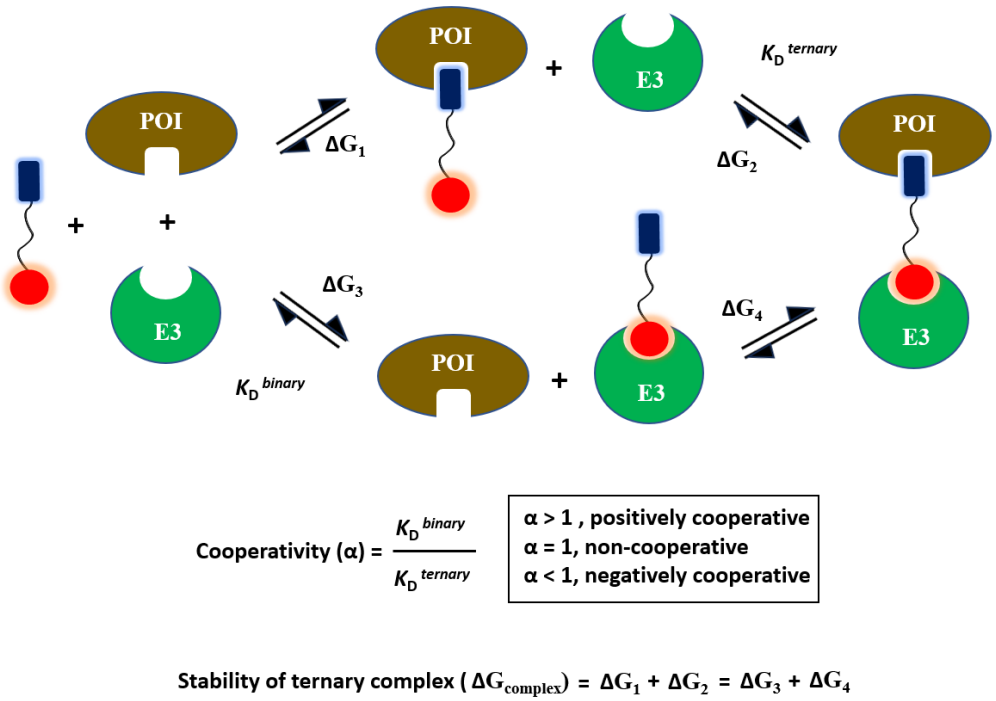

Figure 19. Equilibria of ternary complexes and definitions of cooperativity.

In PROTACs, cooperativity in ternary complex formation is crucial for their mechanism and efficacy (Figure 19).[92] Positive cooperativity ($\alpha > 1$) occurs when interactions between the target protein and the E3 ligase, mediated by the PROTAC, enhance ternary complex stability. This can result from synergistic binding, complementary surface contacts, conformational changes, or allosteric effects, promoting efficient target protein ubiquitination and degradation. Negative cooperativity ($\alpha < 1$) arises when repulsive forces, steric hindrance, or conformational incompatibilities reduce complex stability, impairing target protein recruitment and ubiquitination. This highlights potential challenges in PROTAC design, where such effects can diminish degradation efficiency. Noncooperative systems, characterized by unchanged dissociation constants, show no enhancement or reduction in complex formation. While these systems can achieve ternary complex formation, their efficiency may fall short compared to positively cooperative systems.

8. Overview of The Thesis

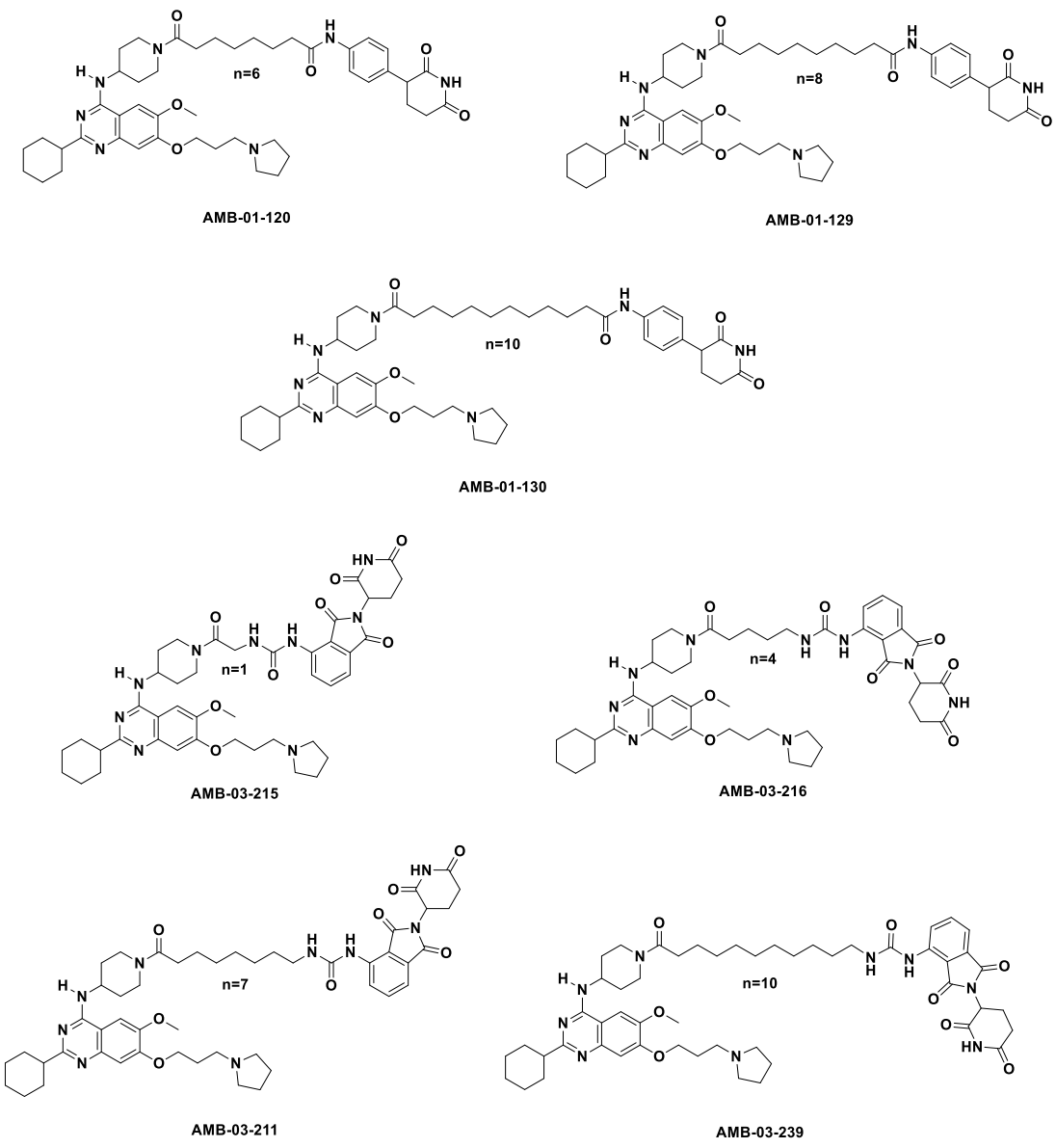

Figure 20. Representative class I G9a/GLP PROTAC candidates.

This thesis presents the design, synthesis, and biological evaluation of several novel G9a/GLP-PROTAC degraders. A diverse set of PROTAC candidates was developed by combining various E3 ligase ligands and G9a/GLP inhibitors with linkers of varying lengths, including alkyl and polyethylene glycol (PEG) linkers. The degradation efficiency of these

candidates was assessed using western blot analysis in human breast cancer MCF-7 cells. Comprehensive investigations identified AMB-03-378 as the most potent PROTAC that degrades G9a/GLP in a dose- and time-dependent manner via the UPS and reduces H3K9me2 levels in cells. Furthermore, AMB-03-378 downregulates HP1γ expression, highlighting G9a's scaffolding function. It also demonstrates potential in promoting neurite outgrowth in the mouse neural crest-derived N2a cell line, suggesting therapeutic implications for neural development and repair. Although AMB-03-378 inhibits the migration of MCF-7 breast cancer cells, it does not exhibit antiproliferative effects in these cells, indicating the need to reevaluate the role of G9a in breast cancer development.

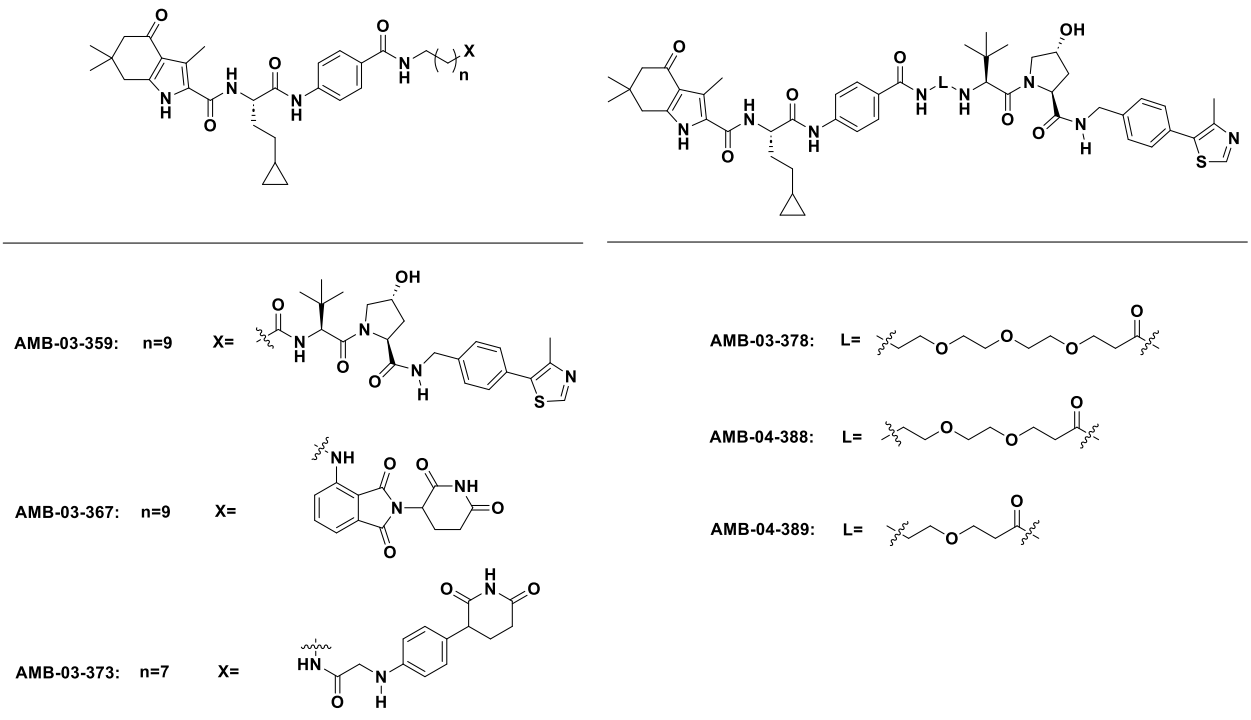

Figure 21. Representative class II G9a/GLP PROTAC candidates.

Chapter 1 describes the design, synthesis, and biological evaluation of class I PROTACs targeting G9a/GLP. Seven PROTAC candidates were synthesized (Figure 20), utilizing

UNC0638, a potent G9a/GLP inhibitor developed at the University of North Carolina (UNC), as the targeting ligand. Phenyl glutarimide (PG) and pomalidomide were employed as recruiters for the cereblon E3 ligase.

In Chapter 2, the design, synthesis, and biological evaluation of class II G9a/GLP PROTACs are described. This class of PROTACs was designed using the highly selective and potent norleucine-based G9a/GLP inhibitor RK-701, which was linked to several different types of E3 ligase recruiting ligands via alkyl and PEG linkers. Six different PROTAC candidates were synthesized (Figure 21), leading to the identification of the most potent G9a/GLP degrader, AMB-03-378.

Chapter 1

Design, Synthesis and Biological Evaluation of Class I G9a/GLP PROTAC Degraders

Abstract

Chapter 1 focuses on the development and assessment of class I PROTACs designed to target G9a/GLP. In this work, seven novel PROTAC candidates were synthesized, featuring UNC0638 as the G9a/GLP-binding ligand and phenyl glutarimide (PG) or pomalidomide as the cereblon-based E3 ligase recruiting moiety. These molecules were evaluated for their biological activity in MCF-7 human breast cancer cells, where they exhibited notable antiproliferative effects. Despite these promising results, no detectable G9a degradation was observed under the experimental conditions, suggesting further optimization is required to achieve effective degradation.

1. Introduction

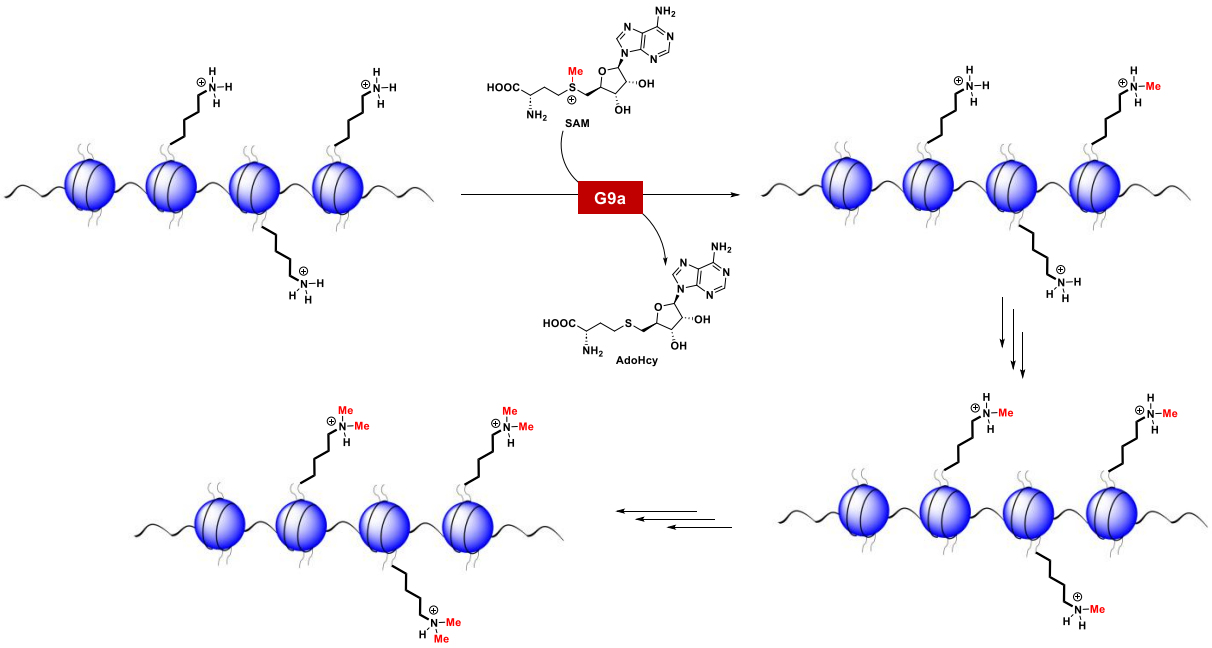

Figure 1. Schematic of the catalytic activity of G9a showing the transfer of methyl group from SAM to H3 lysine.

Histone methylation plays an important role in chromatin structure and epigenetic gene expression. G9a/GLP is a histonemethyltransferase that catalyzes the mono- and di-methylation of histone H3 lysine 9 (H3K9) using SAM as a cofactor.[19] Dysregulation of G9a/GLP has been implicated in various pathological conditions, such as cancers, neurodegenerative disorders and other diseases.[27-42] Consequently, G9a inhibitors have emerged as the potential therapeutic agents for such diseases.[93] While G9a inhibitors have shown potential, their clinical efficacy remains limited, indicating that targeting G9a's enzymatic activity alone may be insufficient. This highlights the need for alternative strategies, such as developing novel G9a modulators with mechanisms that go beyond traditional inhibition.

Recently, targeted protein degradation using proteolysis targeting chimeras (PROTACs) has become an effective therapeutic modality in medicinal chemistry for treating a variety of diseases.[88-91] PROTACs are molecules composed of two parts: a ligand of the protein of interest (POI) and a ligand of ubiquitin ligase (E3) connected through a linker. By inducing ubiquitination and subsequent proteasomal degradation of the POI (Figure 2), PROTACs effectively abrogate its functions, offering a comprehensive strategy to degrade proteins that conventional inhibitors fail to address. Thus, PROTACs were expected not only to inhibit its catalytic function, but also to prevent it from interacting with other proteins.

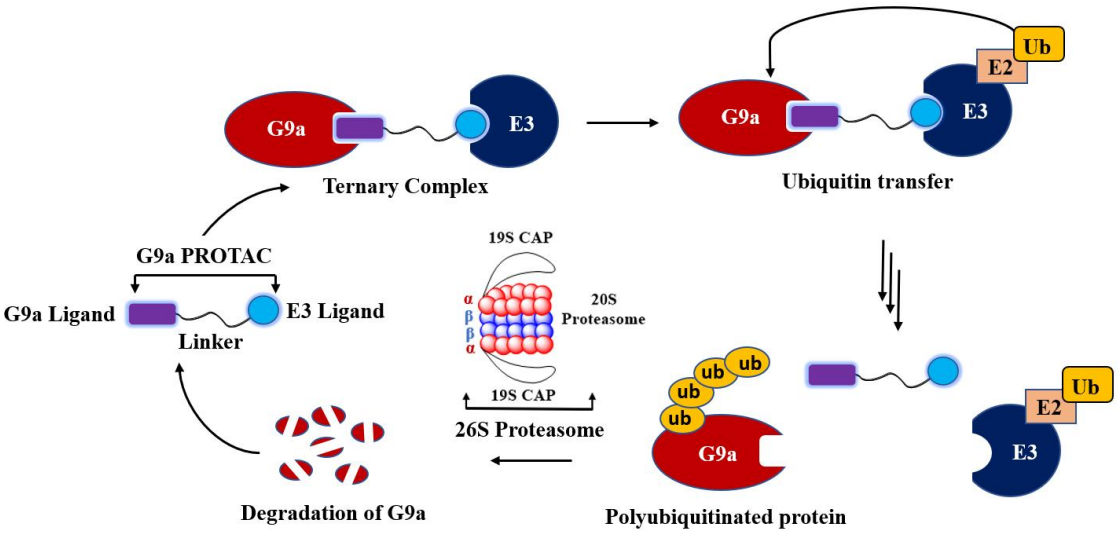

Figure 2. Mechanism of G9a degradation by a PROTAC.

With this advantage in mind, study was conducted to identify G9a/GLP PROTAC degraders. A small molecule inhibitor UNC0638 was used as the G9a/GLP ligand and G9a/GLP PROTACs were designed utilizing phenyl glutarimide (PG) and pomalidomide as the cereblon E3 ligase ligands. Seven PROTAC candidates with different linker lengths were synthesized and their G9a degradation activity was evaluated using western blotting analysis. This analysis revealed that, although the candidates exhibited antiproliferative effects, they were ineffective in achieving the desired targeted degradation of G9a.

2. Results and Discussions

2.1 Design of Class I PROTACs

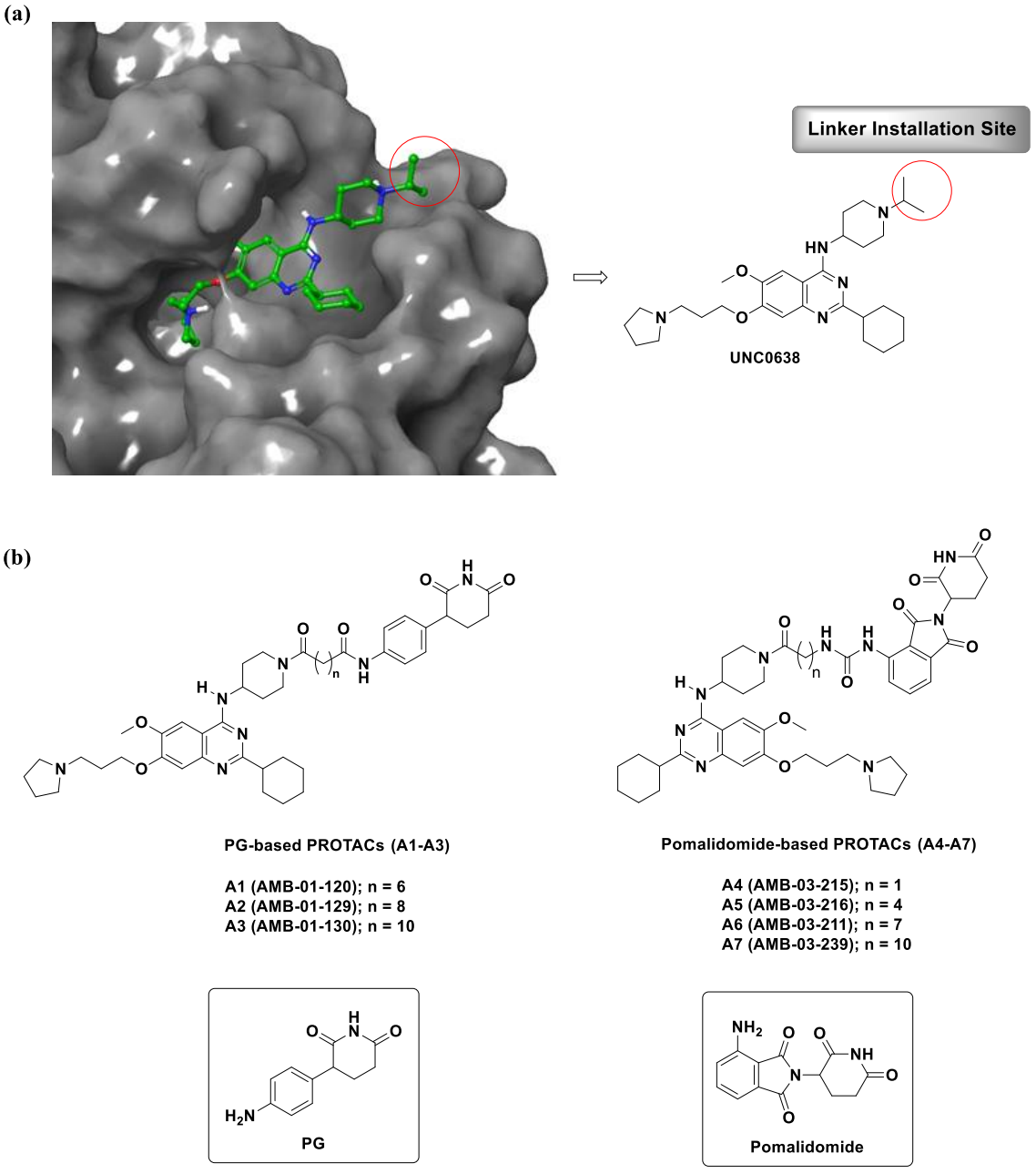

Figure 3. Rational design of G9a/GLP PROTAC degraders. (a) Left, the X-ray cocrystal structure of RK701 bound to G9a (PDB: 3RJW) and right, chemical structure of RK-701 showing the linker attachment site. (b) Designed UNC0638-based class I PROTAC candidates **A1**-**A7**.

To begin, UNC0638 was selected as the G9a/GLP binding ligand for the generation of G9a/GLP PROTAC degraders. X-ray co-crystal structure analysis of UNC0638 bound to G9a (Figure 3a) provided valuable structural insights, revealing that the isopropyl group on the piperidine ring is exposed to the solvent. This exposed position made it an ideal site for linker installation, which is crucial for the development of PROTACs. Consequently, the *N*-isopropyl group (highlighted by the red circle in Figure 3a) was replaced with a hydrogen atom (N-H). Using this modified intermediate, seven G9a/GLP PROTAC candidates (**A1**-**A7** in Figure 3b) were developed, linking it to different alkyl chains which were further conjugated with PG or pomalidomide as CRBN ligand.

2.2 Synthesis of Class I PROTACs

Scheme 1. G9a inhibitor part[a]

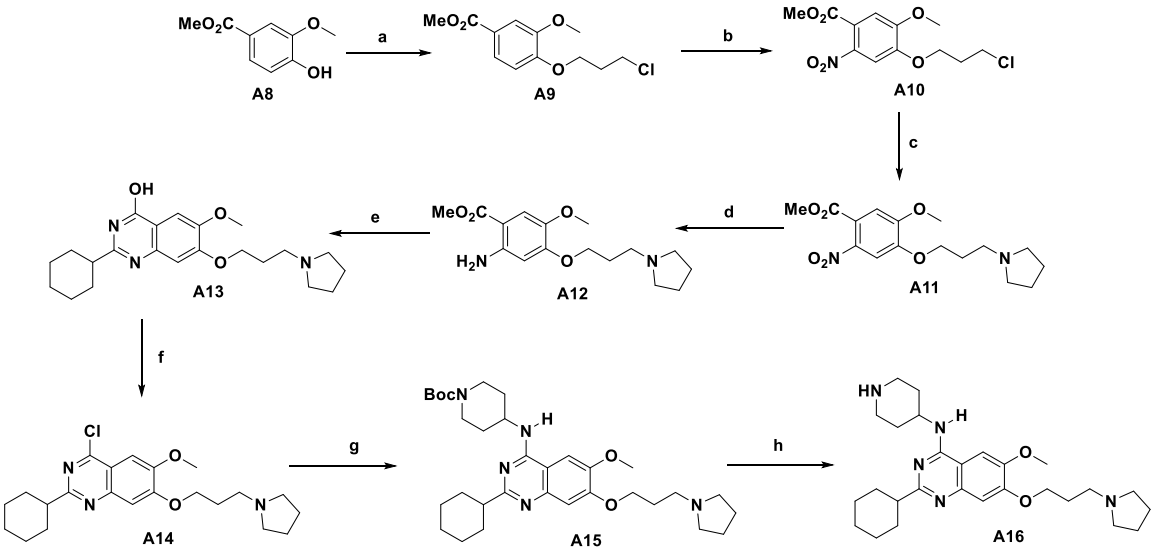

[a]Reaction and conditions: (a) 1-chloro-3-iodopropane, K_2CO_3, CH_3CN, reflux, 2 h; (b) HNO_3, Ac_2O, 0°C-rt, 12 h, 75% over 2 steps; (c) Pyrrolidine, K_2CO_3, NaI, tetrabutylammonium Iodide, CH_3CN, reflux, 3 h, 81%; (d) Fe-Dust, NH_4OAc, EtOAc-H_2O, reflux, 12 h, 63%; (e) Cyclohexanecarbonitrile, 4(N) HCl, dioxane, 100°C, 12 h; (f) *N*,*N*-diethylaniline, $POCl_3$, reflux, 4 h, 35% over 2 steps; (g) *tert*-butyl 4-aminopiperidine-1-carboxylate, K_2CO_3, DMF, 60°C, 12 h; (h) TFA, DCM, rt, 15 h, 30% over 2 steps.

Scheme 2. PG part[b]

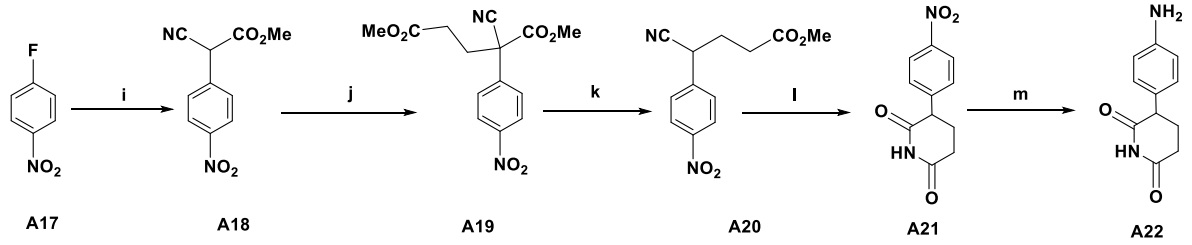

[b]Reaction and conditions: (i) Methyl 2-cyanoacetate, K_2CO_3, DMF, 120ºC, 2 h, (j) Methyl acrylate, NMM, THF, 55ºC, 2 h; (k) Na_2CO_3, THF/H_2O (1:2), 90ºC, 3 h; (l) conc. H_2SO_4, AcOH, 120ºC, 2 h; (m) Fe-dust, NH_4OAc, reflux, 36% over 5 steps.

Scheme 3: PG-linker part[c]

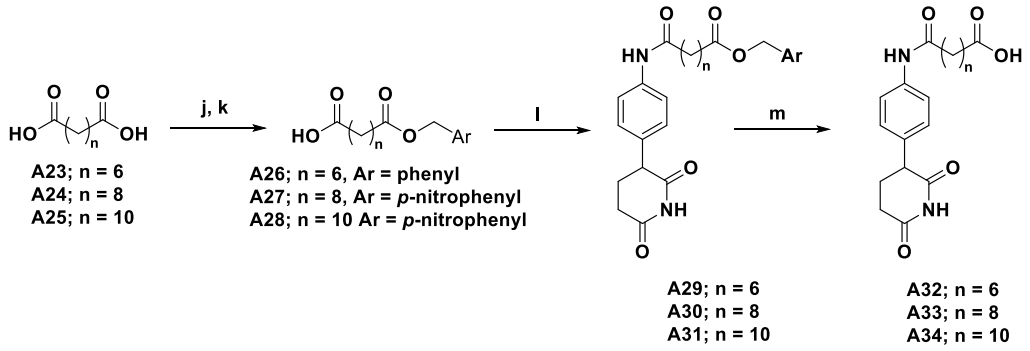

[c]Reaction and conditions: (j) KOH, MeOH, rt, 0.5 h; (k) Respective bromides, tetrabutylammonium bromide, Toluene, 130 °C, 14 h, 36%-40% over 2 steps; (l) **A22**, HATU, DIPEA, DMF, rt (m) 10% Pd/C, H_2, MeOH, rt, 12h.

Scheme 4. Pomalidomide-linker part[d]

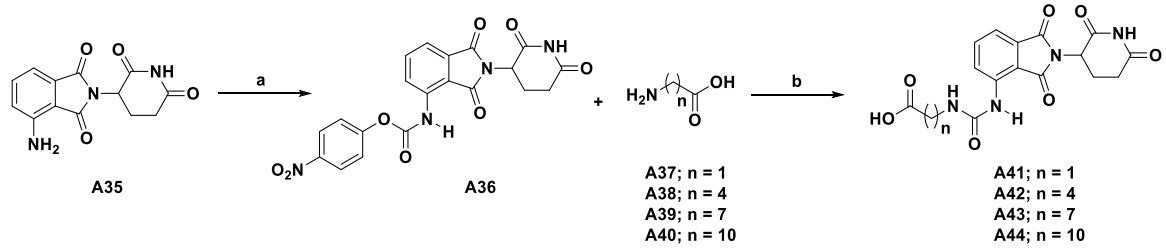

[d](a) 4-nitrophenyl chloroformate, 80°C,4 h, 47%; (b) DMF, rt, 12 h, 47-62%.

Scheme 5. Synthesis of PG-based PROTACs

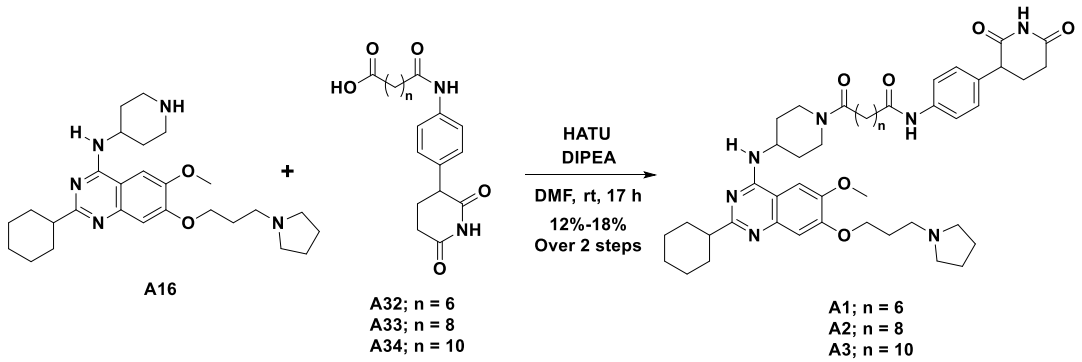

Scheme 6. Synthesis of pomalidomide-based PROTACs

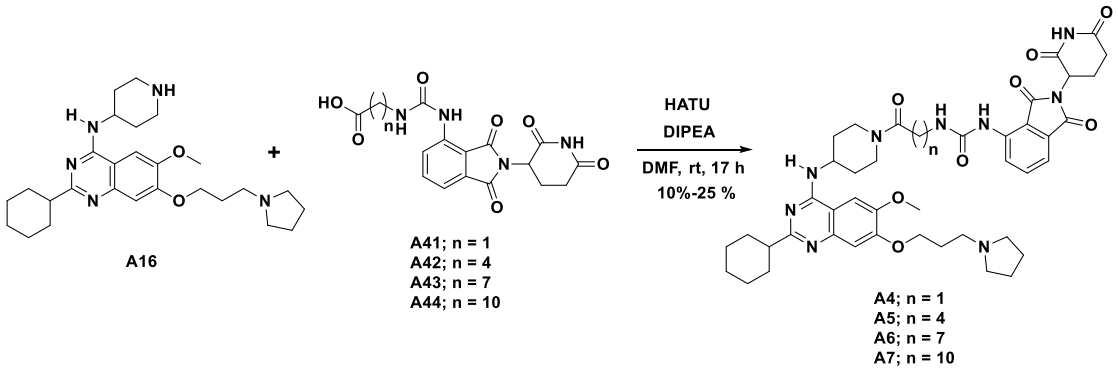

The synthesis of PROTACs **A1**–**A7** is comprehensively outlined in Schemes 1–6. The preparation of the G9a-binding moiety, UNC0638 counterpart **A16**, is depicted in Scheme 1. The synthesis began with commercially available methyl 4-hydroxy-3-methoxybenzoate (**A8**), which was converted to intermediate **A10** in two steps: alkylation with 1-chloro-3-iodopropane followed by nitration. The resulting chloride **A10** underwent nucleophilic substitution with pyrrolidine to produce the nitro derivative **A11**, which was reduced to afford aniline **A12**. Cyclization of **A12** with tetrahydro-2H-pyran-4-carbonitrile yielded the intermediate **A13**, which was subsequently converted to 4-chloroquinazoline **A14**. The chloride in compound **A14** was then displaced with tert-butyl 4-aminopiperidine-1-carboxylate, affording intermediate

A15. The final step involved Boc deprotection, resulting in the desired G9a-binding intermediate **A16**.

The synthesis of the PG intermediate **A22** is shown in Scheme 2. Starting from fluoride **A17**, reaction with methyl 2-cyanoacetate provided compound **A18**. Treatment of **A18** with methyl acrylate in the presence of NMM afforded compound **A19**. Subsequent decarboxylation yielded compound **A20**, which cyclized to form intermediate **A21**. Reduction of **A21** furnished the PG intermediate **A22**.

Scheme 3 represents the linker attachment to PG intermediate **A22**. Dioic acids **A23**–**A25** were first converted into aryl esters **A26**–**A28** through esterification. These aryl esters were conjugated with PG **A22**, yielding intermediates **A29**–**A31**. Hydrolysis of the corresponding esters afforded the linker-bound PG intermediates **A32**–**A34**.

The synthesis of alkyl linker-bound pomalidomide derivatives is outlined in Scheme 4. Pomalidomide **A35** underwent nucleophilic substitution with 4-nitrophenyl chloroformate, resulting in the formation of carbamate intermediate **A36**. Subsequent nucleophilic reactions with the respective amines **A37**–**A40** led to the generation of the linker-conjugated pomalidomide intermediates **A41**–**A44**.

The synthesis of PG-based PROTACs **A1**–**A3** and pomalidomide-based PROTACs **A4–7A** is outlined in Scheme 5 and Scheme 6, respectively. Intermediate **A16** was conjugated with alkyl linker-bound PG intermediates (**A32**–**A34**) and alkyl linker-bound pomalidomide intermediates (**A41**–**A44**) through amide bond formation under optimized coupling conditions. Following purification, the final products, PROTACs **A1**–**A7**, were obtained and prepared for subsequent biological evaluation.

2.3 Biological Evaluation of Class I PROTACs

2.3.1 Degradation Activity of Class I PROTACs

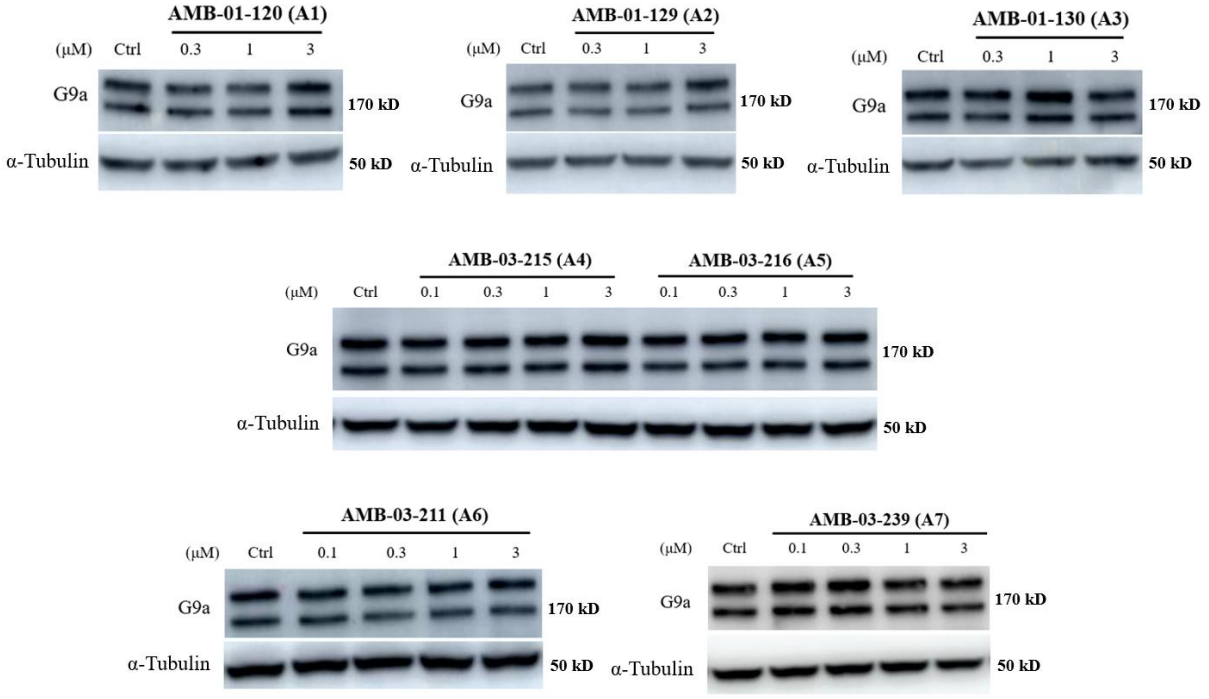

Figure 4. Western blot detection of G9a levels in MCF-7 cells following 24 h treatment with **A1**-**A7**.

After successful synthesis of UNC0638-based PROTACs **A1**-**A7**, their degradation efficacy was evaluated in MCF-7 human breast cancer cells. The western blot analysis was conducted to determine the ability of these PROTACs to induce G9a degradation. MCF-7 cells were treated with each compound at concentrations of 0.3, 1, and 3 μM for 24 hours. As depicted in Figure 4, none of the PROTAC candidates were effective in reducing G9a protein levels under the tested conditions.

2.3.2 Antiproliferative Activity of Class I PROTACs

To further investigate the functional impact of these PROTACs, I assessed their antiproliferative activity using the Alamar Blue assay. This assay measures cell viability and provide insight into the potential cytotoxic effects of the compounds. The results demonstrated

that compound **A2** and **A6** exhibited moderate antiproliferative activity, while compound **A3** and **A7** showed an antiproliferative effect comparable to that of the parent G9a inhibitor UNC0638 (Table 1). The differential activity between the PROTAC candidates highlights the impact of linker composition and overall molecular design on their biological performance. These findings underscore the challenges of achieving targeted protein degradation and suggest that further optimization of the linker architecture, compound stability, or E3 ligase recruitment

Table 1. Effects of the indicated compounds on MCF-7 cell growth after 72 hours of treatment. The dose-response curve was drawn and the IC_{50} value was calculated. The IC_{50} value is the mean ± SD of three experiments.

Compound	n	Cell Viability IC_{50}(μM)
UNC0638	-	3.6 ± 0.52
PG	-	> 30
Pomalidomide	-	> 30
AMB-01-120 (A1)	6	> 30
AMB-01-129 (A2)	8	6.1 ± 0.91
AMB-01-130 (A3)	10	3.1 ± 0.61
AMB-03-215 (A4)	1	> 30
AMB-03-216 (A5)	4	> 30
AMB-03-211 (A6)	7	12.7 ± 1.38
AMB-03-239 (A7)	10	4.3 ± 0.67

efficiency is required to improve PROTAC performance and achieve G9a degradation in cells. Notably, the observed antiproliferative effects of the aforementioned class I PROTAC candidates suggest the potential presence of off-target interactions. These off-target effects may contribute to the observed anticancer activity, independent of G9a degradation.

3. Conclusion

This chapter details the design, synthesis, and initial biological evaluation of class I G9a/GLP-targeting PROTACs. These PROTACs were constructed as bifunctional molecules, employing UNC0638 as the G9a-binding ligand, phenyl glutarimide or pomalidomide as the CRBN-recruiting ligand and a series of alkyl linkers to connect the two functional components. Various alkyl linkers of differing lengths and compositions were explored to strike a balance between structural stability and cellular permeability while maintaining the appropriate proximity between the G9a-binding ligand and the cereblon-recruiting motif. Following successful synthesis, the biological activity of these PROTAC candidates was evaluated in the MCF-7 human breast cancer cell line. Western blot analysis was performed to assess their ability to induce G9a degradation. Surprisingly, despite their rational design, none of the synthesized PROTACs were able to reduce G9a protein levels under the tested conditions. Nevertheless, the antiproliferative effects of the PROTACs were evaluated using the Alamar Blue assay to determine their impact on cell viability. The results demonstrated that certain candidates, particularly compound **A2**, **A3**, **A6** and **A7**, retained notable antiproliferative activity. Compound **A3** and **A7**, in particular, exhibited similar inhibitory effects on cell proliferation as the parent G9a inhibitor UNC0638. These findings highlight the importance of linker optimization and efficient ternary complex formation in achieving targeted protein degradation. Further refinements in PROTAC design, including linker modifications and exploration of alternative E3 ligase ligands, may be required to overcome current limitations and achieve successful G9a degradation in cancer cells. Interestingly, the antiproliferative activity exhibited by the class I PROTAC candidates raises the possibility of off-target effects. Such unintended interactions could account for the observed anticancer properties, even in the absence of G9a degradation.

Chapter 2

Design, Synthesis and Biological Evaluation of Class II G9a/GLP PROTAC Degraders

Abstract

Chapter 2 details the design, synthesis, and biological assessment of class II G9a/GLP PROTACs. These PROTACs were developed by coupling the highly potent and selective norleucine-based G9a/GLP inhibitor RK-701 with various E3 ligase recruiting ligands, connected through alkyl and PEG linkers. From the six synthesized PROTAC candidates, AMB-03-378 (**B4**) emerged as the most effective G9a/GLP degrader.

1. Introduction

Histone methylation plays a pivotal role in controlling chromatin organization and epigenetic gene regulation. G9a/GLP, a histone methyltransferase, catalyzes the mono- and di-methylation of histone H3 at lysine 9 (H3K9) with SAM serving as a cofactor.[19] Aberrant activity of G9a/GLP is associated with conditions such as cancer and neurodegenerative disorders, making it a target for therapeutic intervention.[27-40] Several *in vitro* and *in vivo* studies revealed that inhibiting G9a can reduce neurodegeneration and cognitive impairment, underscoring its potential for treating AD.[41,42] While G9a inhibitors have shown promise,[93] their limited clinical efficacy suggests that enzymatic inhibition alone is insufficient, highlighting the need for alternative approaches.

Proteolysis-targeting chimeras (PROTACs) offer a novel strategy by inducing targeted protein degradation.[88-91] These bifunctional molecules connect the target protein to an E3 ubiquitin ligase, triggering ubiquitination and proteasomal degradation. By eliminating the protein entirely, PROTACs overcome the limitations of traditional inhibitors and hold potential as a next-generation therapeutic approach.

In this chapter, I present the design, synthesis and biological evaluation of G9a/GLP PROTAC degraders based on a recently discovered highly selective Norleucine-based G9a inhibitor RK-701 and several E3 ligase recruiters including cereblon (CRBN) and von Hippel Lindau (VHL). This effort led to the discovery of several active PROTAC degraders targeting G9a and GLP, with AMB-03-378 (**B4**) identified as the most potent degrader. Compound **B4** induced the degradation of G9a/GLP in a dose- and time-dependent manner via the ubiquitin–proteasome system (UPS). It also effectively reduced H3K9me2 levels in MCF-7 cells and lowered HP1γ expression, highlighting the scaffolding role of G9a. Moreover, compound **B4** demonstrated a significant ability to promote neurite outgrowth in the mouse neural crest-

derived N2a cell line. However, despite effectively degrading G9a/GLP, it did not exhibit antiproliferative effects in MCF-7 breast cancer cells. This finding was corroborated by siRNA knockdown experiments, where G9a downregulation did not inhibit cancer cell growth, suggesting the need to re-evaluate the role of G9a/GLP in breast cancer development.

2. Results and Discussion

2.1 Design of Class II PROTACs

As discussed earlier in the general introduction section, UNC compounds are associated with toxicities,[64,72] which may arise from the off-target effects of these inhibitors. Consequently, after failing to achieve G9a degradation with the class I PROTACs, as described in Chapter 1, I prioritized this factor in selecting a suitable G9a-binding ligand for the construction of PROTACs. To address this, the cytotoxicity of UNC0642,[67] a well-known and widely used quinazoline-based inhibitor, was compared with that of RK-701,[71] a recently developed inhibitor that exhibits high selectivity against DNA and histone methyltransferases (DNMTs and HMTs) with an excellent *in vivo* efficacy.[72] As a result of evaluation of their cytotoxic effects on normal mouse embryonic stem cells (mESCs), UNC0642 exhibited high cytotoxicity, but not RK-701 (Figure 1a), despite RK-701 being more effective at reducing H3K9me2 levels

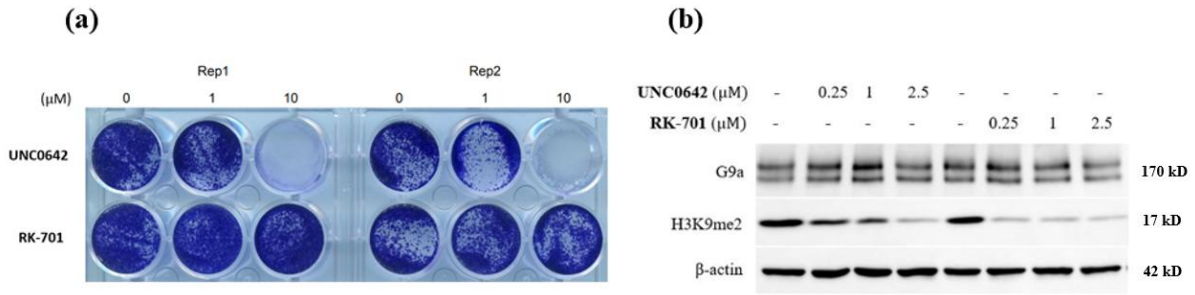

Figure 1. (a) Cell growth following 4 days treatment with UNC0642 and RK-701 at indicated concentrations in mESCs. (b) Western blot detection of G9a and H3K9me2 levels in mESCs treated with the test compounds at indicated concentrations for 72 h.

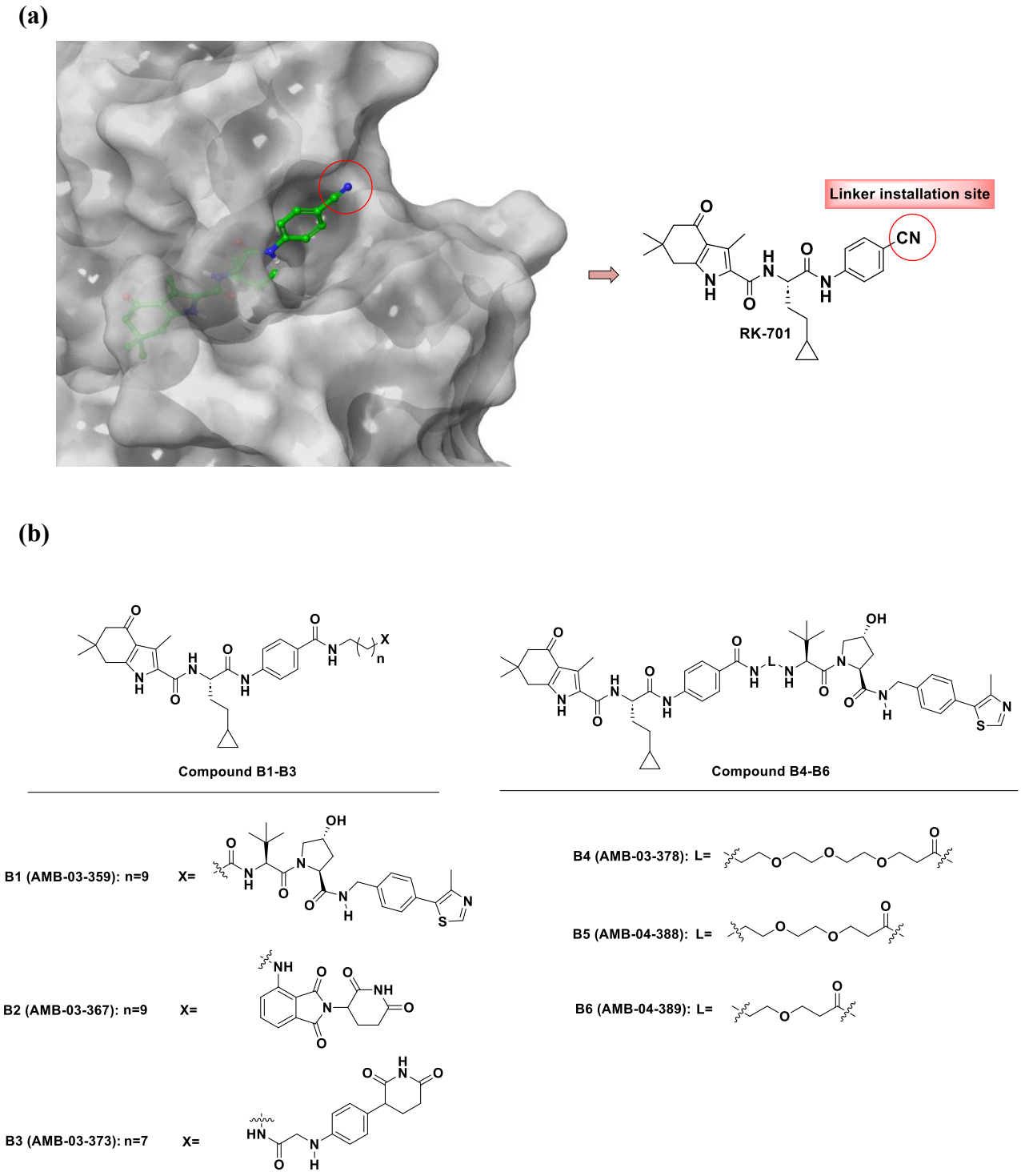

Figure 2. Rational design of G9a/GLP PROTAC degraders. (a) Left, the X-ray cocrystal structure of RK701 bound to G9a (PDB: 7X73), and right, the chemical structure of RK-701 showing the linker attachment site. (b) Chemical structures of the synthesized G9a/GLP PROTAC candidates.

than that of UNC0642 (Figure 1b). Hence, I selected RK-701 as the G9a/GLP binding ligand to generate G9a/GLP PROTAC degraders. The X-ray co-crystal structure analysis of RK-701 bound to G9a revealed that the cyano group on the phenyl ring is exposed to the solvent (red circle in Figure 2a), making it suitable for linker installation. Hence, I replaced the cyano group with a carboxylic acid to attach the linkers. Using this modified intermediate, we then developed a series of G9a/GLP PROTAC candidates (**B1**-**B6**) (Figure 2b), linking it to different alkyl and polyethylene glycol (PEG) chains which were conjugated with VHL-1 and CRBN ligands.

2.2 Synthesis of Class II PROTACs

Scheme 1. Synthesis of E3 ligase counterparts[a]

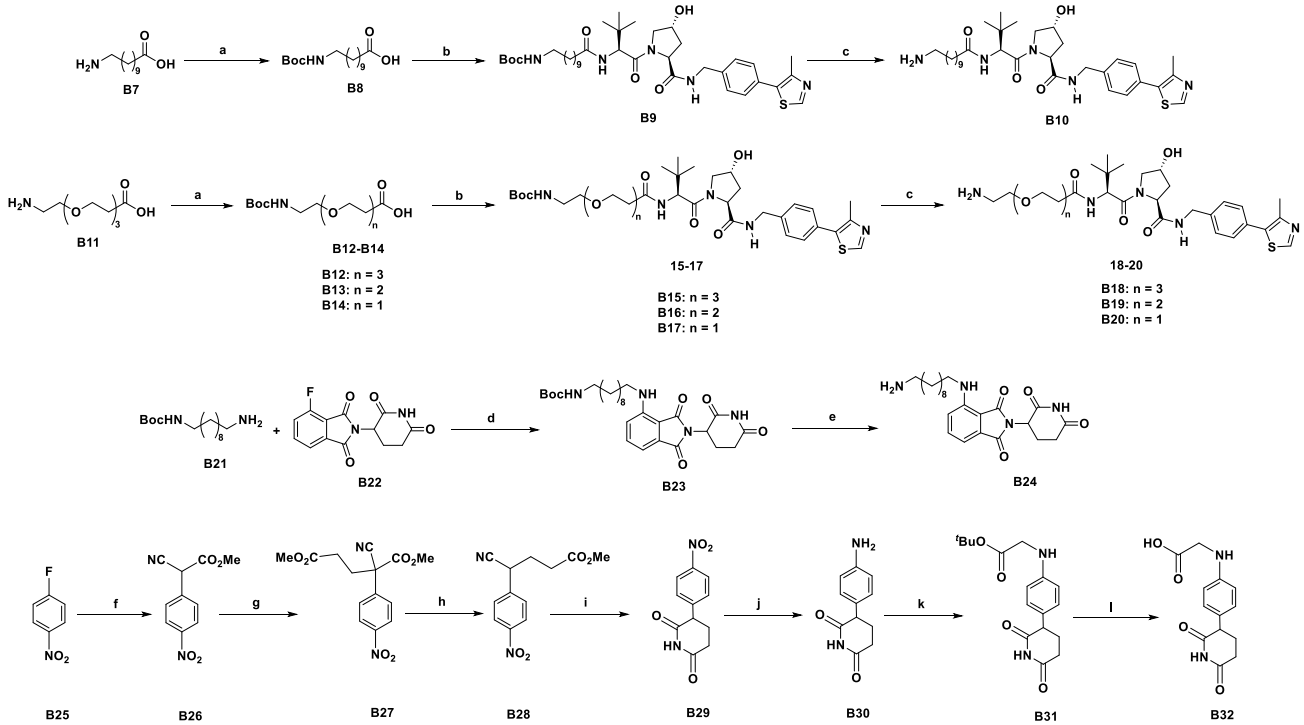

[a]Reaction and conditions: (a) di-*tert*-butyl dicarbonate, NaOH (aq), THF, rt, 15 h, 65-85%; (b) (2*S*,4*R*)-1-((S)-2-amino-3,3-dimethylbutanoyl)-4-hydroxy-*N*-(4-(4-methylthiazol-5-yl)benzyl)pyrrolidine-2-carboxamide hydrochloride (VHL-1), EDCI-HCl, HOBt-H_2O, DIPEA, DMF, rt, 18 h, 62-68% ; (c) TFA, DCM, rt, 2 h, quantitative; (d) DIPEA, DMF, rt, 14 h, 57%; (e) TFA, DCM, rt, 1 h quantitative; (f) Methyl 2-cyanoacetate,

K_2CO_3, DMF, 120 ºC, 2 h, (g) Methyl acrylate, NMM, THF, 55 ºC, 2 h; (h) Na2CO3, THF/H2O (1:2), 90 ºC, 3 h; (i) conc. H_2SO_4, AcOH, 120 ºC, 2 h; (j) Fe-dust, NH_4OAc, reflux, 36% over 5 steps; (k) *tert*-butyl 2-bromoacetate, DIPEA, acetonitrile, 60 °C, 2 h, 42%; (l) TFA, DCM, rt, 5 h, quantitative.

Scheme 2: Synthesis of PROTAC candidates **B1**-**B6**[b]

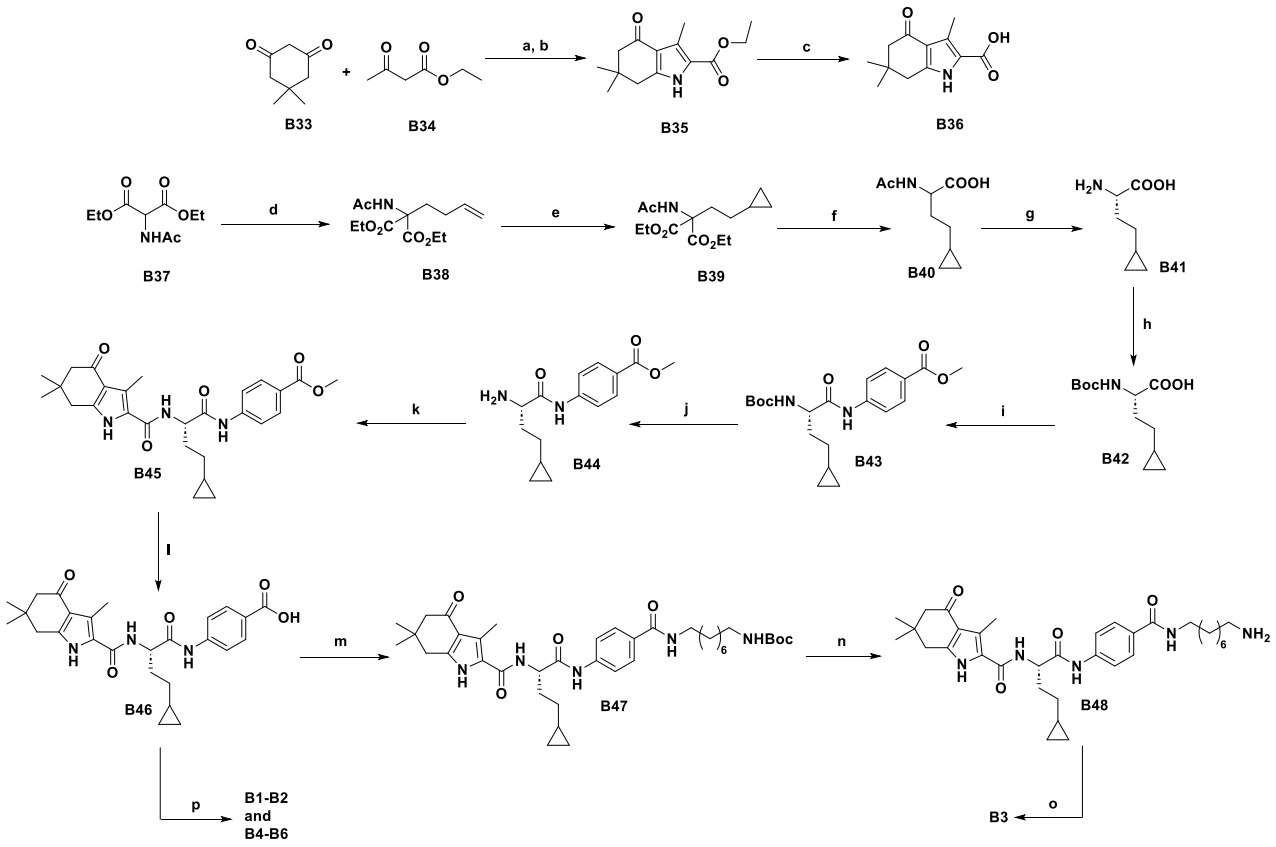

[b]Reaction and conditions: (a) $NaNO_2$, H_2O, AcOH, < 7°C, 0.5 h, rt : 3h, (b) AcONa, Zn, AcOH, reflux, 14 h, 45%; (c) NaOH, MeOH, reflux, 24 h, 2M HCl, 97%; (d) 4-bromobut-1-ene, NaH, DMF, 90°C, 4 h, 75%; (e) diiodomethane, diethylzinc, DCM, 0°C-rt, 24 h, 78%; (f) NaOH, EtOH (aq.), reflux, 16 h, 2M HCl, 87%; (g) Aspergillus genus, NaOH (aq), 37 °C, 12 h; (h) di-*tert*-butyl dicarbonate, Na_2CO_3,THF/H_2O (1:1), 24 h, 1M HCl, 40% over two steps; (i) methyl 4-aminobenzoate, HATU, DIPEA, DMF, rt, 18 h, 48%; (j) TFA, DCM, rt, 2 h; (k) **B36**, EDCI-HCl, HOBt-H_2O, DIPEA, DMF, rt, 18 h, 48% over 2 steps; (l) NaOH, MeOH, rt, 24 h, 2M HCl, 78%; (m) *tert*-butyl (8-aminooctyl)carbamate, EDCI-HCl, HOBt.H_2O, DIPEA, DMF, rt, 18 h, 43%; (n) TFA, DCM, rt, 3 h, quantitative. (o) **B32**, EDCI-HCl, HOBt-H_2O, DIPEA, DMF, rt ,18 h, 26% over 4 steps; (p) **B10**, **B24** or, **B18**-**B20**, EDCI-HCl, HOBt-H_2O, DIPEA, DMF, rt, 18 h, 34-44% over 2 steps.

Figure 2 presents the compounds investigated in this study, while Schemes 1 and 2 depict the synthetic pathways for compounds **B1**-**B6**. Scheme 1 outlines the preparation of the E3 ligase counterparts, specifically compounds **B10**, **B18**-**B20**, and **B32**. Starting with Boc-protected intermediates **B7** and **B11**, compounds **B8** and **B12** were formed. Intermediates **B8** and **B12-B14** were then underwent coupling with the commercially available VHL-1 ligand. Following Boc deprotection, compounds **B10** and **B18-B20** were obtained. For pomalidomide-based compound **B24**, the nucleophilic substitution of fluoride **B22** with amine **B21**, followed by Boc deprotection, completed its synthesis. The phenyl-glutarimide-based intermediate **B32** was synthesized as per previously established methods.[24] Further, fluoride **B25** reacted with methyl 2-cyanoacetate to yield compound **B26**, which, after treatment with methyl acrylate and NMM, formed compound **B27**. Decarboxylation of **B27** led to compound **B28**, which was then cyclized to yield compound **B29**, and subsequently reduced to compound **B30**. Lastly, the nucleophilic substitution of *tert*-butyl 2-bromoacetate with **B30**, followed by TFA treatment, afforded compound **B32**. Scheme 2 shows the synthesis of PROTAC candidates **B1**-**B6**. The synthesis began with the Knorr pyrrole reaction using compound **B33**, followed by ester hydrolysis to yield intermediate **B36**. This was followed by a Michael addition using intermediate **B37**, resulting in the formation of compound **B38**. Next, a Simmons-Smith reaction was performed on **B38**, followed by a decarboxylation, leading to intermediate **B40**. Enzymatic reaction then produced the *s*-isomer **B41**. Subsequently, Boc protection was applied, and coupling with methyl 4-aminobenzoate gave intermediate **B43**. After Boc deprotection, intermediate **B44** was coupled with **B36**, yielding **B45**. Ester hydrolysis of **B45**, followed by conjugation with intermediates **B10**, **B24**, or **B18-B20**, resulted in the PROTAC candidates **B1**-**B2** and **B4**-**B6**. On a separate path, coupling *tert*-butyl (8-aminooctyl)carbamate with **B46**, followed by Boc deprotection, produced intermediate **B48**, which was then coupled with acid **B32** to afford PROTAC candidate **B3**.

2.3 Biological Evaluation of Class II PROACs

2.3.1 Assessing the G9a/GLP Degradation Efficacy of the Class II PROTACs

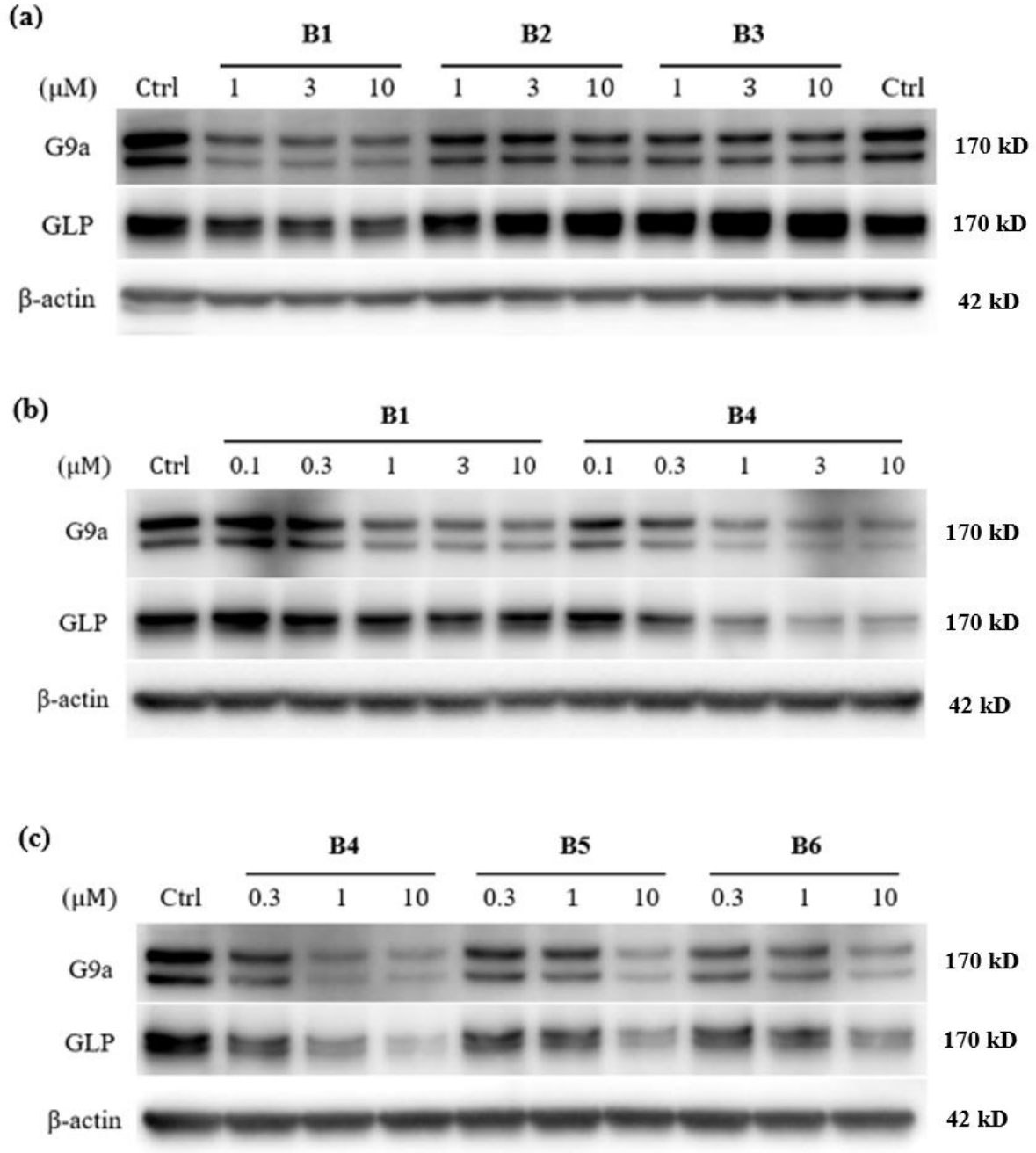

Figure 3. Western blot analysis of G9a and GLP levels in MCF-7 cells following 24 h treatment with various synthesized PROTAC candidates at the indicated concentrations. (a) Comparison of alkyl linker-based PROTACs **B1**–**B3**, each containing different E3 ligase ligands. (b) Comparison of degradation efficiency between compound **B1** and compound **B4**. (c) Structure-activity relationship (SAR) analysis of PEG linker-based PROTACs **B4**–**B6**.

We initially assessed the potential of G9a/GLP PROTAC candidates **B1**-**B3** in the MCF-7 breast cancer cell line by performing a western blotting analysis. The cells were treated with each degrader at concentrations of 1, 3 and 10 μM for 24 hours. As shown in Figure 3a the VHL-1 ligand-based compound **B1** successfully induced degradation of G9a and GLP, while the pomalidomide-based compound **B2** and the phenyl glutarimide-based compound **B3** did not produce significant degradation effects. However, compound **B1** showed very weak G9a inhibitory activity *in vitro* with an IC_{50} of 8.4 μM (Figure 4). The high ClogP value of 9.01 suggests that compound **B1** may have solubility issues. To enhance solubility, I replaced the alkyl linker with a PEG linker, leading to the synthesis of compound **B4**. As expected, compound **B4** demonstrated a significantly stronger degradation effect compared to compound **B1** (Figure 3b) with a ClogP value of 5.67. Interestingly, compound **B4** exhibited a 44-fold increase in inhibitory activity *in vitro*, achieving an IC_{50} of 190 nM (Figure 4). In my efforts to identify the most effective degrader, I conducted a comprehensive structure-activity relationship (SAR) study. This involved systematically varying the lengths of the PEG linker to assess how these changes influenced the compound's degradation potency. I synthesized two new compounds, compound **B5** and compound **B6**, each featuring progressively shorter linker lengths. As evident from the western blot analysis (Figure 3c) compound **B4** produced a more pronounced degradation effect than both compound **B5** and compound **B6**. This observation underscores the critical influence of linker length on the degrader's efficacy of G9a and GLP. Specifically, the data suggest that a longer linker, as seen in compound **B4**, is essential for achieving best degradation activity.

2.3.2 Dose- and Time-Dependent Degradation of G9a/GLP by PROTAC B4

Next, we treated MCF-7 breast cancer cells with varying concentrations of compound **B4** over a 24-hour period to evaluate its ability to degrade G9a and GLP. As shown in Figure 4a, compound **B4** effectively reduced the levels of G9a and GLP in a dose-dependent manner,

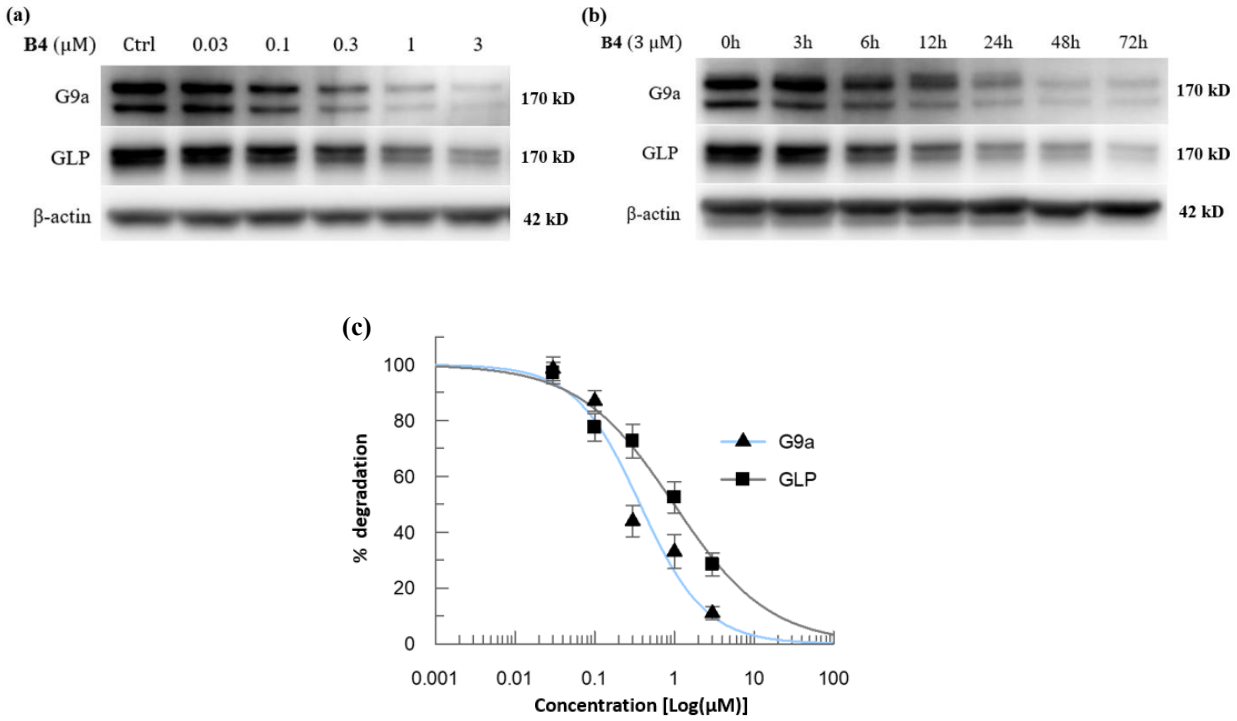

Compound	G9a DC_{50} (nM)	GLP DC_{50} (nM)	G9a D_{max} (%)	GLP D_{max} (%)
B4 (AMB-03-378)	336.2 ± 0.1	988.5 ± 0.2	89	71

Figure 4. Western blot detection of G9a and GLP levels in MCF-7 cells. (a) Following 24 h treatment with **B4** at indicated concentrations. (b) Following treatment with 3 μM of **B4** at indicated time points. (c) DC_{50} value and D_{max} determination. The dose-response curve was drawn and the DC_{50} value was calculated based on values of G9a/GLP ratio determined by optical density measurement of the blots. The DC_{50} value is the mean ± SD of three experiments.

indicating its potency in downregulating these proteins. To further investigate the kinetics of this degradation, I conducted a time course study to observe the effects of compound **B4** over a range of time points. As illustrated in Figure 4b, compound **B4** progressively induced the degradation of both G9a and GLP, with significant reductions observed as early as 6 hours post-treatment and sustained activity observed at later time points. These results demonstrate that compound **B4** exhibits robust activity in inducing the degradation of G9a and GLP in both a

concentration- and time-dependent manner. The half-maximal degradation concentrations (DC_{50}) were determined to be 336 nM for G9a and 988 nM for GLP (Figure 4c). Additionally, the maximum degradation (D_{max}) achieved was 89% for G9a and 71% for GLP respectively.

2.3.3 Mechanistic Analysis

To gain a deeper understanding of compound **B4**-induced G9a and GLP degradation, we performed a mechanistic analysis. We investigated the effects of the original G9a/GLP inhibitor RK-701, the VHL-1 ligand, and a combination of both RK-701 and VHL-1 ligand on the levels of G9a and GLP. As shown in Figure 6a, compound **B4** significantly reduced G9a and GLP levels in MCF-7 breast cancer cells, while neither RK-701 nor the VHL-1 ligand had any effect. Furthermore, the combination of RK-701 and the VHL-1 ligand did not alter G9a or GLP levels (Figure 5a). These findings suggest that the conjugation of the G9a/GLP inhibitor with the E3 ligase ligand is critical for the reduction of G9a and GLP levels induced by compound **B4**. Next, we co-treated MCF-7 cells with compound **B4** and the proteasome inhibitor bortezomib[94]. As anticipated, bortezomib effectively blocked the reduction of G9a and GLP induced by compound **B4** (Figure 5b). This finding suggests that compound **B4** induced the degradation of G9a and GLP through the ubiquitin-proteasome system (UPS). Next, we investigated whether G9a/GLP reduction induced by compound **B4** is affected by the treatment with RK-701 or VHL-1 ligand. As shown in Figure 5c the reduction of G9a/GLP upon treatment of compound **B4** was inhibited in the presence of RK-701 or VHL-1 ligand, which indicates that compound **B4** competes with RK-701 and VHL-1 ligand. Notably, 20 μM of RK-701 and 200 μM of VHL-1 ligand were required to completely inhibit the compound 4-induced G9a/GLP degradation (Figure 5c), suggesting that compound **B4** is a highly potent PROTAC degrader. Therefore, G9a/GLP degradation by compound **B4** is dependent on its binding to both G9a/GLP and E3 ligase. Overall, the mechanistic study suggests that compound **B4** works as a typical PROTAC degrader.

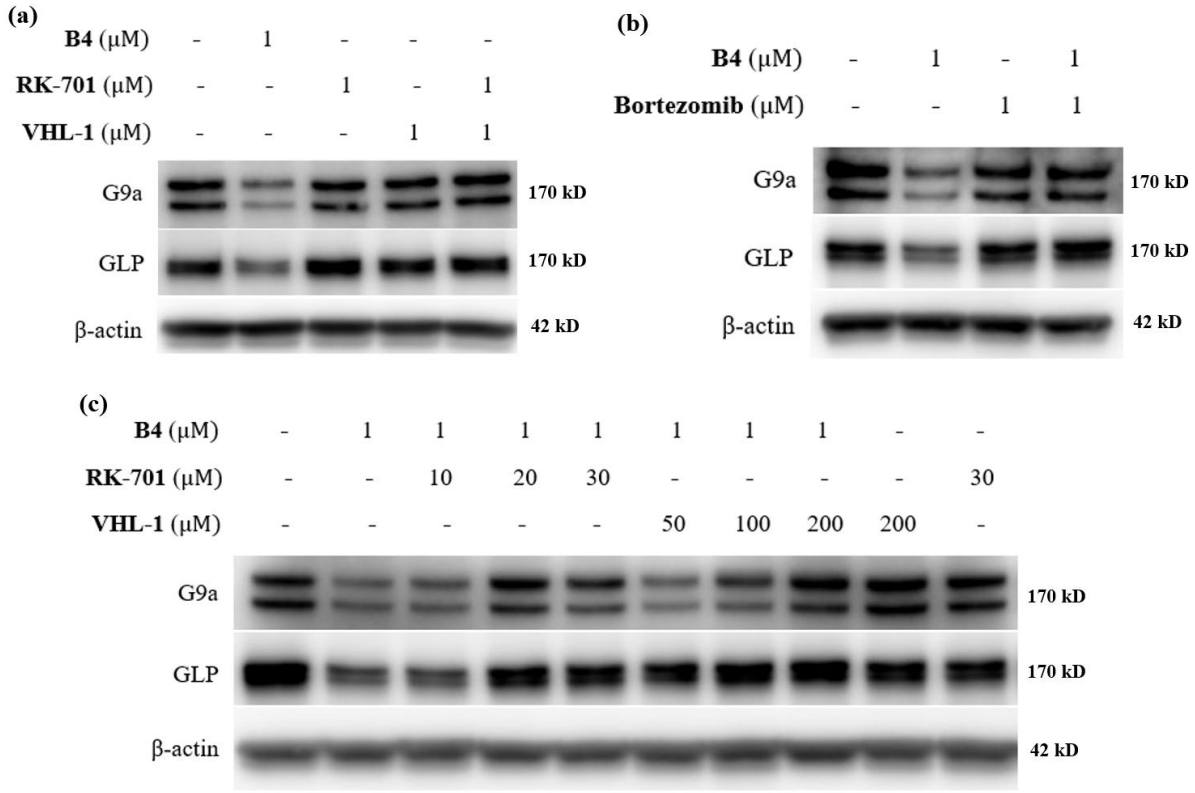

Figure 5. Western blot detection of G9a and GLP levels in MCF-7 cells treated with the test compounds. (a) 24 h treatment with compound **B4**, RK-701, VHL-1 ligand and co-treatment with RK-701 and VHL-1 ligand. (b) 22.5 h treatment with compound **B4** in the presence of a proteasome inhibitor bortezomib. The cells were pre-treated with bortezomib for 1.5 h before addition of **B4**. (c) 24 h treatment with compound **B4** in the presence of RK-701 and VHL-1 ligand.

2.3.4 *In vitro* and *in cell* G9a Inhibitory Activity of the Class II PROTACs

Next, I evaluated the *in vitro* G9a inhibitory activity of class I PROTACs using the AlphaScreen assay, which revealed that compound **B4** exhibited ten-fold lower potency compared to the parent inhibitor RK-701 (Figure 6a-c). Subsequently, I assessed the effects of compounds **B1** and **B4** on H3K9me2 levels in MCF-7 cells. As shown in Figure 6d, a significant reduction in H3K9me2 levels was observed after three days of treatment. This reduction aligns with the degradation of G9a and GLP, demonstrating a strong correlation between enzyme degradation and decreased H3K9me2 levels, comparable to the effect of RK-

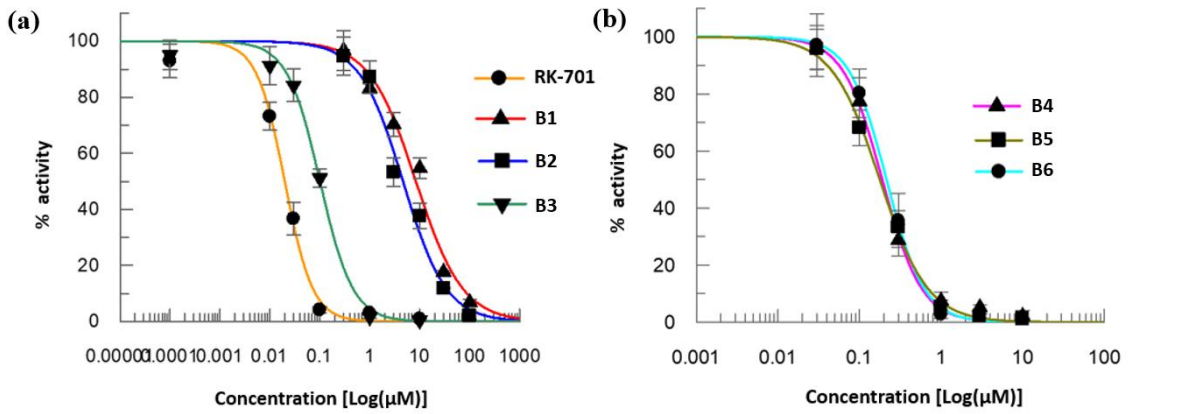

(c)

Compound	G9a IC_{50}
RK-701	19.7 ± 1.8 nM
B1	8.4 ± 1.4 μM
B2	4.7 ± 0.7 μM
B3	101.4 ± 13.3 nM
B4	190.4 ± 11.9 nM
B5	175.9 ± 9.7 nM
B6	214.7 ± 6.0 nM

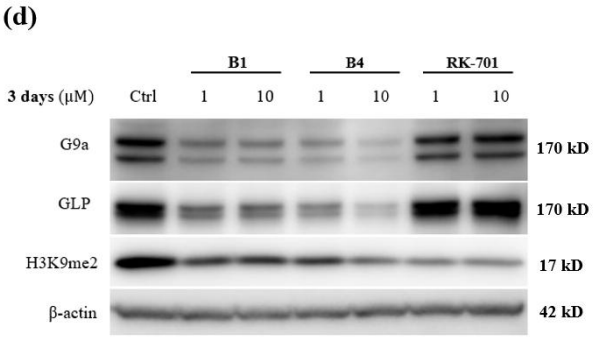

Figure 6. (a-c) *In vitro* G9a inhibition by RK-701 and compounds **B1**-**B6**. The dose-response curve was drawn and the IC_{50} value was calculated. The IC_{50} value is the mean ± SD of three experiments. (d) Western blot detection of G9a, GLP and H3K9me2 levels in MCF-7 cells treated with the test compounds at indicated concentrations for 72 h.

701. Moreover, the alkyl linker-based PROTAC 1 demonstrated weaker inhibition of H3K9me2 compared to PROTAC **B4**, underscoring the enhanced efficacy of compound **B4** in modulating histone methylation via G9a/GLP degradation. Collectively, these findings suggest that compound **B4** effectively inhibits the catalytic activity of G9a and GLP.

2.3.5 Evaluating the Scaffolding Function of G9a/GLP by PROTAC B4

As mentioned earlier, G9a forms a complex with GLP. and this G9a-GLP complex is reported to bind with heterochromatin protein 1 (HP1) [specifically, it interacts with the γ isoform of HP1, one of the three known isoforms], which recognizes the methylated H3K9 and associated with the silencing of heterochromatin (Figure 7a).[95] We hypothesize that the G9a

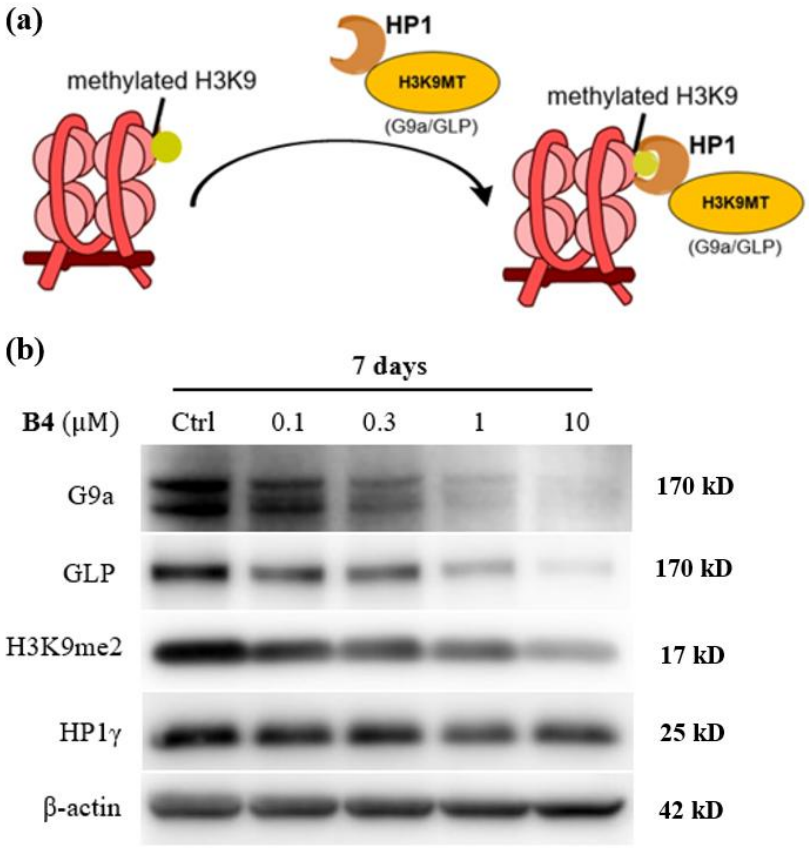

Figure 7. (a) Scaffolding function of G9a. H3K9MT denotes H3K9 methyl transferase. (b) Western blot detection of G9a, GLP, H3K9me2 and HP1γ levels in MCF-7 cells treated with compound **B4** at indicated concentrations for 7 days.

and GLP degradation could potentially disrupt their interaction with HP1γ. To investigate this, we assessed the impact of compound **B4** on HP1γ expression levels. As shown in Figure 7b, treatment with compound **B4** for 7 days resulted in a dose-dependent reduction of HP1γ levels in MCF-7 cells. Therefore, compound **B4** not only inhibits the catalytic activity of G9a/GLP but also disrupts their ability to interact with other proteins. Additionally, with extended treatment using compound **B4** over a 7-day period, the G9a protein band was completely eliminated. Accordingly, the H3K9me2 levels were also found to be reduced with great extent. These findings also highlight the stability of PROTAC **B4** in the cellular environment, as it maintains its degradation efficacy even after prolonged exposure, supporting its potential for sustained therapeutic action in long-term treatments.

2.3.6 PROTAC B4 Exhibited Neurite Outgrowth Promoting Activity

Studies have shown that inhibiting G9a can significantly improve cognitive function.[41,42] This inhibition is associated with reduced DNA methylation, increased hydroxymethylation, and lower levels of H3K9me2 in the hippocampus. Additionally, it helps prevent the accumulation of β-amyloid plaques, while also enhancing synaptic plasticity and boosting neuronal health markers. Based on these findings, we examined the effect of compound **B4** on N2a cell differentiation, using Vorinostat as a positive control. As shown in Figure 8a-b, PROTAC **B4** induced neurite outgrowth more effectively than the parent inhibitor, RK-701. This suggests that disrupting G9a interactions with other proteins may also play a key role in targeting neurological disorders.

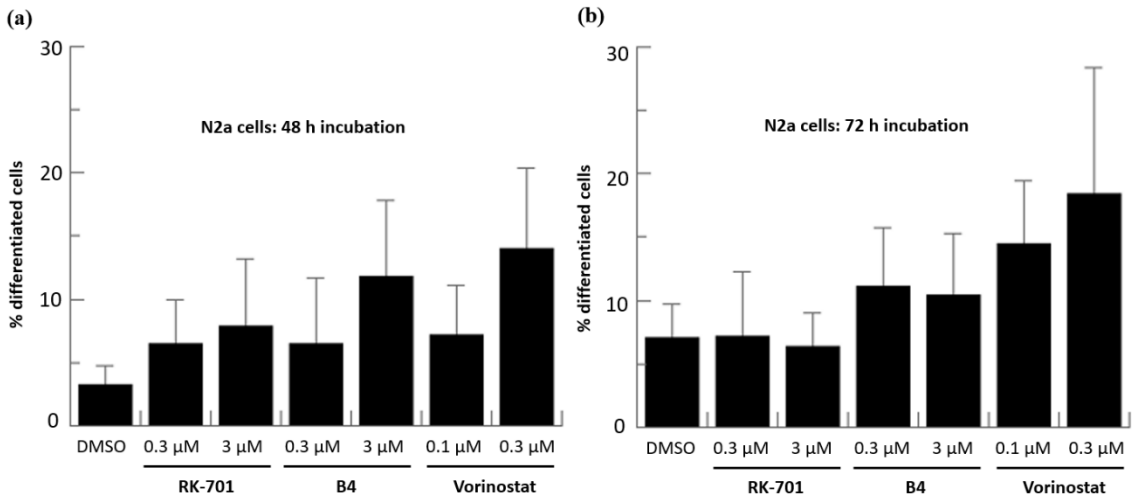

Figure 8. Effect of RK-701, **B4** and Vorinostat on N2a differentiation after treatment for 48 h (a) and 72 h (b) respectively with indicated concentrations. The results shown are the mean values ± SD from three experiments.

2.3.7 Effect of Compound B4 on the Growth and Migration of MCF-7 Cells

Despite its strong ability to degrade G9a and GLP, compound **B4** failed to inhibit the growth of MCF-7 breast cancer cells, as demonstrated in Figure 9c. To validate this finding, we performed siRNA-mediated knockdown of G9a in MCF-7 cells to assess whether reducing G9a expression alone could impact cell proliferation. Similar to **B4**, siRNA-mediated down-

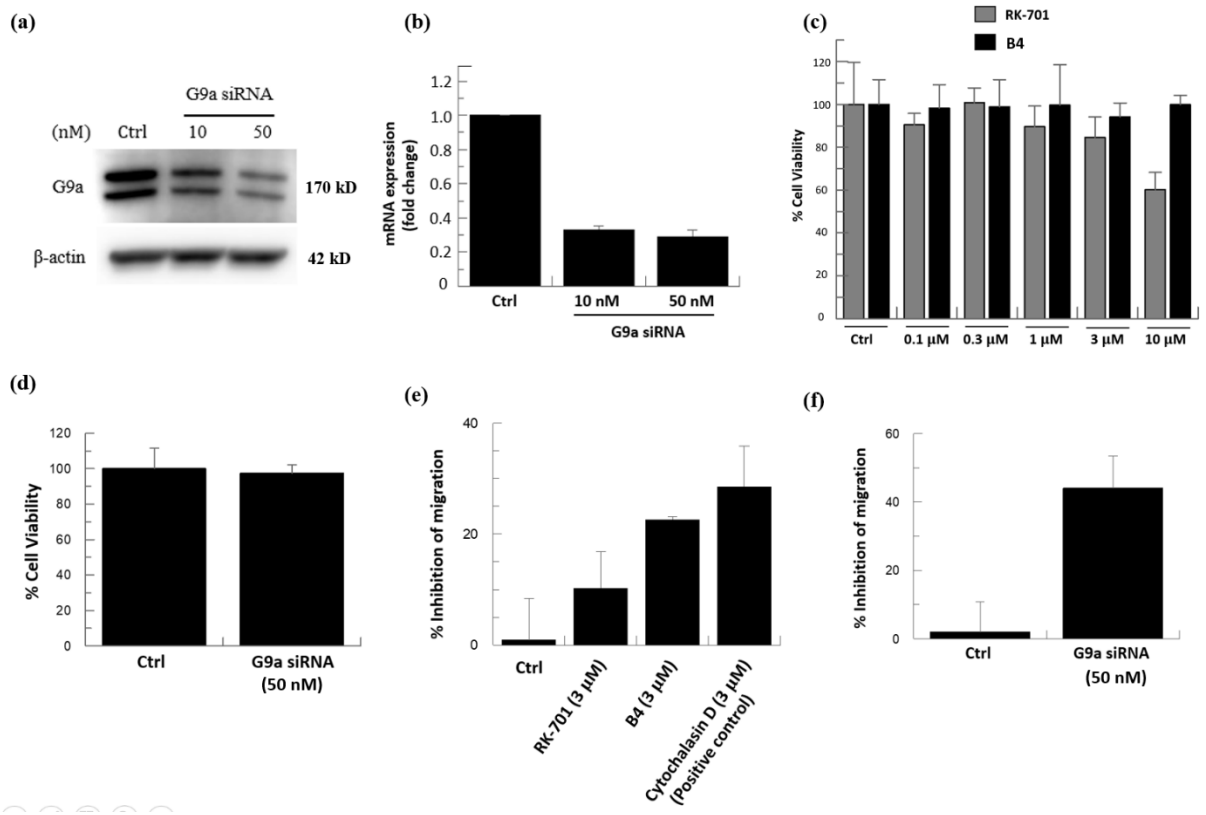

Figure 9. (a) Western blot detection of G9a levels after 36 h treatment with siRNA at indicated concentrations. (b) qPCR determination of mRNA expression in MCF-7 cells after 36 h treatment with siRNA at indicated concentrations. Results shown are the mean values ± SD of two experiments. (c, d) Effects of RK-701 and compound **B4** (AMB-03-378) (c) and G9a siRNA (d) on MCF-7 cell growth after 72 hours of treatment. Results shown are the mean values ± SD of three experiments. (e, f) Quantification of MCF-7 cell migration after treatment with RK-701, compound **B4**, and cytochalasin D (e) or G9a siRNA (f) at the indicated concentrations for 24 hours. Results shown are the mean values ± SD of two experiments.

regulation of G9a (Figure 9a and 9b) did not result in a significant reduction in cancer cell growth (Figure 9d), aligning with our observations from the treatment with compound **B4**. These results suggest that G9a/GLP activity may not play a critical role in regulating the proliferation of MCF-7 breast cancer cells. This raises important questions about the previously assumed role of G9a/GLP in breast cancer development and progression. The lack of an antiproliferative effect, even with effective G9a/GLP degradation or knockdown, suggests that

these proteins may have limited or context-dependent contributions to breast cancer cell survival. Consequently, further studies are needed to thoroughly investigate the function of G9a/GLP in breast cancer biology. Previous studies have demonstrated that downregulation of G9a through siRNA or shRNA knockdown can inhibit the migration of MCF-7 breast cancer cells.[96,97] To build on these findings, we examined the effect of compound **B4** on the migratory behaviour of MCF-7 cells and compared it to the impact of siRNA-mediated G9a knockdown. As shown in Figures 9e-f, both the degradation of G9a/GLP induced by compound **B4** and the siRNA-mediated knockdown of G9a significantly reduced MCF-7 cell migration. These findings indicate that compound **B4** inhibits breast cancer cell migration by promoting G9a/GLP degradation.

3. Conclusion

This chapter presents the rational design and discovery of PROTAC **B4** (AMB-03-378), a highly effective degrader of G9a/GLP, derived from the selective inhibitor RK-701. PROTAC **B4** demonstrates potent activity in degrading G9a and GLP in a dose- and time-dependent manner through the ubiquitin-proteasome system (UPS), significantly reducing H3K9me2 levels in cells. In addition to its impact on histone modification, PROTAC **B4** also lowers the expression of HP1γ, further emphasizing the scaffolding role of G9a/GLP in maintaining chromatin structure and regulating gene expression. Despite its impressive degradation activity, PROTAC **B4** did not affect the proliferation of MCF-7 breast cancer cells, which is particularly intriguing given the well-established role of G9a/GLP in various cancers, including breast cancer. This finding was further supported by siRNA knockdown experiments, where G9a downregulation did not inhibit cancer cell growth, suggesting the need to re-evaluate the role of G9a/GLP in breast cancer development. This unexpected result raises important questions about the previously assumed involvement of G9a/GLP in cancer cell proliferation, suggesting that their functions in breast cancer progression might be more complex or context-dependent than previously thought. Although compound **B4** inhibits the migration of MCF-7 breast cancer cells, siRNA-mediated knockdown of G9a exhibits a stronger effect in reducing migratory activity, highlighting the greater significance of gene knockdown over protein knockdown in migration inhibition. Given these observations, PROTAC **B4** holds the potential as a valuable tool for investigating the multifaceted role of G9a/GLP in breast cancer biology. Additionally, PROTAC **B4**'s ability to stimulate neurite outgrowth in N2a cells points to its possible utility in exploring G9a's involvement in neurological disorders.

Experimental Section

1. Chemistry

General. Proton (^{1}H) and carbon (^{13}C) nuclear magnetic resonance spectra were recorded using a JEOL JNM-LA500, JEOL JNM-A500, JEOL ECA-600 or Bruker AVANCE III700 spectrometer, with the solvent specified for each case. Chemical shifts (δ) are presented in parts per million relative to the internal reference of tetramethylsilane. The format of chemical shift was reported as follows: chemical shift, multiplicity (s = singlet, d =doublet, t = triplet, q = quartet, m = multiplet), coupling constant (J values in Hz), and integration. Mass spectrometry was performed using a Bruker HCTplus mass spectrometer equipped with electrospray ionization (ESI). High-performance liquid chromatography (HPLC) was conducted with a Cosmosil 5C18-AR-II column (150 mm × φ4.6 mm), a Hitachi L-6050 intelligent pump, and a Hitachi L-4000 UV detector. The samples were dissolved in MeCN, and the elution process involved a linear gradient of Solvent A (water containing 0.1% trifluoroacetic acid (TFA)) and Solvent B (MeCN containing 0.1% TFA) as follows: 0 minutes (10% B), 20 minutes (90% B), 30 minutes (90% B), and 40 minutes (10% B). Detection occurred at 254 nm. All biologically tested compounds exhibited greater than 95% purity as confirmed by HPLC analysis. Reagents and solvents, obtained from Aldrich, Merck, Nacalai Tesque, Tokyo Kasei Kogyo, Wako Pure Chemical Industries, Kishida Kagaku, and Kanto Kagaku, were used without further purification. Flash column chromatography was carried out with silica gel from Merck or Toyota Silica Gel.

Methyl 4-(3-chloropropoxy)-5-methoxy-2-nitrobenzoate (A10). To a suspension of methyl 3-methoxy-4-hydroxy benzoate, **A8** (10.9 g, 60 mmol) and K_2CO_3 (20.7 g, 150 mmol) in acetonitrile (120 mL), 1-chloro-3-iodopropane (25.0 g, 122 mmol) was added and the reaction mixture was heated at reflux for 2 h. The solid material was filtered and washed with ethyl acetate (100 mL). The filtrate was concentrated under reduced pressure, the residue was then

dissolved in acetic anhydride (120 mL) and 69 wt% nitric acid (15.4 mL, 0.24 mol) was added slowly at 0 °C. The reaction mixture was stirred overnight at room temperature, poured into ice water and extracted with ethyl acetate (3 x 60 mL). The combined organic phases were collected, washed with saturated aq $NaHCO_3$, brine, and dried over Na_2SO_4. The solvent was removed under reduced pressure to give a brown oil which was purified by flash column chromatography on silica gel (0%-30% ethyl acetate/hexane) to afford the title compound **A10** as a yellow solid (75% over two steps).1H-NMR (400 MHz, $CDCl_3$) δ 7.49 (s, 1H), 7.08 (s, 1H), 4.25 (t, J = 6.0 Hz, 2H), 3.97 (s, 3H), 3.90 (d, J = 5.5 Hz, 3H), 3.78 (t, J = 6.2 Hz, 2H), 2.36-2.30 (m, 2H).

Methyl 5-methoxy-2-nitro-4-(3-(pyrrolidin-1-yl)propoxy)benzoate (A11). A suspension of compound **A10** (7.0 g, 22.9 mmol), NaI (6.8 g, 45 mmol) and tetrabutylammonium iodide (0.37 g, 1.0 mmol) in acetonitrile (60 mL) was heated at reflux for 15 min. Pyrrolidine (5.8 mL, 70 mmol) and K_2CO_3 (8.2 g, 60 mmol) were then added and this mixture was stirred for 3 h at reflux. The solid material was filtered and washed with ethyl acetate (50 mL). The filtrate was concentrated and purified column chromatography on silica gel (0%-10% MeOH (1% NH_3) / DCM) to afford the title compound **A11** as a yellow oil (81% yield).1H-NMR (400 MHz, $CDCl_3$) δ 7.52 (s, 1H), 7.07 (s, 1H), 4.19 (t, J = 6.6 Hz, 2H), 3.96 (s, 3H), 3.91 (s, 3H), 2.65 (t, J = 7.3 Hz, 2H), 2.56-2.53 (m, 4H), 2.14-2.07 (m, 2H), 1.84-1.76 (m, 4H).

***Methyl 2-amino-5-methoxy-4-(3-(pyrrolidin-1-yl)propoxy)benzoate (A12*).** A mixture of compound **A11** (6.3 g, 18.62 mmol), iron dust (4.2 g, 75 mmol) and ammonium acetate (8.7 g, 113 mmol) in ethyl acetate : water (70 mL : 30 mL) was stirred overnight at reflux. The resulting mixture was filtered and washed with 5% methanol in dichloromethane (150 mL). The combined organic layers were dried, concentrated and purified by flash column chromatography (0%-100% ethyl acetate / hexane on N-H silica) to afford the title compound **A12** as a brown oil (63% yield). 1H-NMR (400 MHz, $CDCl_3$) δ 7.29 (s, 1H), 6.17-6.20 (1H),

5.55 (s, 2H), 4.07 (t, J = 6.9 Hz, 2H), 3.84 (s, 3H), 3.81 (s, 3H), 2.61 (t, J = 7.3 Hz, 2H), 2.54-2.49 (m, 4H), 2.09-2.04 (m, 2H), 1.81-1.76 (m, 4H).

4-Chloro-2-cyclohexyl-6-methoxy-7-(3-(pyrrolidin-1-yl)propoxy)quinazoline (A14). In a sealed tube, a mixture of compound **A12** (0.75 g, 2.43 mmol), cyclohexanecarbonitrile (3.0 mL, 24.3 mmol) and HCl (4N solution in dioxane, 10 mL, 40 mmol) was stirred overnight at 100 °C. The reaction mixture was poured into water and neutralized with $NaHCO_3$. The resulting precipitate was collected and dried to provide the desired crude product **A13** (0.65 g). A mixture of the crude compound **A13** (0.65 g, 1.68 mmol) and N,N–diethylaniline (0.27 mL, 1.68 mmol) in $POCl_3$ (15 mL) was heated at reflux for 4h. The reaction mixture was concentrated in vacuo and saturated aq $NaHCO_3$ (20 mL) was added. The resulting mixture was extracted with chloroform (20 mL × 3). The combined organic layers were dried, concentrated and purified by column chromatography (0%-30% ethyl acetate / hexane on N-H silica) to afford the title compound **A14** as a yellow solid (35% over two steps). 1H-NMR (400 MHz, $CDCl_3$) δ 7.34 (s, 1H), 7.31 (s, 1H), 4.28 (t, J = 6.6 Hz, 2H), 4.04 (s, 3H), 2.94 (tt, J = 11.8, 3.4 Hz, 1H), 2.66 (t, J = 7.1 Hz, 2H), 2.53 (d, J = 6.4 Hz, 4H), 2.19-2.12 (m, 2H), 2.11-2.00 (m, 2H), 1.90-1.76 (m, 5H), 1.74-1.67 (m, 4H), 1.50-1.26 (m, 3H).

2-cyclohexyl-6-methoxy-N-(piperidin-4-yl)-7-(3-(pyrrolidin-1-yl)propoxy)quinazolin-4-amine (A16). A solution of compound **A14** (0.404 g, 1 mmol), N-Boc-4-aminopiperidine (0.24 g, 1.2 mmol) and K_2CO_3 (0.29 g, 2 mmol) in DMF was stirred overnight at 100 °C. The solution was cooled to room temperature, diluted with ice water (20 ml) and extracted with ethyl acetate and the organic layer was washed with brine and then dried over anhy. Na_2SO_4, filtered and concentrated to obtain the crude tert-butyl 4-((2-cyclohexyl-6-methoxy-7-(3-(pyrrolidin-1-yl)propoxy)quinazolin-4-yl)amino)piperidine-1-carboxylate **A15** (0.205 g), which was used directly in the next step. Crude **A15** (0.205 g, 0.36 mmol) and TFA (3.3ml, 43.2 mmol) were dissolved in DCM (5ml) and stirred at room temperature for 15h under argon atmosphere. Then

the reaction mixture was concentrated in vacuo and further purified by column chromatography (0%-5% methanol gradient in DCM on N-H silica) to afford the title compound **A16** as a yellowish white solid (30% over two steps).^{1}H-NMR (400 MHz, $CDCl_3$) δ 7.16 (s, 1H), 6.78 (s, 1H), 5.06 (d, J = 6.9 Hz, 1H), 4.37-4.29 (m, 1H), 4.18 (t, J = 6.6 Hz, 2H), 3.94 (d, J = 14.7 Hz, 3H), 3.17 (d, J = 12.4 Hz, 2H), 2.83 (t, J = 11.0 Hz, 2H), 2.70 (tt, J = 11.7, 3.3 Hz, 1H), 2.62 (t, J = 7.6 Hz, 2H), 2.51 (s, 4H), 2.18 (t, J = 10.1 Hz, 2H), 2.14-2.07 (m, 2H), 1.97 (d, J = 12.8 Hz, 2H), 1.84-1.60 (m, 8H), 1.51-1.23 (m, 7H). ^{13}C-NMR (101 MHz, $CDCl_3$) δ 169.5, 157.7, 153.7, 148.5, 147.4, 108.6, 106.7, 99.8, 67.6, 56.5, 54.3, 53.0, 48.5, 48.0, 45.7, 33.6, 32.0, 28.5, 26.5, 26.3, 23.6. HRMS (ESI) calcd. for $C_{27}H_{42}N_5O_2$ $[M+H]^+$ 468.3339, found 468.3330.

3-(4-aminophenyl)piperidine-2,6-dione (A22 or, B30). To a solution of compound **A17/B25** (5.00 g, 35.4 mmol, 1.00 eq) in DMF (35.0 mL) was added compound Methyl 2-cyanoacetate (5.27 g, 53.2 mmol, 1.50 eq) and K_2CO_3 (9.79 g, 70.9 mmol, 2.00 eq), then the mixture was stirred at 120 °C for 2 hrs under N_2 atmosphere. TLC showed compound A was consumed completely and one new spot was formed. The reaction mixture was cooled to 20 °C and filtered. The filter liquor was poured into H_2O (70.0 mL) and stirred for 0.5 hr. The pH value of the solution was acidified to 2 ~ 3 with 1 N HCl. The solution was extracted with ethyl acetate (50.0 mL x 3). The combined organic phase was washed with brine (50.0 mL x 3), dried over Na_2SO_4, filtered and concentrated in vacuum to give a crude of compound **A18/B26** (8.00 g). The crude was used for the next step without further purification.

To a solution of compound **A18/B26** (8.00 g, 36.3 mmol, 1.00 eq) in THF (60.0 mL) was added NMM (5.51 g, 54.5 mmol, 1.50 eq) and compound Methyl acrylate (4.96 g, 57.6 mmol, 1.59 eq), then the mixture was stirred at 55 °C for 4 hrs. TLC showed compound **A18/B26** was consumed completely and one new spot was formed. The reaction mixture was poured into H_2O (60.0 mL) and extracted with ethyl acetate (50.0 mL). The combined organic phase was

washed with brine (50.0 mL), dried over Na_2SO_4, filtered and concentrated in vacuum to give a crude of compound **A19/B27** (5.00 g). The crude was used for the next step without further purification.

To a solution of compound **A19/B27** (5.00 g, 16.3 mmol, 1.00 eq) in THF (15.0 mL) and H_2O (30.0 mL) was added Na_2CO_3 (3.46 g, 32.7 mmol, 2.00 eq), then the mixture was stirred at 90 °C for 1.5 hrs under N_2 atmosphere. TLC showed compound **A19/B27** was consumed completely and one new spot was formed. The reaction mixture was cooled to 20 °C and the pH value of the solution was acidified to 5 with 1 N HCl. The solution was extracted with ethyl acetate (50.0 mL x 3). The combined organic phase was washed with brine (50.0 mL x 3), dried over Na_2SO_4, filtered and concentrated in vacuum to give a crude. The crude was used for the next step without further purification. Compound **A20/B28** (3.80 g, crude) was obtained as black oil.

To a solution of compound **A20/B28** (3.00 g, 12.1 mmol, 1.00 eq) in AcOH (18.0 mL) was added H_2SO_4 (948 mg, 9.67 mmol, 515 uL, 0.8 eq), then the mixture was stirred at 120 °C for 2 hrs under N_2 atmosphere. TLC showed compound **A20/B28** was consumed completely and one new spot was formed. The reaction mixture was cooled to 20 °C, poured into H_2O (30.0 mL) and stirred for 0.5 hr. The solution was filtered and the filter cake was washed by H_2O (10.0 mL x 2) to give a residue. The residue was triturated with MeOH (10.0 mL) at 25 °C for 0.5 hr. Then the solution was filtered and concentrated in vacuum. Compound **A21/B29** (2.30 g) was obtained as an off-white solid. The crude was used for the next step without further purification.

A mixture of compound **A21/B29** (2 g, 8.5 mmol), and iron fillings (2.4 g, 5.0 equiv) in ethanol (40 mL) and water (10 mL) was cooled to 0 °C. To the stirred mixture was added a solution of concentrated hydrochloric acid (6.0 equiv) dropwise. The suspension was stirred at 90 °C in an

oil bath for 1.5 h, then cooled to room temperature, filtered through a short pad of celite. The celite pad was further washed with ethanol (50 mL). The combined solution was concentrated in vacuo and the residue was purified by column chromatography (10%-100% EtOAc-Hexane) afforded compound **A22**/**B30** as a white sold (36% over 5 steps). 1H NMR (400 MHz, DMSO-D6) δ 10.72 (s, 1H), 6.84 (d, J = 8.4 Hz, 2H), 6.51 (d, J = 8.4 Hz, 2H), 4.97 (s, 2H), 3.61 (dd, J = 10.5, 5.0 Hz, 1H), 2.59 (ddd, J = 16.4, 10.8, 5.4 Hz, 1H), 2.43 (dt, J = 17.3, 4.7 Hz, 1H), 2.12 – 2.02 (m, 1H), 2.02 – 1.94 (m, 1H).

8-(benzyloxy)-8-oxooctanoic acid (A26). KOH (79.2 mg, 1.41 mmol) was added to a solution of suberic acid **A23** (258 mg, 1.48 mmol) in MeOH (11.4 mL) at room temperature. After being stirred at room temperature for 20 min, the reaction mixture was concentrated and dissolved in toluene (2.5 mL). n-Bu4NBr (48.1 mg, 0.149 mmol) and benzyl bromide (p-NO_2-BnBr, 0.20 mL, 1.7 mmol) were successively added to the solution at room temperature. After the reaction mixture was stirred at 130 °C for 13 h, 1 M aqueous HCl (1.7 mL, 1.7 mmol) was added to the mixture at room temperature. The resultant mixture was extracted with Et_2O (10 mL x3). The combined organic layers were washed with H_2O (10 mL) and brine (10 mL), dried over Na_2SO_4, filtered, and concentrated. The residue was purified by flash column chromatography on silica gel (hexane/EtOAc = 1/0 to 3/1) to afford the title carboxylic acid **A26** (40% over 2 steps) as a colourless oil. 1H-NMR (400 MHz, CHLOROFORM-D) δ 7.39-7.30 (m, 5H), 5.11 (s, 2H), 2.38-2.29 (m, 4H), 1.69-1.59 (m, 4H), 1.39-1.25 (m, 4H).

10-((4-nitrobenzyl)oxy)-10-oxodecanoic acid (A27). KOH (79.2 mg, 1.41 mmol) was added to a solution of sebacic acid **A24** (299 mg, 1.48 mmol) in MeOH (11.4 mL) at room temperature. After being stirred at room temperature for 20 min, the reaction mixture was concentrated and dissolved in toluene (2.5 mL). n-Bu4NBr (48.1 mg, 0.149 mmol) and p-NO_2-benzyl bromide (p-NO2-BnBr, 367.2 mg, 1.7 mmol) were successively added to the solution at room temperature. After the reaction mixture was stirred at 130 °C for 13 h, 1 M aqueous HCl (1.7

mL, 1.7 mmol) was added to the mixture at room temperature. The resultant mixture was extracted with Et_2O (10 mL x3). The combined organic layers were washed with H_2O (10 mL) and brine (10 mL), dried over Na_2SO_4, filtered, and concentrated. The residue was purified by flash column chromatography on silica gel (hexane/EtOAc = 1/0 to 3/1) to afford the title carboxylic acid **A27** (36% over 2 steps) as white solid. 1H-NMR (400 MHz, CHLOROFORM-D) δ 8.23 (d, J = 6.9 Hz, 2H), 7.51 (d, J = 8.7 Hz, 2H), 5.21 (s, 2H), 2.42-2.30 (m, 4H), 1.63 (dt, J = 19.4, 7.2 Hz, 4H), 1.31-1.26 (m, 8H). 13C-NMR (101 MHz, CHLOROFORM-D) δ 179.7, 173.5, 147.8, 143.5, 128.5, 123.9, 64.7, 34.2, 34.0, 29.1, 29.1, 24.9, 24.7. HRMS (ESI) calcd. for $C_{17}H_{23}NO_6Na$ $[M+Na]^+$ 360.1423, found 360.1414.

12-((4-nitrobenzyl)oxy)-12-oxododecanoic acid (A28). KOH (79.2 mg, 1.41 mmol) was added to a solution of dodecanedioic acid **A25** (340 mg, 1.48 mmol) in MeOH (11.4 mL) at room temperature. After being stirred at room temperature for 20 min, the reaction mixture was concentrated and dissolved in toluene (2.5 mL). n-Bu4NBr (48.1 mg, 0.149 mmol) and p-NO_2-benzyl bromide (p-NO2-BnBr, 367.2 mg, 1.7 mmol) were successively added to the solution at room temperature. After the reaction mixture was stirred at 130 °C for 13 h, 1 M aqueous HCl (1.7 mL, 1.7 mmol) was added to the mixture at room temperature. The resultant mixture was extracted with Et_2O (10 mL x3). The combined organic layers were washed with H_2O (10 mL) and brine (10 mL), dried over Na_2SO_4, filtered, and concentrated. The residue was purified by flash column chromatography on silica gel (hexane/EtOAc = 1/0 to 3/1) to afford the title carboxylic acid **A28** (39% over 2 steps) as white solid. 1H-NMR (400 MHz, CHLOROFORM-D) δ 8.23 (d, J = 8.7 Hz, 2H), 7.51 (d, J = 9.2 Hz, 2H), 5.21 (s, 2H), 2.42-2.28 (m, 4H), 1.67-1.59 (m, 4H), 1.29-1.24 (m, 12H). 13C-NMR (101 MHz, CHLOROFORM-D) δ 179.6, 173.5, 147.8, 143.6, 128.5, 123.9, 64.7, 34.3, 34.1, 29.5, 29.3, 29.2, 29.1, 25.0, 24.8. HRMS (ESI) calcd. for $C_{19}H_{27}NO_6$ $[M+Na]^+$ 388.1736, found 388.1727.

Benzyl 8-((4-(2,6-dioxopiperidin-3-yl)phenyl)amino)-8-oxooctanoate (A29). To the 8-(benzyloxy)-8-oxooctanoic acid **A26** (84 mg, 0.32 mmol), 3-(4-aminophenyl)piperidine-2,6-dione (66 mg, 0.32 mmol), HATU (243 mg, 0.64 mmol) in DMF (5 ml) was added DIPEA (0.28 mL, 1.6 mmol) and the reaction mixture was stirred at 23 °C for 18 h. Then diluted with water and extracted with ethyl acetate and the organic layer was washed with brine and then dried over anhy. Na_2SO_4, filtered and concentrated to obtain the crude product. The crude product was purified on silica gel column using EtOAc-Hexane gradient (50%) to give the title compound (48%) as an off-white solid. 1H-NMR (400 MHz, CHLOROFORM-D) δ 8.07 (s, 1H), 7.53 (d, J = 8.2 Hz, 2H), 7.40-7.33 (m, 5H), 7.16 (d, J = 8.7 Hz, 2H), 5.12 (s, 2H), 3.80-3.74 (m, 1H), 2.77-2.61 (m, 2H), 2.39-2.18 (m, 6H), 1.69 (td, J = 14.8, 7.1 Hz, 5H), 1.38-1.29 (m, 4H). 13C-NMR (151 MHz, CHLOROFORM-D) δ 173.8, 173.2, 172.3, 171.5, 137.7, 136.2, 132.7, 128.8, 128.7, 128.3, 120.3, 66.3, 47.5, 37.6, 34.3, 31.0, 28.8, 28.7, 26.5, 25.4, 24.8. HRMS (ESI) calcd. for $C_{26}H_{30}N_2O_5Na$ $[M+Na]^+$ 473.2052, found 473.2042.

4-nitrobenzyl 10-((4-(2,6-dioxopiperidin-3-yl)phenyl)amino)-10-oxodecanoate (A30). To the 10-((4-nitrobenzyl)oxy)-10-oxodecanoic acid **A27** (108 mg, 0.32 mmol), 3-(4-aminophenyl)piperidine-2,6-dione (66 mg, 0.32 mmol), HATU (243 mg, 0.64 mmol) in DMF (5 ml) was added DIPEA (0.28 mL, 1.6 mmol) and the reaction mixture was stirred at 23 °C for 18 h. Then diluted with water and extracted with ethyl acetate and the organic layer was washed with brine and then dried over anhy. Na_2SO_4, filtered and concentrated to obtain the crude product. The crude product was purified on silica gel column using EtOAc-Hexane gradient (0-50%) to give the desired product **30** (49%) as an off-white solid. 1H-NMR (600 MHz, CHLOROFORM-D) δ 8.22 (d, J = 8.2 Hz, 2H), 8.09 (s, 1H), 7.53-7.51 (m, 4H), 7.31 (s, 1H), 7.15 (d, J = 8.2 Hz, 2H), 5.20 (s, 2H), 3.75 (q, J = 4.8 Hz, 1H), 2.75-2.62 (m, 2H), 2.39 (t, J = 7.6 Hz, 2H), 2.34 (t, J = 7.6 Hz, 2H), 2.30-2.19 (m, 2H), 1.72-1.65 (m, 5H), 1.31 (s, 8H). 13C-NMR (151 MHz, CHLOROFORM-D) δ 173.7, 173.5, 172.5, 171.7, 148.0, 143.8, 137.9,

132.9, 129.0, 128.7, 124.1, 120.5, 64.9, 47.7, 38.0, 34.4, 31.2, 29.4, 29.3, 26.7, 25.8, 25.2. HRMS (ESI) calcd. for $C_{28}H_{33}N_3O_7$ $[M+Na]^+$ 546.2216, found 546.2205.

4-nitrobenzyl 12-((4-(2,6-dioxopiperidin-3-yl)phenyl)amino)-12-oxododecanoate (A31). To the 12-((4-nitrobenzyl)oxy)-12-oxododecanoic acid **A28** (117 mg, 0.32 mmol), 3-(4-aminophenyl)piperidine-2,6-dione (66 mg, 0.32 mmol), HATU (243 mg, 0.64 mmol) in DMF (5 ml) was added DIPEA (0.28 mL, 1.6 mmol) and the reaction mixture was stirred at 23 °C for 18 h. Then diluted with water and extracted with ethyl acetate and the organic layer was washed with brine and then dried over anhy. Na_2SO_4, filtered and concentrated to obtain the crude product. The crude product was purified on silica gel column using EtOAc-Hexane gradient (0-50%) to give the desired product **A31** (46%) as an off-white solid. 1H-NMR (600 MHz, CHLOROFORM-D) δ 8.22 (d, J = 8.9 Hz, 2H), 8.09 (s, 1H), 7.52 (t, J = 7.9 Hz, 4H), 7.32 (s, 1H), 7.15 (d, J = 8.2 Hz, 2H), 5.21 (t, J = 15.8 Hz, 2H), 3.76 (q, J = 5.0 Hz, 1H), 2.75-2.62 (m, 2H), 2.40 (t, J = 7.2 Hz, 2H), 2.34 (t, J = 7.2 Hz, 2H), 2.29-2.19 (m, 2H), 1.73-1.63 (m, 5H), 1.35-1.23 (m, 12H). 13C-NMR (151 MHz, CHLOROFORM-D) δ 173.5, 173.2, 172.3, 171.6, 147.8, 143.6, 137.7, 132.7, 128.8, 128.5, 123.9, 120.3, 64.7, 47.5, 37.9, 34.3, 31.0, 29.4, 29.3, 29.3, 29.2, 26.5, 25.7, 25.0. HRMS (ESI) calcd. for $C_{30}H_{37}N_3O_7Na$ $[M+Na]^+$ 574.2529, found 574.2518.

4-nitrophenyl (2-(2,6-dioxopiperidin-3-yl)-1,3-dioxoisoindolin-4-yl)carbamate (A36). To a solution of pomalidomide **A35** (2 g, 7.33 mmol, 1.0 equiv.) in THF (20 mL), 4-Nitrophenyl chloroformate (2.2 g, 10.99 mmol, 1.5 equiv.) was added. The mixture was stirred at reflux for 4 h. After the reaction completed, the mixture was slowly cooled to room temperature, filtered and washed with THF to produce the title compound **A36** as white solid (47%). 1H NMR (400 MHz, DMSO-d6) δ 11.01 (s, 1H), 10.28 (s, 1H), 8.17 (d, J = 5.3 Hz, 2H), 7.51 (dd, J = 5.5, 1.7 Hz, 1H), 7.43–7.32 (m, 4H), 5.12 (d, J = 5.0 Hz, 1H), 3.14–2.98 (m, 1H), 2.59 (d, J = 12.0 Hz, 1H), 2.41–2.23 (m, 1H), 2.10–1.95 (m, 1H).

((2-(2,6-dioxopiperidin-3-yl)-1,3-dioxoisoindolin-4-yl)carbamoyl)glycine (A41). To a solution of **A36** (500 mg, 1.14 mmol, 1.0 equiv.) in DMF (7 mL), glycine **A37** (128 mg, 1.71 mmol, 1.5 equiv.) was added. The mixture was stirred at room temperature overnight. The reaction mixture was then diluted with cold water and extracted 3 times with EtOAc. The combined organic layers were then washed saturated brine, dried over anhydrous Na_2SO_4, concentrated in vacuo and purified by flash column chromatography with 0-100% EtOAc/Hexane gradient to obtain the title compound (47%) as a white solid.

5-(3-(2-(2,6-dioxopiperidin-3-yl)-1,3-dioxoisoindolin-4-yl)ureido)pentanoic acid (A42). To a solution of **A36** (500 mg, 1.14 mmol, 1.0 equiv.) in DMF (7 mL), 5-aminopentanoic acid **A38** (200 mg, 1.71 mmol, 1.5 equiv.) was added. The mixture was stirred at room temperature overnight. The reaction mixture was then diluted with cold water and extracted 3 times with EtOAc. The combined organic layers were then washed saturated brine, dried over anhydrous Na_2SO_4, concentrated in vacuo and purified by flash column chromatography with 0-9% MeOH/DCM gradient to obtain the title compound (62%) as white solid. 1H-NMR (600 MHz, DMSO-D6) δ 12.05 (s, 1H), 11.17 (s, 1H), 8.79 (s, 1H), 8.63-8.59 (m, 1H), 7.75-7.67 (m, 2H), 7.41 (d, J = 6.9 Hz, 1H), 5.12 (dd, J = 12.7, 5.2 Hz, 1H), 3.16-3.09 (m, 2H), 2.89 (ddd, J = 18.4, 13.2, 4.6 Hz, 1H), 2.61 (d, J = 17.2 Hz, 1H), 2.52 (d, J = 4.8 Hz, 1H), 2.24 (t, J = 7.2 Hz, 2H), 2.08-2.06 (m, 1H), 1.56-1.43 (m, 4H). 13C-NMR (151 MHz, DMSO-D6) δ 174.6, 173.0, 170.1, 168.5, 167.1, 154.4, 139.3, 136.1, 131.5, 124.3, 115.9, 113.7, 49.0, 33.5, 31.1, 29.0, 22.3, 22.1. HRMS (ESI) calcd. for $C_{19}H_{20}N_4O_7Na$ $[M+Na]^+$ 439.1230, found 439.1218.

8-(3-(2-(2,6-dioxopiperidin-3-yl)-1,3-dioxoisoindolin-4-yl)ureido)octanoic acid (A43). To a solution of **A36** (500 mg, 1.14 mmol, 1.0 equiv.) in DMF (7 mL), 8-aminooctanoic acid **A39** (272 mg, 1.71 mmol, 1.5 equiv.) was added. The mixture was stirred at room temperature overnight. The reaction mixture was then diluted with cold water and extracted 3 times with EtOAc. The combined organic layers were then washed saturated brine, dried over anhydrous

Na_2SO_4, concentrated in vacuo and purified by flash column chromatography with 0-5% MeOH/DCM gradient to obtain the title compound (59%) as white solid. 1H-NMR (600 MHz, DMSO-D6) δ 11.99 (s, 1H), 11.17 (s, 1H), 8.76 (d, J = 23.4 Hz, 1H), 8.59 (d, J = 8.2 Hz, 1H), 7.71 (t, J = 7.9 Hz, 2H), 7.41 (d, J = 6.9 Hz, 1H), 5.12 (q, J = 6.2 Hz, 1H), 3.08 (q, J = 6.4 Hz, 2H), 2.89 (ddd, J = 18.4, 12.9, 4.3 Hz, 1H), 2.62-2.54 (m, 1H), 2.54-2.49 (m, 1H), 2.19 (t, J = 7.2 Hz, 2H), 2.08-2.05 (m, 1H), 1.51-1.42 (m, 4H), 1.25 (d, J = 33.0 Hz, 6H). 13C-NMR (151 MHz, DMSO-D6) δ 174.7, 173.0, 170.1, 168.5, 167.1, 154.4, 139.3, 136.1, 131.5, 124.3, 115.9, 113.7, 49.0, 33.8, 31.1, 29.4, 28.7, 28.7, 26.5, 24.6, 22.3. HRMS (ESI) calcd. for $C_{22}H_{26}N_4O_7Na$ $[M+Na]^+$ 481.1699, found 481.1691.

11-(3-(2-(2,6-dioxopiperidin-3-yl)-1,3-dioxoisoindolin-4-yl)ureido)undecanoic acid (A44). To a solution of **A36** (500 mg, 1.14 mmol, 1.0 equiv.) in DMF (7 mL), 11-aminoundecanoic acid **A40** (344 mg, 1.71 mmol, 1.5 equiv.) was added. The mixture was stirred at room temperature overnight. The reaction mixture was then diluted with cold water and extracted 3 times with EtOAc. The combined organic layers were then washed saturated brine, dried over anhydrous Na_2SO_4, concentrated in vacuo and purified by flash column chromatography with 0-5% MeOH/DCM gradient to obtain the title compound (61%) as white solid. ^{1}H-NMR (400 MHz, DMSO-D6) δ 11.97 (s, 1H), 11.16 (s, 1H), 8.78 (s, 1H), 8.60 (d, J = 8.7 Hz, 1H), 7.74-7.70 (m, 2H), 7.41 (d, J = 7.3 Hz, 1H), 5.12 (dd, J = 12.8, 5.5 Hz, 1H), 3.09 (q, J = 6.4 Hz, 2H), 2.94-2.85 (m, 1H), 2.63-2.55 (m, 1H), 2.17 (t, J = 7.3 Hz, 2H), 2.09-2.05 (m, 1H), 1.49-1.42 (m, 4H), 1.25 (s, 12H). ^{13}C-NMR (101 MHz, DMSO-D6) δ 174.8, 173.1, 170.2, 168.5, 167.1, 154.4, 139.4, 136.1, 131.6, 124.3, 115.9, 113.7, 49.0, 33.9, 31.2, 29.5, 29.2, 29.1, 29.0, 28.8, 26.6, 24.7, 22.3.

8-(4-((2-cyclohexyl-6-methoxy-7-(3-(pyrrolidin-1-yl)propoxy)quinazolin-4-yl)amino)piperidin-1-yl)-N-(4-(2,6-dioxopiperidin-3-yl)phenyl)-8-oxooctanamide (A1). To a solution of Benzyl 8-((4-(2,6-dioxopiperidin-3-yl)phenyl)amino)-8-oxooctanoate **A29** (60 mg,

0.13 mmol) was added Pd-C (10% Pd, 5.3 mg, 0.045 mmol) under an inert atmosphere and then the reaction mixture was stirred overnight under a hydrogen atmosphere at room temperature. The reaction mixture was then filtered through a short pad of celite and washed with ethyl acetate and concentrated to dryness. The crude white solid product **A32** was directly used in the next step without further purification. To the 8-((4-(2,6-dioxopiperidin-3-yl)phenyl)amino)-8-oxooctanoic acid **A32** (20 mg, 0.056 mmol), **A16** (26 mg, 0.056 mmol), HATU (43 mg, 0.119 mmol) in DMF (1.5 ml) was added DIPEA (50 µL, 0.28 mmol) and the reaction mixture was stirred at 23 °C for 18 h. Then diluted with water and extracted with ethyl acetate and the organic layer was washed with brine and then dried over anhy. Na_2SO_4, filtered and concentrated to obtain the crude product. The crude product was purified on N-H silica gel column using acetone/CH_2Cl_2 = 2/3 followed by preparative HPLC (30%-70% MeCN-Miliq for 50 minutes) to give the title compound (12% over two steps) as a white solid. 1H-NMR (400 MHz, METHANOL-D4) δ 7.79 (s, 1H), 7.51 (d, J = 8.2 Hz, 2H), 7.14 (d, J = 7.3 Hz, 3H), 4.64 (d, J = 12.8 Hz, 2H), 4.31 (t, J = 5.3 Hz, 2H), 4.10-4.04 (m, 1H), 3.97 (s, 3H), 3.80-3.76 (m, 3H), 3.44 (t, J = 7.1 Hz, 2H), 3.11 (t, J = 8.5 Hz, 2H), 2.80 (dd, J = 26.8, 12.6 Hz, 2H), 2.70-2.54 (m, 2H), 2.50-2.32 (m, 6H), 2.18-2.11 (m, 4H), 2.08-1.98 (m, 4H), 1.91 (d, J = 12.4 Hz, 2H), 1.80-1.58 (m, 9H), 1.38 (dq, J = 60.6, 12.8 Hz, 7H). 13C-NMR (151 MHz, METHANOL-D4) δ 176.4, 175.6, 174.6, 174.1, 166.9, 160.7, 156.8, 151.7, 139.1, 136.5, 135.4, 129.9, 121.3, 107.1, 104.1, 101.0, 68.2, 57.2, 55.4, 54.2, 51.3, 46.0, 45.6, 42.0, 37.8, 33.9, 32.8, 32.1, 32.0, 31.9, 30.0, 29.9, 27.8, 26.8, 26.6, 26.6, 26.5, 24.0. HRMS (ESI) calcd. for $C_{46}H_{64}N_7O_6$ $[M+H]^+$ 810.4918, found 810.4901.

10-(4-((2-cyclohexyl-6-methoxy-7-(3-(pyrrolidin-1-yl)propoxy)quinazolin-4-yl)amino)piperidin-1-yl)-N-(4-(2,6-dioxopiperidin-3-yl)phenyl)-10-oxodecanamide (A2). To a solution of 4-nitrobenzyl 10-((4-(2,6-dioxopiperidin-3-yl)phenyl)amino)-10-oxodecanoate **A30** (81 mg, 0.15 mmol) was added Pd-C (10% Pd, 7.0 mg, 0.06 mmol) under an inert

atmosphere and then the reaction mixture was stirred overnight under a hydrogen atmosphere at room temperature. The reaction mixture was then filtered through a short pad of celite and washed with ethyl acetate and concentrated to dryness. The crude white solid product **A33** was directly used in the next step without further purification. 10-((4-(2,6-dioxopiperidin-3-yl)phenyl)amino)-10-oxodecanoic acid **A33** (32 mg, 0.082 mmol), **A16** (38.5 mg, 0.082 mmol), HATU (62.3 mg, 0.164 mmol) in DMF (2 ml) was added DIPEA (71 µL, 0.41mmol) and the reaction mixture was stirred at 23 °C for 18 h. Then diluted with water and extracted with ethyl acetate and the organic layer was washed with brine and then dried over anhy. Na_2SO_4, filtered and concentrated to obtain the crude product. The crude product was purified on N-H silica gel column using acetone/CH_2Cl_2 = 2/3 followed by preparative HPLC (30%-70% MeCN-Miliq for 50 minutes) to give the title compound (18% over two seps) as a white solid. 1H-NMR (600 MHz, METHANOL-D4) δ 7.81 (s, 1H), 7.53 (d, J = 8.9 Hz, 2H), 7.17 (d, J = 6.9 Hz, 3H), 4.71-4.65 (m, 2H), 4.32 (t, J = 5.5 Hz, 2H), 4.11-4.07 (m, 1H), 3.99 (s, 3H), 3.80 (q, J = 5.3 Hz, 3H), 3.46 (t, J = 7.2 Hz, 2H), 3.15-3.11 (m, 2H), 2.87-2.79 (m, 2H), 2.71-2.65 (m, 1H), 2.59 (dt, J = 17.6, 4.6 Hz, 1H), 2.44 (dq, J = 31.8, 7.6 Hz, 2H), 2.35 (q, J = 7.1 Hz, 4H), 2.21-2.16 (m, 4H), 2.11 (d, J = 12.4 Hz, 1H), 2.06-2.00 (m, 3H), 1.92 (d, J = 13.1 Hz, 2H), 1.81-1.61 (m, 9H), 1.51-1.44 (m, 2H), 1.38-1.33 (m, 9H). 13C-NMR (151 MHz, METHANOL-D4) δ 176.4, 175.6, 174.7, 174.2, 166.9, 162.3, 162.0, 160.7, 156.8, 151.7, 139.1, 136.5, 135.4, 129.9, 121.3, 107.1, 104.2, 101.0, 68.2, 57.2, 55.4, 54.2, 51.3, 46.0, 45.6, 42.0, 37.9, 34.1, 32.8, 32.1, 32.0, 31.9, 30.3, 30.2, 27.8, 26.8, 26.8, 26.6, 26.6, 24.0. HRMS (ESI) calcd. for $C_{48}H_{67}N_7O_6$ Na$[M+Na]^+$ 860.5051, found 860.5001.

12-(4-((2-cyclohexyl-6-methoxy-7-(3-(pyrrolidin-1-yl)propoxy)quinazolin-4-yl)amino)piperidin-1-yl)-N-(4-(2,6-dioxopiperidin-3-yl)phenyl)-12-oxododecanamide (A3).

To a solution of 4-nitrobenzyl 12-((4-(2,6-dioxopiperidin-3-yl)phenyl)amino)-12-oxododecanoate **A31** (85 mg, 0.15 mmol) was added Pd-C (10% Pd, 7.0 mg, 0.06 mmol) under

an inert atmosphere and then the reaction mixture was stirred overnight under a hydrogen atmosphere at room temperature. The reaction mixture was then filtered through a short pad of celite and washed with ethyl acetate and concentrated to dryness. The crude white solid product **A34** was directly used in the next step without further purification. To the 8-((4-(2,6-dioxopiperidin-3-yl)phenyl)amino)-8-oxooctanoic acid **A34** (28 mg, 0.067 mmol), **A16** (31.5 mg, 0.067 mmol), HATU (51 mg, 0.134 mmol) in DMF (2 ml) was added DIPEA (59 µL, 0.34 mmol) and the reaction mixture was stirred at 23 °C for 18 h. Then diluted with water and extracted with ethyl acetate and the organic layer was washed with brine and then dried over anhy. Na_2SO_4, filtered and concentrated to obtain the crude product. The crude product was purified on N-H silica gel column using acetone/CH_2Cl_2 = 2/3 followed by preparative HPLC (30%-70% MeCN-Miliq for 50 minutes) to give the title compound (16% over two steps) as a white solid. 1H-NMR (400 MHz, METHANOL-D4) δ 7.79 (s, 1H), 7.51 (d, J = 8.2 Hz, 2H), 7.17-7.14 (m, 3H), 4.69-4.63 (m, 2H), 4.30 (t, J = 5.5 Hz, 2H), 4.09 (t, J = 6.9 Hz, 1H), 3.98 (s, 3H), 3.79 (dd, J = 9.8, 5.7 Hz, 3H), 3.44 (t, J = 7.3 Hz, 2H), 3.14-3.08 (m, 2H), 2.89-2.77 (m, 2H), 2.71-2.55 (m, 2H), 2.42 (qd, J = 7.6, 5.4 Hz, 2H), 2.37-2.30 (m, 4H), 2.24-2.12 (m, 4H), 2.08-1.99 (m, 4H), 1.92 (t, J = 12.4 Hz, 2H), 1.80-1.58 (m, 9H), 1.51-1.26 (m, 15H). 13C-NMR (101 MHz, METHANOL-D4) δ 176.5, 175.7, 174.7, 174.2, 166.9, 160.7, 156.8, 151.7, 139.1, 136.5, 135.4, 129.9, 121.3, 107.1, 104.1, 101.0, 68.2, 57.2, 55.4, 54.1, 51.3, 46.0, 45.6, 42.0, 38.0, 34.1, 32.8, 32.2, 32.0, 31.9, 30.5, 30.4, 30.4, 30.3, 27.8, 26.9, 26.8, 26.7, 26.6, 24.0. HRMS (ESI) calcd. for $C_{50}H_{71}N_7O_6$ $[M+Na]^+$ 888.5364, found 888.5345.

1-(2-(4-((2-cyclohexyl-6-methoxy-7-(3-(pyrrolidin-1-yl)propoxy)quinazolin-4-yl)amino)piperidin-1-yl)-2-oxoethyl)-3-(2-(2,6-dioxopiperidin-3-yl)-1,3-dioxoisoindolin-4-yl)urea (A4). To the mixture of **A41** (40 mg, 0.11 mmol), **A16** (50 mg, 0.11 mmol), HATU (84 mg, 0.22 mmol) in DMF (2 ml) was added DIPEA (96 µL, 0.55 mmol) and the reaction mixture was stirred at 23 °C for 18 h. Then diluted with water and extracted with ethyl acetate and the

organic layer was washed with brine and then dried over anhy. Na_2SO_4, filtered and concentrated to obtain the crude product. The crude product was purified on N-H silica gel column using acetone/CH_2Cl_2 = 2/3 followed by preparative HPLC (15%-30% MeCN-Miliq for 30 minutes then 50% for 30-50 min) to obtain the title compound (11%) as white solid. 1H-NMR (600 MHz, METHANOL-D4) δ 8.56 (dd, J = 8.6, 2.4 Hz, 1H), 7.84 (d, J = 15.1 Hz, 1H), 7.67 (q, J = 8.2 Hz, 1H), 7.43 (dd, J = 24.4, 7.2 Hz, 1H), 7.17 (d, J = 8.2 Hz, 1H), 5.12 (dd, J = 12.7, 5.2 Hz, 1H), 4.74-4.65 (m, 2H), 4.32 (t, J = 5.5 Hz, 2H), 4.26 (dd, J = 17.2, 6.2 Hz, 1H), 4.15-4.08 (m, 2H), 4.00 (s, 3H), 3.82 (s, 2H), 3.47 (t, J = 7.2 Hz, 2H), 3.15 (t, J = 8.6 Hz, 3H), 2.93-2.84 (m, 3H), 2.78-2.69 (m, 2H), 2.38-2.34 (m, 2H), 2.25-2.15 (m, 5H), 2.07-2.02 (m, 4H), 1.94 (d, J = 13.1 Hz, 2H), 1.82-1.68 (m, 5H), 1.49 (q, J = 12.8 Hz, 2H), 1.41-1.28 (m, 1H). 13C-NMR (151 MHz, METHANOL-D4) δ 174.7, 171.6, 170.1, 169.8, 168.6, 167.0, 160.8, 157.2, 156.9, 151.8, 140.3, 136.9, 136.6, 133.2, 125.6, 117.6, 116.1, 107.3, 104.3, 101.1, 68.3, 57.3, 55.5, 54.3, 51.3, 50.6, 45.7, 44.9, 42.6, 32.6, 32.3, 32.1, 31.9, 26.9, 26.8, 24.1, 23.8. HRMS (ESI) calcd. for $C_{43}H_{54}N_9O_8$ $[M+H]^+$ 824.4095, found 824.4078.

1-(5-(4-((2-cyclohexyl-6-methoxy-7-(3-(pyrrolidin-1-yl)propoxy)quinazolin-4-yl)amino)piperidin-1-yl)-5-oxopentyl)-3-(2-(2,6-dioxopiperidin-3-yl)-1,3-dioxoisoindolin-4-yl)urea (A5). To the mixture of **A42** (46 mg, 0.11 mmol), **A16** (50 mg, 0.11 mmol), HATU (84 mg, 0.22 mmol) in DMF (2 ml) was added DIPEA (96 µL, 0.55 mmol) and the reaction mixture was stirred at 23 °C for 18 h. Then diluted with water and extracted with ethyl acetate and the organic layer was washed with brine and then dried over anhy. Na_2SO_4, filtered and concentrated to obtain the crude product. The crude product was purified on N-H silica gel column using acetone/CH_2Cl_2 = 2/3 followed by preparative HPLC (15%-30% MeCN-Miliq for 30 minutes then 50% for 30-50 min) to obtain the title compound (25%) as white solid. 1H-NMR (600 MHz, METHANOL-D4) δ 8.56-8.52 (m, 1H), 7.77 (d, J = 4.8 Hz, 1H), 7.58 (t, J = 7.9 Hz, 1H), 7.32 (d, J = 4.8 Hz, 1H), 7.16 (s, 1H), 5.09 (t, J = 6.2 Hz, 1H), 4.67 (d, J = 11.0

Hz, 2H), 4.33 (s, 2H), 4.14 (d, J = 13.7 Hz, 1H), 3.99-3.97 (m, 3H), 3.81 (s, 2H), 3.47 (t, J = 6.9 Hz, 2H), 3.31-3.23 (m, 5H), 3.13 (s, 3H), 2.84-2.80 (m, 3H), 2.76-2.67 (m, 2H), 2.57-2.44 (m, 2H), 2.36 (t, J = 5.5 Hz, 2H), 2.20-2.01 (m, 9H), 1.92 (d, J = 13.1 Hz, 2H), 1.79-1.63 (m, 10H), 1.48 (q, J = 12.8 Hz, 2H), 1.39-1.28 (m, 1H). 13C-NMR (151 MHz, METHANOL-D4) δ 174.5, 173.8, 171.4, 170.1, 168.4, 166.8, 160.5, 156.8, 151.6, 140.4, 136.7, 136.4, 132.9, 125.2, 117.1, 107.0, 104.1, 101.0, 68.2, 57.2, 55.4, 54.1, 51.2, 50.4, 45.9, 45.5, 42.0, 33.6, 32.8, 32.1, 31.9, 31.8, 30.5, 26.7, 26.5, 24.0, 23.8, 23.6. HRMS (ESI) calcd. for $C_{46}H_{60}N_9O_8$ $[M+H]^+$ 866.4565, found 866.4557.

1-(8-(4-((2-cyclohexyl-6-methoxy-7-(3-(pyrrolidin-1-yl)propoxy)quinazolin-4-yl)amino)piperidin-1-yl)-8-oxooctyl)-3-(2-(2,6-dioxopiperidin-3-yl)-1,3-dioxoisoindolin-4-yl)urea (A6). To the mixture of **A43** (34.4 mg, 0.075 mmol), **A16** (35 mg, 0.075 mmol), HATU (57 mg, 0.15 mmol) in DMF (2 ml) was added DIPEA (65 µL, 0.375 mmol) and the reaction mixture was stirred at 23 °C for 18 h. Then diluted with water and extracted with ethyl acetate and the organic layer was washed with brine and then dried over anhy. Na_2SO_4, filtered and concentrated to obtain the crude product. The crude product was purified on N-H silica gel column using acetone/CH_2Cl_2 = 2/3 followed by preparative HPLC (15%-30% MeCN-Miliq for 30 minutes then 50% for 30-50 min) to obtain the title compound (10%) as white solid. 1H-NMR (600 MHz, METHANOL-D4) δ 8.55 (d, J = 8.2 Hz, 1H), 7.81 (d, J = 18.6 Hz, 1H), 7.64 (t, J = 6.9 Hz, 1H), 7.38 (d, J = 6.9 Hz, 1H), 7.16 (d, J = 7.6 Hz, 1H), 5.11 (q, J = 6.0 Hz, 1H), 4.68 (t, J = 11.7 Hz, 2H), 4.33 (t, J = 5.5 Hz, 2H), 4.12 (d, J = 14.4 Hz, 1H), 3.99 (d, J = 8.2 Hz, 3H), 3.81 (s, 2H), 3.47 (t, J = 7.2 Hz, 2H), 3.22 (t, J = 6.9 Hz, 2H), 3.15 (d, J = 11.0 Hz, 2H), 2.90-2.70 (m, 5H), 2.51-2.41 (m, 2H), 2.41-2.35 (m, 2H), 2.21-2.02 (m, 9H), 1.94-1.92 (m, 2H), 1.82-1.57 (m, 9H), 1.52-1.29 (m, 9H). 13C-NMR (151 MHz, METHANOL-D4) δ 174.5, 174.2, 171.4, 168.5, 166.9, 161.9, 161.7, 160.6, 156.9, 156.8, 151.6, 140.5, 136.8, 133.0, 125.3, 117.2, 107.1, 104.1, 100.9, 68.2, 57.2, 55.4, 54.2, 51.3, 50.4, 46.0, 45.6, 42.0, 34.1, 32.8,

32.2, 32.0, 31.9, 30.8, 30.3, 30.1, 27.7, 26.8, 26.6, 26.6, 24.0, 23.7. HRMS (ESI) calcd. for $C_{49}H_{66}N_9O_8$ $[M+H]^+$ 908.5034, found 908.5020.

1-(11-(4-((2-cyclohexyl-6-methoxy-7-(3-(pyrrolidin-1-yl)propoxy)quinazolin-4-yl)amino)piperidin-1-yl)-11-oxoundecyl)-3-(2-(2,6-dioxopiperidin-3-yl)-1,3-dioxoisoindolin-4-yl)urea (A7). To the mixture of **A44** (37.5 mg, 0.075 mmol), **A16** (35 mg, 0.075 mmol), HATU (57 mg, 0.15 mmol) in DMF (2 ml) was added DIPEA (65 µL, 0.375 mmol) and the reaction mixture was stirred at 23 °C for 18 h. Then diluted with water and extracted with ethyl acetate and the organic layer was washed with brine and then dried over anhy. Na_2SO_4, filtered and concentrated to obtain the crude product. The crude product was purified on N-H silica gel column using acetone/CH_2Cl_2 = 2/3 followed by preparative HPLC (15%-30% MeCN-Miliq for 30 minutes then 50% for 30-50 min) to obtain the title compound (17%) as white solid. ^{1}H-NMR (600 MHz, METHANOL-D4) δ 8.56 (d, J = 8.9 Hz, 1H), 7.80 (s, 1H), 7.66 (t, J = 7.9 Hz, 1H), 7.38 (d, J = 6.5 Hz, 1H), 7.16 (s, 1H), 5.12 (q, J = 6.0 Hz, 1H), 4.70-4.66 (m, 2H), 4.33 (t, J = 5.5 Hz, 2H), 4.12 (d, J = 13.7 Hz, 1H), 3.99 (s, 3H), 3.82 (s, 2H), 3.49-3.43 (m, 2H), 3.20 (t, J = 7.2 Hz, 2H), 3.15 (dd, J = 18.6, 7.6 Hz, 2H), 2.90-2.81 (m, 3H), 2.77-2.69 (m, 2H), 2.44 (dd, J = 7.7, 6.0 Hz, 2H), 2.38-2.34 (m, 2H), 2.22-2.02 (m, 9H), 1.93 (d, J = 11.7 Hz, 2H), 1.82-1.60 (m, 6H), 1.57-1.46 (m, 3H), 1.37-1.29 (m, 15H). ^{13}C-NMR (151 MHz, METHANOL-D4) δ 173.2, 172.9, 170.1, 168.8, 167.2, 165.5, 159.3, 155.4, 150.3, 139.2, 135.4, 135.1, 131.7, 124.0, 115.8, 105.8, 102.8, 99.6, 66.9, 55.8, 54.1, 52.8, 50.0, 49.1, 44.7, 44.2, 40.6, 32.8, 31.4, 30.8, 30.6, 30.5, 29.5, 29.2, 29.1, 29.0, 29.0, 26.5, 25.4, 25.3, 25.2, 22.6, 22.3. HRMS (ESI) calcd. for $C_{52}H_{72}N_9O_8$ $[M+H]^+$ 950.5504, found 950.5514.

11-((tert-butoxycarbonyl)amino)undecanoic acid (B8). A solution of 11-aminoundecanoic acid **B7** (1 g, 4.98 mmol) in THF (14 mL) was prepared, and an aqueous solution of sodium hydroxide (238 mg, 5.97 mmol in 1.8 mL of water) was added. At 0°C, Boc_2O (2.7 g, 12.4 mmol) was introduced, and the reaction mixture was allowed to warm to room temperature.

After stirring for 15 hours, the reaction mixture was quenched with water and extracted three times with EtOAc (50 mL). The combined organic layers were washed with water and brine, dried over anhydrous sodium sulfate, and concentrated under reduced pressure. The residue was purified by flash column chromatography, using a gradient of 0-30% EtOAc-Hexane, to yield the title compound (85%) as a white solid. ^{1}H-NMR (400 MHz, CHLOROFORM-D) δ 4.54 (s, 1H), 3.10 (d, J = 6.4 Hz, 2H), 2.34 (t, J = 7.3 Hz, 2H), 1.67-1.59 (m, 2H), 1.44 (s, 11H), 1.27 (s, 12H). ^{13}C-NMR (101 MHz, CHLOROFORM-D) δ 179.4, 156.2, 79.2, 40.7, 34.2, 30.1, 29.5, 29.4, 29.3, 29.1, 28.6, 26.9, 24.8. HRMS (ESI) calcd. for $C_{16}H_{31}NO_4Na$ $[M+Na]^+$ 324.2151, found 324.2141.

tert-butyl-(11-(((S)-1-((2R,4R)-4-hydroxy-2-((4-(4-methylthiazol-5-yl)benzyl)carbamoyl)pyrrolidin-1-yl)-3,3-dimethyl-1-oxobutan-2-yl)amino)-11-oxoundecyl)carbamate (B9). A solution of **B8** (349 mg, 1.16 mmol), (2R,4R)-1-((S)-2-amino-3,3-dimethylbutanoyl)-4-hydroxy-N-(4-(4-methylthiazol-5-yl)benzyl)pyrrolidine-2-carboxamide (VHL-1 ligand) (542 mg, 1.16 mmol), and HOBt·H_2O (266 mg, 1.74 mmol) in DMF (7 mL) was prepared. To this solution, DIPEA (1 mL, 5.8 mmol) and EDCI·HCl (334 mg, 1.74 mmol) were added at 0°C under an argon atmosphere. The reaction mixture was stirred overnight at room temperature, then quenched with water. The aqueous layer was separated and extracted with ethyl acetate. The combined organic layers were washed with water and brine, dried over anhydrous sodium sulfate, filtered, and concentrated under reduced pressure. The residue was purified by flash column chromatography, using a 0-7% methanol-dichloromethane gradient, to yield the title compound (62%) as a white solid. ^{1}H-NMR (600 MHz, CHLOROFORM-D) δ 8.69 (s, 1H), 7.38-7.30 (m, 5H), 6.18 (d, J = 8.2 Hz, 1H), 4.71 (t, J = 7.9 Hz, 1H), 4.58-4.49 (m, 4H), 4.34 (dd, J = 14.8, 5.2 Hz, 1H), 4.08 (d, J = 11.7 Hz, 1H), 3.62 (dd, J = 11.0, 3.4 Hz, 2H), 3.09 (d, J = 6.2 Hz, 2H), 2.49 (dd, J = 7.9, 5.2 Hz, 4H), 2.18 (d, J = 7.6 Hz, 2H), 2.05-2.12 (1H), 1.58 (q, J = 6.6 Hz, 2H), 1.44 (s, 11H), 1.25 (d, J = 6.9 Hz,

12H), 0.93 (s, 9H). ^{13}C-NMR (101 MHz, CHLOROFORM-D) δ 173.7, 171.8, 170.7, 155.9, 150.3, 148.4, 138.0, 131.5, 130.9, 129.4, 128.0, 78.9, 69.9, 58.5, 57.3, 56.6, 43.2, 40.5, 36.4, 35.8, 34.9, 29.9, 29.3, 29.1, 28.4, 26.7, 26.3, 25.5, 16.0. HRMS (ESI) calcd. for $C_{38}H_{59}N_5O_6SNa$ $[M+Na]^+$ 736.4084, found 736.4070.

2,2-dimethyl-4-oxo-3,8,11,14-tetraoxa-5-azaheptadecan-17-oic acid (B12). A solution of 3-(2-(2-(2-aminoethoxy)ethoxy)ethoxy)propanoic acid **B11** (1.1 g, 4.98 mmol) in THF (14 mL) was prepared, and an aqueous solution of sodium hydroxide (238 mg, 5.97 mmol in 1.8 mL of water) was added. At 0°C, Boc_2O (2.7 g, 12.4 mmol) was introduced, and the reaction mixture was allowed to warm to room temperature. After stirring for 15 hours, the reaction mixture was quenched with water and extracted three times with EtOAc (50 mL). The combined organic layers were washed with water and brine, dried over anhydrous sodium sulfate, and concentrated under reduced pressure. The residue was purified by flash column chromatography, using a gradient of 0-10% MeOH-DCM, to yield the title compound (55%) as a sticky solid. ^{1}H-NMR (600 MHz, CHLOROFORM-D) δ 5.18 (s, 1H), 3.77 (d, J = 3.1 Hz, 2H), 3.65-3.63 (m, 8H), 3.54 (d, J = 19.2 Hz, 2H), 3.30 (d, J = 22.0 Hz, 2H), 2.64-2.58 (m, 2H), 1.45 (s, 9H). ^{13}C-NMR (151 MHz, CHLOROFORM-D) δ 175.0, 156.4, 79.6, 70.7, 70.4, 69.9, 66.6, 66.3, 41.8, 40.5, 35.0, 28.5. HRMS (ESI) calcd. for $C_{14}H_{28}NO_7$ $[M+H]^+$ 322.1866, found 322.1858.

tert-butyl ((S)-14-((2S,4R)-4-hydroxy-2-((4-(4-methylthiazol-5-yl)benzyl)carbamoyl)pyrrolidine-1-carbonyl)-15,15-dimethyl-12-oxo-3,6,9-trioxa-13-azahexadecyl)carbamate (B15). A solution of **B12** (372 mg, 1.16 mmol), VHL-1 ligand (542 mg, 1.16 mmol), and HOBt·H_2O (266 mg, 1.74 mmol) in DMF (7 mL) was prepared. To this solution, DIPEA (1 mL, 5.8 mmol) and EDCI·HCl (334 mg, 1.74 mmol) were added at 0°C under an argon atmosphere. The reaction mixture was stirred overnight at room temperature, then quenched with water. The aqueous layer was separated and extracted with ethyl acetate.

The combined organic layers were washed with water and brine, dried over anhydrous sodium sulfate, filtered, and concentrated under reduced pressure. The residue was purified by flash column chromatography, using a 0-8% methanol-dichloromethane gradient, to yield the title compound (65%) as a white solid. ^{1}H-NMR (600 MHz, CHLOROFORM-D) δ 8.68 (s, 1H), 8.01 (s, 1H), 7.46 (s, 1H), 7.37-7.34 (m, 4H), 7.00 (d, J = 7.9 Hz, 1H), 5.25 (s, 1H), 4.71 (t, J = 8.2 Hz, 1H), 4.58-4.50 (m, 3H), 4.35 (dd, J = 15.1, 5.5 Hz, 1H), 4.10-4.03 (m, 2H), 3.81-3.68 (m, 2H), 3.64-3.57 (m, 9H), 3.49 (dd, J = 24.7, 4.8 Hz, 2H), 3.30 (d, J = 4.8 Hz, 2H), 2.94-2.99 (2H), 2.88 (s, 2H), 2.53-2.49 (m, 6H), 2.34 (s, 5H), 2.17-2.13 (m, 1H), 0.95 (s, 9H). ^{13}C-NMR (151 MHz, CHLOROFORM-D) δ 172.2, 171.7, 171.1, 162.7, 156.2, 150.4, 148.5, 138.3, 131.7, 131.0, 129.6, 128.2, 79.3, 70.5, 70.4, 70.2, 67.2, 58.7, 57.7, 56.9, 43.3, 40.5, 36.7, 36.6, 36.2, 35.1, 31.6, 28.5, 26.5, 16.1. HRMS (ESI) calcd. for $C_{36}H_{55}N_5O_9SNa$ $[M+Na]^+$ 756.3618, found 756.3676.

tert-butyl (2-(2-(3-(((S)-1-((2S,4R)-4-hydroxy-2-((4-(4-methylthiazol-5-yl)benzyl)carbamoyl)pyrrolidin-1-yl)-3,3-dimethyl-1-oxobutan-2-yl)amino)-3-oxopropoxy)ethoxy)ethyl)carbamate(B16). A solution of **B13** (321 mg, 1.16 mmol), VHL-1 ligand (542 mg, 1.16 mmol), and HOBt·H_2O (266 mg, 1.74 mmol) in DMF (7 mL) was prepared. To this solution, DIPEA (1 mL, 5.8 mmol) and EDCI·HCl (334 mg, 1.74 mmol) were added at 0°C under an argon atmosphere. The reaction mixture was stirred overnight at room temperature, then quenched with water. The aqueous layer was separated and extracted with ethyl acetate. The combined organic layers were washed with water and brine, dried over anhydrous sodium sulfate, filtered, and concentrated under reduced pressure. The residue was purified by flash column chromatography, using a 0-8% methanol-dichloromethane gradient, to yield the title compound (68%) as a white solid.

tert-butyl (2-(3-(((S)-1-((2S,4R)-4-hydroxy-2-((4-(4-methylthiazol-5-yl)benzyl)carbamoyl)pyrrolidin-1-yl)-3,3-dimethyl-1-oxobutan-2-yl)amino)-3-

oxopropoxy)ethyl)carbamate (B17). A solution of **B14** (270 mg, 1.16 mmol), VHL-1 ligand (542 mg, 1.16 mmol), and HOBt·H_2O (266 mg, 1.74 mmol) in DMF (7 mL) was prepared. To this solution, DIPEA (1 mL, 5.8 mmol) and EDCI·HCl (334 mg, 1.74 mmol) were added at 0°C under an argon atmosphere. The reaction mixture was stirred overnight at room temperature, then quenched with water. The aqueous layer was separated and extracted with ethyl acetate. The combined organic layers were washed with water and brine, dried over anhydrous sodium sulfate, filtered, and concentrated under reduced pressure. The residue was purified by flash column chromatography, using a 0-8% methanol-dichloromethane gradient, to yield the title compound (66%) as a white solid.

tert-butyl(10-((2-(2,6-dioxopiperidin-3-yl)-1,3-dioxoisoindolin-4-yl)amino)decyl)carbamate (B23). To a mixture of tert-butyl (10-aminodecyl)carbamate **B21** (1.48, 5.4 mmol) and DIPEA (~3.8mL, 21.6 mmol) in DMF (11 mL) was added thalidomide 4-fluoride **B22** (1 g, 3.6 mmol). The reaction mixture was stirred under reflux for 14 h, then cooled to room temperature, diluted with water, and extracted with AcOEt. The organic layer was washed with brine and dried over Na_2SO_4. Filtration, concentration, and purification by flash column chromatography (0-40% AcOEt/Hexane) afforded the title compound (57%) as a yellow solid. ^{1}H-NMR (400 MHz, DMSO-D6) δ 11.09 (s, 1H), 7.57 (t, J = 7.8 Hz, 1H), 7.08 (d, J = 8.7 Hz, 1H), 7.01 (d, J = 6.9 Hz, 1H), 6.74 (s, 1H), 6.52 (t, J = 5.7 Hz, 1H), 5.04 (dd, J = 12.8, 5.5 Hz, 1H), 3.32-3.25 (m, 4H), 2.92-2.84 (m, 3H), 2.03-1.98 (m, 1H), 1.56 (t, J = 6.4 Hz, 2H), 1.35-1.17 (m, 23H).

tert-butyl (4-(2,6-dioxopiperidin-3-yl)phenyl)glycinate (B31). To 3-(4-aminophenyl)piperidine-2,6-dione (50 mg, 0.25 mmol) in acetonitrile (1 mL) at room temperature was added N,N-diisopropylethylamine (0.085 mL, 0.49 mmol) followed by tert-butyl bromoacetate (0.040 mL, 0.27 mmol). The reaction mixture was stirred at 60 °C for 2 h, then cooled to room temperature. The crude mixture was diluted with ethyl acetate (15 mL) and washed with brine (3 x 10 mL). The organic phase was dried over anhydrous sodium sulfate,

filtered, and concentrated in vacuo. Purification was done on N-H silica gel column using 10%-50% ethyl acetate gradient in hexanes to provide the title compound (32.5 mg, 42% yield). 1H-NMR (400 MHz, CHLOROFORM-D) δ 7.95 (s, 1H), 7.03 (dd, J = 6.4, 1.8 Hz, 2H), 6.59 (dd, J = 6.6, 2.1 Hz, 2H), 4.33 (s, 1H), 3.79 (s, 2H), 3.70 (q, J = 4.7 Hz, 1H), 2.76-2.58 (m, 2H), 2.29-2.16 (m, 2H), 1.50 (s, 9H).

ethyl 3,6,6-trimethyl-4-oxo-4,5,6,7-tetrahydro-1H-indole-2-carboxylate (B35). To a stirred solution of ethyl acetoacetate **B34** (464 mg, 3.57 mmol, 1 eq) in glacial acetic acid (3 ml) cooled to 5°C was added dropwise a solution of $NaNO_2$ (239 mg, 3.46 mmol, 0.97 eq) in distilled water (0.5 ml) at a rate such that the temperature does not exceed about 7°C. The reaction mixture was stirred at 5°C for about 30 min before allowing to stand at ambient for around 3 h. A solution of 95% Zn dust (490 mg, 7.14 mmol, 2 eq), sodium acetate (1.2 g, 14.28 mmol, 4 eq) and 5,5-dimethylcyclohexane-1,3-dione **B33** (500 mg, 3.57 mmol, 1 eq) in glacial acetic acid (6 ml) was then added to the reaction mixture before refluxing the fully charged vessel for approximately 1 hour. The reaction mixture was then poured over distilled water and, having left to stand overnight, the product was filtered by suction, washed (H_2O) and subjected to flash column chromatography (0%-15% EtOAc/Hexane) to obtain the title compound (45%) as beige solid. 1H-NMR (400 MHz, CHLOROFORM-D) δ 9.00 (s, 1H), 4.34 (q, J = 7.2 Hz, 2H), 2.66 (s, 2H), 2.60 (s, 3H), 2.35 (s, 2H), 1.38 (t, J = 7.1 Hz, 3H), 1.11 (s, 6H). 13C-NMR (101 MHz, CHLOROFORM-D) δ 194.9, 162.1, 144.2, 128.4, 120.0, 119.4, 60.6, 53.1, 37.1, 35.4, 28.6, 14.6, 11.6. HRMS (ESI) calcd. for $C_{14}H_{20}NO_3$ $[M+H]^+$ 250.1443, found 250.1435.

3,6,6-trimethyl-4-oxo-4,5,6,7-tetrahydro-1H-indole-2-carboxylic acid (B36). To a suspension of **B35** (35 mg, 0.14 mmol) in ethanol (2 mL), 30% NaOH (0.5 mL) was added. The mixture was heated under reflux for overnight, then cooled and washed with ethyl ether. The aqueous extract was acidified with 6 N HCl and the solid precipitated was filtered off and dried to furnish the title compound (97%) as beige solid. 1H-NMR (600 MHz, METHANOL-D4) δ

2.67 (d, J = 17.9 Hz, 2H), 2.54 (s, 3H), 2.32 (s, 2H), 1.09 (s, 6H). 13C-NMR (151 MHz, METHANOL-D4) δ 197.7, 164.5, 147.2, 129.3, 121.7, 119.6, 53.7, 37.3, 36.2, 28.6, 11.7. HRMS (ESI) calcd. for $C_{12}H_{16}NO_3$ $[M+H]^+$ 222.1130, found 222.1122.

diethyl 2-acetamido-2-(but-3-en-1-yl)malonate (B38). A stirred suspension of sodium hydride (4.60 g of 60% NaH in mineral oil, 115 mmol) in anhydrous DMF (100 mL) was cooled to 0°C, under an argon atmosphere. A solution of diethyl acetamidomalonate **B37** (22.68 g, 105 mmol) in anhydrous DMF (80 mL) was then added over a period of 10 minutes via a syringe with an efficient exit ensured to compensate for effervescence of H_2. The ice bath was removed and the reaction mixture was stirred for 20 minutes at room temperature before adding 4-bromo-1-butene (7.5 mL, 74.1 mmol). The light brown solution was then stirred at 90°C for 4 hours before re-cooling to 0°C. The reaction was then quenched with saturated NH_4Cl (aq) until no bubbling was observed and then diluted with water (600 mL). The mixture was extracted with Et_2O (100 mL) and the two layers were separated. The aqueous layer was extracted with EtOAC (200 mL) twice and the combined organic extracts were washed with water (200 mL) and brine (150 mL), dried over sodium sulphate and concentrated under reduced pressure to yield a dark yellow which was purified using flash column chromatography with gradient 0-40% EtOAc-Hexane to afford the title compound (75%) as clear oil that crystallized on storage at −20 °C. ^{1}H-NMR (600 MHz, CHLOROFORM-D) δ 6.79 (s, 1H), 5.78-5.71 (m, 1H), 5.03-4.95 (m, 2H), 4.26-4.23 (m, 4H), 2.46-2.43 (m, 2H), 2.04 (s, 3H), 1.93-1.89 (m, 2H), 1.30-1.23 (m, 6H).

diethyl 2-acetamido-2-(2-cyclopropylethyl)malonate (B39). To a stirred solution of **B38** in DCM (70 mL) at 0°C, diiodomethane (7.7 mL, 96 mmol) and diethyl zinc (48 mL of ZnEt2, 1 M in hexane solution, 48 mmol) were added, respectively. The reaction mixture was then stirred for an additional 10 minutes at 0°C. Subsequently, the reaction mixture was allowed to come to room temperature and stirred for 24 h. The reaction mixture was quenched with 1M HCl.

DCM and hexane were removed under reduced pressure, and the residue was dissolved in EtOAc (150 mL), filtered, and extracted with water. The aqueous layer was separated and extracted twice with ethyl acetate (50 mL). The combined organic layer was washed with water and brine, dried over anhydrous sodium sulphate, and concentrated under reduced pressure. The residue was purified using flash column chromatography with a gradient of 0-40% EtOAc-Hexane to afford the title compound (78%) as a colourless oil. ^{1}H-NMR (600 MHz, CHLOROFORM-D) δ 6.73 (s, 1H), 4.22 (q, J = 7.1 Hz, 4H), 2.44-2.41 (m, 2H), 2.01 (s, 3H), 1.24 (t, J = 7.2 Hz, 6H), 1.02-0.98 (m, 2H), 0.65-0.59 (m, 1H), 0.39 (q, J = 6.0 Hz, 2H), -0.05 (q, J = 4.8 Hz, 2H). ^{13}C-NMR (151 MHz, CHLOROFORM-D) δ 169.0, 168.4, 77.4, 77.2, 76.9, 66.5, 62.6, 32.2, 29.1, 23.2, 14.1, 10.6, 4.7. HRMS (ESI) calcd. for $C_{14}H_{23}NO_5Na$ $[M+Na]^+$ 308.1474, found 308.1464.

2-acetamido-4-cyclopropylbutanoic acid (B40). Sodium hydroxide (818 mg, 20.5 mmol) was added in one portion to a solution of **B39** (5.3 g, 18.6 mmol) in water and ethanol (1 : 1, 40 mL). After stirring at reflux for 16 h the reaction mixture was cooled and ethanol was removed under reduced pressure. The remaining aqueous solution was washed with Et_2O (100 mL) and then acidified with 2 M HCl. The resulting emulsion was extracted three times with EtOAc and the combined organic layers were dried over sodium sulphate and concentrated under reduced pressure to yield the title compound (87%) as white solid. ^{1}H-NMR (600 MHz, METHANOL-D4) δ 4.40 (q, J = 4.8 Hz, 1H), 1.97 (d, J = 7.2 Hz, 3H), 1.97-1.92 (m, 1H), 1.80-1.74 (m, 1H), 1.32-1.26 (m, 2H), 0.72-0.65 (m, 1H), 0.45-0.41 (m, 2H), 0.04 (td, J = 5.3, 4.1 Hz, 2H). ^{13}C-NMR (151 MHz, METHANOL-D4) δ 175.7, 173.4, 53.5, 32.6, 32.0, 22.3, 11.2, 5.1, 4.6. HRMS (ESI) calcd. for $C_9H_{15}NO_3Na$ $[M+Na]^+$ 208.0950, found 208.0942.

(S)-2-((tert-butoxycarbonyl)amino)-4-cyclopropylbutanoic acid (B42). **B40** (3 g, 16.2 mmol) was dissolved in water (43 mL) and the pH was adjusted to 7.5 with 5 M NaOH solution, warmed up to 37°C. Aspergillus genus (600 mg) was added with gentle stirring and the pH was

maintained to 7.5. The reaction mixture was then allowed to stir at room temperature for 12 h. The volume of the solution was then reduced in vacuo (20 mL), ethanol (500 mL) was added and the resulting white solid was collected by filtration. The volume of the filtrate was again reduced in vacuo and more ethanol (400 mL) was added and a second precipitate was collected. Finally, 1.2 g (80% with respect to one isomer) of (S)-2-amino-4-cyclopropylbutanoic acid **B41** was obtained as an off-white solid which was directly used in the next step without further purification. Now, **B41** (1 g, 7 mmol) and sodium carbonate (2.4 g, 22.6 mmol) were dissolved in a water/THF mixture (20 ml, 1 : 1). Boc_2O (2.7 g, 12.4 mmol) was added at 0°C and the reaction mixture was allowed to warm to room temperature. After 24 h stirring the reaction mixture was acidified (pH = 2) with 1 M HCl and extracted thrice with EtOAc (50 mL). The combined organic layer was washed with water and brine, dried over anhydrous sodium sulphate, and concentrated under reduced pressure. The residue was purified using flash column chromatography with a gradient of 0-50% EtOAc-Hexane to afford the title compound (40% over two steps). 1H-NMR (400 MHz, CHLOROFORM-D) δ 4.99 (d, J = 7.8 Hz, 1H), 4.34 (d, J = 5.0 Hz, 1H), 1.98 (s, 1H), 1.77 (q, J = 6.6 Hz, 1H), 1.45 (s, 9H), 1.31-1.24 (m, 2H), 0.70-0.63 (m, 1H), 0.44 (d, J = 8.2 Hz, 2H), 0.09-0.04 (m, 2H). ^{13}C-NMR (101 MHz, CHLOROFORM-D) δ 178.2, 156.1, 80.7, 53.6, 32.7, 30.8, 28.8, 10.8, 5.0, 4.8. HRMS (ESI) calcd. for $C_{12}H_{21}NO_4Na$ $[M+Na]^+$ 266.1368, found 266.1361.

methyl (S)-4-(2-((tert-butoxycarbonyl)amino)-4-cyclopropylbutanamido)benzoate (B43). To the solution of **B42** (843 mg, 3.5 mmol), methyl 4-aminobenzoate (529 mg, 3.5 mmol), HATU (2.7 g, 7 mmol) in DMF (10 ml) was added DIPEA (3 mL, 17.5 mmol) and the reaction mixture was stirred at room temperature for 18 h. Then diluted with water and extracted with ethyl acetate and the organic layer was washed with brine and then dried over anhy. Na_2SO_4, filtered and concentrated to obtain the crude product. The crude product was purified with flash column chromatography with gradient 0 to 25 % ethyl acetate-hexane to afford the title compound

(48 %) as a white solid. ^{1}H-NMR (400 MHz, CHLOROFORM-D) δ 8.93 (s, 1H), 7.97-7.88 (m, 2H), 7.55 (d, J = 8.7 Hz, 2H), 5.21-5.16 (m, 1H), 4.30 (s, 1H), 3.90 (s, 3H), 2.08-1.99 (m, 1H), 1.83-1.75 (m, 1H), 1.45 (s, 9H), 1.37-1.24 (m, 2H), 0.72-0.63 (m, 1H), 0.47-0.39 (m, 2H), 0.07-0.00 (m, 2H). ^{13}C-NMR (101 MHz, CHLOROFORM-D) δ 171.2, 166.7, 156.7, 142.2, 130.8, 125.6, 119.0, 80.9, 55.3, 52.1, 31.7, 30.9, 28.4, 10.5, 4.7, 4.5. HRMS (ESI) calcd. for $C_{20}H_{28}N_2O_5Na$ $[M+Na]^+$ 399.1896, found 399.1891.

methyl (S)-4-(4-cyclopropyl-2-(3,6,6-trimethyl-4-oxo-4,5,6,7-tetrahydro-1H-indole-2-carboxamido)butanamido)benzoate (B45). To the solution of **B43** at room temperature in DCM (13 mL) under a nitrogen atmosphere was added trifluoroacetic acid (7.3 mL, 96 mmol). After 1.5 h the reaction mixture was concentrated in vacuo to provide the crude amine which was further purified by flash column chromatography with gradient 0-10% MeOH-DCM to provide the corresponding amine **B44** as a white solid. Now, to a solution of **B36** (200 mg, 0.9 mmol), **B44** (249 mg, 0.9 mmol), and HOBt-H_2O (165 mg, 1.08 mmol) in DMF (4.5 mL) were added DIPEA (0.6 ml, 3.6 mmol) and EDCI-HCl (207 mg, 1.08 mmol) at 0°C under argon atmosphere. The reaction mixture was stirred overnight at ambient temperature before being quenched with water. The aqueous layer was separated and extracted with ethyl acetate. The combined organic layer was washed with water and brine, dried over anhydrous sodium sulphate, and concentrated under reduced pressure after filtration. The residue was purified with flash column chromatography with gradient 0 to 70 % ethyl acetate-hexane to afford the title compound (48% over 2 steps) as white solid. ^{1}H-NMR (600 MHz, DMSO-D6) δ 11.67 (s, 1H), 10.50 (s, 1H), 7.95-7.89 (m, 2H), 7.76 (t, J = 8.9 Hz, 2H), 7.70 (d, J = 7.6 Hz, 1H), 4.58 (td, J = 8.3, 5.4 Hz, 1H), 3.82 (s, 3H), 2.64 (d, J = 1.7 Hz, 2H), 2.46 (s, 3H), 2.22 (s, 2H), 1.93-1.79 (m, 2H), 1.37-1.24 (m, 2H), 1.02 (d, J = 2.7 Hz, 6H), 0.75-0.68 (m, 1H), 0.40-0.35 (m, 2H), 0.05--0.01 (m, 2H). 13C-NMR (151 MHz, DMSO-D6) δ 194.0, 171.9, 166.0, 161.3, 143.6, 143.5, 130.5, 124.2, 122.8, 122.6, 118.8, 117.6, 53.8, 52.8, 52.1, 36.0, 35.1, 32.1, 30.7, 28.2,

28.2, 11.4, 10.5, 4.7, 4.4. HRMS (ESI) calcd. for $C_{27}H_{34}N_3O_5$ $[M+H]^+$ 480.2498, found 480.2487.

N-((S)-4-cyclopropyl-1-((4-((11-(((S)-1-((2R,4R)-4-hydroxy-2-((4-(4-methylthiazol-5-yl)benzyl)carbamoyl)pyrrolidin-1-yl)-3,3-dimethyl-1-oxobutan-2-yl)amino)-11-oxoundecyl)carbamoyl)phenyl)amino)-1-oxobutan-2-yl)-3,6,6-trimethyl-4-oxo-4,5,6,7-tetrahydro-1H-indole-2-carboxamide (B1). An aqueous solution of NaOH (4N, 1.8 ml) was added to a solution of **B45** (284 mg, 0.6 mmol) in MeOH (3 ml), and the mixture was stirred at room temperature overnight. The solvent was removed under reduced pressure and extracted three times with AcOEt and water. Water layer was collected and acidified to pH 4 using 2 N HCl, extracted thrice with ethyl acetate and the combined organic layer was washed with water and brine, dried over anhydrous sodium sulphate, and concentrated under reduced pressure after filtration to afford the corresponding acid **B46** (78%) as a white solid and was directly used without further purification.

To a solution of **B9** (300 mg, 0.42 mmol) in DCM (5 mL) at room temperature under a nitrogen atmosphere, trifluoroacetic acid (3.3 mL, 43.3 mmol) was added. After 2 hours, the reaction mixture was concentrated in vacuo to yield the crude amine, which was then purified by flash column chromatography using a 0-10% MeOH-dichloromethane gradient using amino silica, affording the corresponding amine **B10** as a white solid.

Subsequently, to a solution of **B46** (40 mg, 0.086 mmol), **B10** (53 mg, 0.086 mmol), and HOBt·H_2O (27 mg, 0.172 mmol) in DMF (1.5 mL), DIPEA (75 µL, 0.43 mmol) and EDCI·HCl (33 mg, 0.172 mmol) were added at 0°C under an argon atmosphere. The reaction mixture was stirred overnight at room temperature, then quenched with water. The aqueous layer was separated and extracted with ethyl acetate. The combined organic layers were washed with water and brine, dried over anhydrous sodium sulfate, filtered, and concentrated under reduced

pressure. The residue was purified by flash column chromatography, using a 0-5% methanol-chloroform gradient, to afford the title compound (42% over 2 steps) as a white solid. ^{1}H-NMR (600 MHz, CHLOROFORM-D) δ 10.37 (s, 1H), 9.94 (s, 1H), 8.67 (s, 1H), 7.68 (d, *J* = 10.5 Hz, 1H), 7.55 (s, 2H), 7.43 (d, J = 6.2 Hz, 2H), 7.34-7.29 (m, 5H), 6.94 (s, 1H), 6.66 (s, 1H), 4.83 (s, 1H), 4.77-4.75 (m, 1H), 4.59 (d, *J* = 8.6 Hz, 1H), 4.53 (s, 1H), 4.40-4.34 (m, 3H), 4.10 (d, *J* = 10.3 Hz, 1H), 3.66 (d, *J* = 8.1 Hz, 1H), 3.40-3.35 (m, 2H), 2.56 (s, 3H), 2.48 (s, 3H), 2.37 (s, 1H), 2.30-2.23 (m, 1H), 2.20-2.12 (m, 2H), 2.07-2.02 (m, 2H), 1.88 (s, 7H), 1.58 (s, 2H), 1.45 (s, 2H), 1.33-1.25 (m, 7H), 1.14 (s, 7H), 1.02 (d, *J* = 13.1 Hz, 4H), 0.97-0.93 (m, 9H), 0.58 (s, 1H), 0.31 (d, *J* = 7.4 Hz, 2H), -0.09 (d, *J* = 4.8 Hz, 2H). ^{13}C-NMR (176 MHz, CDCl3) δ 195.3, 173.9, 171.9, 171.1, 167.6, 162.3, 150.4, 148.3, 144.2, 140.6, 138.1, 131.6, 130.8, 130.3, 129.4, 127.9, 127.8, 127.7, 121.7, 119.0, 118.8, 69.9, 59.0, 57.7, 57.1, 54.5, 52.9, 42.9, 39.9, 36.7, 36.6, 36.3, 36.2, 35.2, 35.1, 35.0, 32.1, 31.9, 30.9, 30.8, 29.7, 29.6, 29.3, 29.3, 29.1, 28.9, 28.9, 28.7, 28.4, 26.5, 26.4, 25.5, 22.7, 16.0, 14.1, 11.6, 10.4, 4.7, 4.6, 4.4, 4.4, 1.8, 1.1, 1.0, -0.03. HRMS (ESI) calcd. for $C_{59}H_{80}N_8O_8SNa$ $[M+Na]^+$ 1083.5718, found 1083.5698.

N-((2S)-4-cyclopropyl-1-((4-((10-((2-(2,6-dioxopiperidin-3-yl)-1,3-dioxoisoindolin-4-yl)amino)decyl)carbamoyl)phenyl)amino)-1-oxobutan-2-yl)-3,6,6-trimethyl-4-oxo-4,5,6,7-tetrahydro-1H-indole-2-carboxamide (B2). To a solution of **B23** (700 mg, 1.3 mmol) in DCM (15 mL) at room temperature under a nitrogen atmosphere, trifluoroacetic acid (10 mL) was added. After 1 hour, the reaction mixture was concentrated in vacuo to yield the crude amine, which was further purified by flash column chromatography using a 0-10% MeOH-DCM gradient to afford the corresponding amine **B24** as a yellow solid.

Subsequently, to a mixture of **B46** (50 mg, 0.11 mmol), **B24** (46 mg, 0.11 mmol), and HOBt·H_2O (34 mg, 0.22 mmol) in DMF (1.5 mL), DIPEA (100 µL, 0.55 mmol) and EDCI·HCl (42 mg, 0.22 mmol) were added at 0°C under an argon atmosphere. The reaction mixture was stirred overnight at room temperature, then quenched with water. The aqueous layer was

separated and extracted with ethyl acetate. The combined organic layers were washed with water and brine, dried over anhydrous sodium sulfate, filtered, and concentrated under reduced pressure. The residue was purified by flash column chromatography using a 0-5% methanol-chloroform gradient, followed by preparative HPLC, to yield the title compound (34% over 2 steps) as a yellow solid. ^{1}H-NMR (700 MHz, METHANOL-D4) δ 7.79 (d, *J* = 8.6 Hz, 2H), 7.70 (d, *J* = 8.6 Hz, 2H), 7.53 (t, *J* = 7.7 Hz, 1H), 7.01 (d, *J* = 7.7 Hz, 2H), 5.05 (dd, *J* = 13.3, 4.7 Hz, 1H), 4.68 (dd, *J* = 8.6, 5.6 Hz, 1H), 3.36-3.34 (m, 1H), 2.87-2.82 (m, 1H), 2.75-2.68 (m, 4H), 2.56 (s, 3H), 2.32 (s, 2H), 2.10-2.03 (m, 2H), 1.96-1.92 (m, 1H), 1.65-1.58 (m, 4H), 1.41-1.25 (m, 18H), 1.09 (s, 6H), 0.78-0.73 (m, 1H), 0.45 (d, *J* = 7.3 Hz, 2H), 0.10 (s, 1H), 0.05 (d, *J* = 4.7 Hz, 2H). ^{13}C-NMR (176 MHz, METHANOL-D4) δ 198.0, 174.9, 173.6, 172.0, 169.7, 169.6, 164.0, 148.5, 146.7, 142.9, 137.5, 134.1, 131.4, 129.4, 125.3, 124.5, 120.7, 119.5, 118.2, 111.9, 111.1, 55.7, 54.0, 50.4, 43.6, 41.2, 37.6, 36.5, 33.8, 32.5, 32.4, 30.7, 30.7, 30.7, 30.6, 30.6, 30.5, 28.8, 28.2, 28.2, 24.0, 11.9, 11.6, 5.4, 5.1. HRMS (ESI) calcd. for $C_{49}H_{61}N_7O_8Na$ $[M+Na]^+$ 898.4479, found 898.4476.

N-((2S)-4-cyclopropyl-1-((4-((8-(2-((4-(2,6-dioxopiperidin-3-yl)phenyl)amino)acetamido)octyl)carbamoyl)phenyl)amino)-1-oxobutan-2-yl)-3,6,6-trimethyl-4-oxo-4,5,6,7-tetrahydro-1H-indole-2-carboxamide (B3)

To a solution of **B46** (175 mg, 0.38 mmol), tert-butyl (8-aminooctyl)carbamate (110 mg, 0.45 mmol), and HOBt·H_2O (116 mg, 0.76 mmol) in DMF (4 mL), DIPEA (330 µL, 1.9 mmol) and EDCI·HCl (146 mg, 0.76 mmol) were added at 0°C under an argon atmosphere. The reaction mixture was stirred overnight at room temperature, then quenched with water. The aqueous layer was separated and extracted with ethyl acetate. The combined organic layers were washed with water and brine, dried over anhydrous sodium sulfate, filtered, and concentrated under reduced pressure. The residue was purified by flash column chromatography, using a 30-80%

EtOAc-hexane gradient, to afford **B47** (63%) as a sticky solid. HRMS (ESI) calcd. for $C_{39}H_{57}N_5O_6Na$ $[M+Na]^+$ 714.4207, found 714.4202.

To a solution of **B47** (140 mg, 0.2 mmol) in DCM (2 mL) at room temperature under a nitrogen atmosphere, trifluoroacetic acid (1.6 mL, 20.6 mmol) was added. After 3 hours, the reaction mixture was concentrated in vacuo to yield the crude amine **B48**, which was directly used without further purification.

To a solution of **B31** (120 mg, 0.38 mmol) at room temperature in DCM (6 mL) under a nitrogen atmosphere was added trifluoroacetic acid (3 mL, 39.16 mmol). After 5 h the reaction mixture was concentrated in vacuo to provide the crude acid product **B32** which was used without purification.

To a mixture of amine **B48** (88 mg, 0.15 mmol), acid **B32** (59 mg, 0.23 mmol), and HATU (143 mg, 0.38 mmol) in DMF (2 mL), DIPEA (130 µL, 0.75 mmol) was added. The reaction mixture was stirred at 23°C for 18 hours, then diluted with water and extracted with ethyl acetate. The combined organic layers were washed with water and brine, dried over anhydrous sodium sulfate, filtered, and concentrated under reduced pressure. The residue was purified by flash column chromatography using a 0-12% methanol-chloroform gradient, followed by preparative HPLC, to yield the title compound (26% over 4 steps) as a white solid. ^{1}H-NMR (600 MHz, METHANOL-D4) δ 7.79-7.77 (m, 2H), 7.69 (d, *J* = 8.9 Hz, 2H), 7.43 (d, *J* = 8.9 Hz, 2H), 7.34 (d, *J* = 8.2 Hz, 2H), 4.69 (q, *J* = 4.8 Hz, 1H), 4.34 (s, 2H), 3.92 (q, *J* = 5.5 Hz, 1H), 3.72 (dd, *J* = 7.9, 5.2 Hz, 1H), 3.35 (t, *J* = 7.2 Hz, 2H), 3.17 (t, *J* = 6.9 Hz, 2H), 2.76-2.62 (m, 4H), 2.56 (s, 3H), 2.32 (s, 2H), 2.30-2.15 (m, 2H), 2.06 (dq, *J* = 18.7, 5.2 Hz, 1H), 1.95 (tt, *J* = 13.7, 4.8 Hz, 1H), 1.88-1.85 (m, 1H), 1.59 (q, *J* = 6.9 Hz, 2H), 1.49-1.44 (m, 2H), 1.43-1.28 (m, 10H), 1.08 (s, 6H), 0.76-0.71 (m, 1H), 0.47-0.41 (m, 2H), 0.07-0.03 (m, 2H). ^{13}C-NMR (151 MHz, METHANOL-D4) δ 197.9, 176.0, 175.7, 173.5, 169.6, 168.8, 164.0, 146.6,

142.8, 141.5, 140.6, 131.3, 130.9, 129.7, 129.3, 125.4, 124.4, 120.6, 119.4, 69.0, 55.7, 55.5, 53.9, 41.1, 40.6, 37.5, 36.4, 33.7, 32.5, 32.3, 30.6, 30.4, 30.4, 30.4, 28.7, 28.7, 28.1, 27.9, 27.8, 26.6, 11.9, 11.5, 5.3, 5.0. HRMS (ESI) calcd. for $C_{47}H_{61}N_7O_7Na$ $[M+Na]^+$ 858.4530, found 858.4539.

N-((S)-4-cyclopropyl-1-((4-(((S)-14-((2S,4R)-4-hydroxy-2-((4-(4-methylthiazol-5-yl)benzyl)carbamoyl)pyrrolidine-1-carbonyl)-15,15-dimethyl-12-oxo-3,6,9-trioxa-13-azahexadecyl)carbamoyl)phenyl)amino)-1-oxobutan-2-yl)-3,6,6-trimethyl-4-oxo-4,5,6,7-tetrahydro-1H-indole-2-carboxamide (B4). To a solution of **B15** (308 mg, 0.42 mmol) in DCM (5 mL) at room temperature under a nitrogen atmosphere, trifluoroacetic acid (3.3 mL, 43.3 mmol) was added. After 2 hours, the reaction mixture was concentrated in vacuo to yield the crude amine, which was then purified by flash column chromatography using a 0-10% MeOH-dichloromethane gradient using amino silica, affording the corresponding amine **B18** as a white solid.

Subsequently, to a solution of **B46** (40 mg, 0.086 mmol), **B18** (55 mg, 0.086 mmol), and HOBt·H_2O (27 mg, 0.172 mmol) in DMF (1.5 mL), DIPEA (75 µL, 0.43 mmol) and EDCI·HCl (33 mg, 0.172 mmol) were added at 0°C under an argon atmosphere. The reaction mixture was stirred overnight at room temperature, then quenched with water. The aqueous layer was separated and extracted with ethyl acetate. The combined organic layers were washed with water and brine, dried over anhydrous sodium sulfate, filtered, and concentrated under reduced pressure. The residue was purified by flash column chromatography, using a 0-5% methanol-chloroform gradient, to afford the title compound (41% over 2 steps) as a white solid. ^{1}H-NMR (600 MHz, CHLOROFORM-D) δ 10.24 (s, 1H), 9.68 (s, 1H), 8.67 (s, 1H), 7.83 (s, 1H), 7.62 (d, *J* = 7.6 Hz, 2H), 7.47 (d, *J* = 8.2 Hz, 2H), 7.34 (s, 4H), 7.20 (d, *J* = 6.9 Hz, 1H), 6.77 (s, 1H), 4.76-4.36 (m, 7H), 4.11 (t, *J* = 10.3 Hz, 1H), 3.75-3.35 (m, 17H), 2.61 (m, 4H), 2.49 (s, 3H), 2.36-2.27 (m, 5H), 2.16 (d, *J* = 16.5 Hz, 1H), 2.05 (s, 1H), 1.95-1.85 (m, 1H), 1.31-1.26

(m, 3H), 1.04-0.97 (m, 14H), 0.63 (s, 1H), 0.36 (d, J = 7.6 Hz, 2H), 0.00--0.05 (m, 2H). ^{13}C-NMR (151 MHz, CHLOROFORM-D) δ 195.3, 172.0, 171.6, 171.6, 171.3, 167.3, 162.4, 150.5, 148.5, 144.2, 140.9, 138.5, 131.8, 130.9, 130.0, 129.5, 128.2, 128.1, 123.4, 122.6, 119.4, 118.9, 70.6, 70.3, 70.2, 69.6, 67.1, 59.2, 57.9, 57.2, 54.3, 53.1, 43.2, 40.0, 37.4, 36.9, 36.4, 35.5, 35.3, 32.5, 30.8, 28.6, 28.5, 26.6, 26.5, 16.2, 11.6, 10.6, 4.8, 4.6. HRMS (ESI) calcd. for $C_{57}H_{76}N_8O_{11}SNa$ $[M+Na]^+$ 1103.5252, found 1103.5255.

N-((S)-4-cyclopropyl-1-((4-((2-(2-(3-(((S)-1-((2S,4R)-4-hydroxy-2-((4-(4-methylthiazol-5-yl)benzyl)carbamoyl)pyrrolidin-1-yl)-3,3-dimethyl-1-oxobutan-2-yl)amino)-3-oxopropoxy)ethoxy)ethyl)carbamoyl)phenyl)amino)-1-oxobutan-2-yl)-3,6,6-trimethyl-4-oxo-4,5,6,7-tetrahydro-1H-indole-2-carboxamide (B5). To a solution of **B16** (290 mg, 0.42 mmol) in DCM (5 mL) at room temperature under a nitrogen atmosphere, trifluoroacetic acid (3.3 mL, 43.3 mmol) was added. After 2 hours, the reaction mixture was concentrated in vacuo to yield the crude amine, which was then purified by flash column chromatography using a 0-10% MeOH-dichloromethane gradient using amino silica, affording the corresponding amine **B19** as a white solid.

Subsequently, to a solution of **B46** (40 mg, 0.086 mmol), **B19** (51 mg, 0.086 mmol), and HOBt·H_2O (27 mg, 0.172 mmol) in DMF (1.5 mL), DIPEA (75 µL, 0.43 mmol) and EDCI·HCl (33 mg, 0.172 mmol) were added at 0°C under an argon atmosphere. The reaction mixture was stirred overnight at room temperature, then quenched with water. The aqueous layer was separated and extracted with ethyl acetate. The combined organic layers were washed with water and brine, dried over anhydrous sodium sulfate, filtered, and concentrated under reduced pressure. The residue was purified by flash column chromatography, using a 0-8% methanol-chloroform gradient, to afford the title compound (43% over 2 steps) as a white solid. ^{1}H-NMR (600 MHz, CHLOROFORM-D) δ 10.60 (s, 1H), 9.86 (s, 1H), 8.67 (s, 1H), 7.91 (s, 1H), 7.68 (d, *J* = 38.5 Hz, 2H), 7.53-7.45 (m, 2H), 7.40-7.30 (m, 5H), 6.76 (s, 1H), 4.69 (d, *J* = 6.2 Hz,

1H), 4.61-4.41 (m, 5H), 4.30 (dd, *J* = 15.1, 4.8 Hz, 1H), 3.99 (d, *J* = 11.0 Hz, 1H), 3.66-3.47 (m, 12H), 3.24 (s, 1H), 2.66 (s, 1H), 2.61 (s, 4H), 2.49 (s, 3H), 2.29-2.24 (m, 4H), 2.11 (s, 1H), 2.05-1.97 (m, 1H), 1.92-1.85 (m, 1H), 1.30 (m, 3H), 1.02 (m, 14H), 0.59 (s, 1H), 0.38-0.30 (m, 2H), -0.06 (m, 2H). ^{13}C-NMR (151 MHz, CHLOROFORM-D) δ 195.3, 172.0, 171.6, 167.3, 162.7, 150.4, 148.4, 144.5, 140.7, 138.7, 131.8, 130.7, 129.4, 128.2, 127.9, 122.4, 119.5, 118.7, 70.3, 70.0, 69.8, 69.0, 66.9, 59.4, 57.7, 56.9, 54.7, 53.1, 43.2, 39.7, 37.5, 36.9, 36.3, 35.7, 35.3, 32.1, 31.0, 28.6, 28.5, 26.7, 16.2, 11.7, 10.4, 4.8, 4.6. HRMS (ESI) calcd. for $C_{55}H_{72}N_8O_{10}SNa$ $[M+Na]^+$ 1059.4990, found 1059.4980.

N-((S)-4-cyclopropyl-1-((4-((2-(3-(((S)-1-((2S,4R)-4-hydroxy-2-((4-(4-methylthiazol-5-yl)benzyl)carbamoyl)pyrrolidin-1-yl)-3,3-dimethyl-1-oxobutan-2-yl)amino)-3-oxopropoxy)ethyl)carbamoyl)phenyl)amino)-1-oxobutan-2-yl)-3,6,6-trimethyl-4-oxo-4,5,6,7-tetrahydro-1H-indole-2-carboxamide (B6). To a solution of **B17** (271 mg, 0.42 mmol) in DCM (5 mL) at room temperature under a nitrogen atmosphere, trifluoroacetic acid (3.3 mL, 43.3 mmol) was added. After 2 hours, the reaction mixture was concentrated in vacuo to yield the crude amine, which was then purified by flash column chromatography using a 0-10% MeOH-dichloromethane gradient using amino silica, affording the corresponding amine **B20** as a white solid.

Subsequently, to a solution of **B46** (40 mg, 0.086 mmol), **B20** (47 mg, 0.086 mmol), and HOBt·H_2O (27 mg, 0.172 mmol) in DMF (1.5 mL), DIPEA (75 µL, 0.43 mmol) and EDCI·HCl (33 mg, 0.172 mmol) were added at 0°C under an argon atmosphere. The reaction mixture was stirred overnight at room temperature, then quenched with water. The aqueous layer was separated and extracted with ethyl acetate. The combined organic layers were washed with water and brine, dried over anhydrous sodium sulfate, filtered, and concentrated under reduced pressure. The residue was purified by flash column chromatography, using a 0-8% methanol-chloroform gradient, to afford the title compound (44% over 2 steps) as a white solid. ^{1}H-NMR

(600 MHz, CHLOROFORM-D) δ 10.52 (s, 1H), 9.70 (s, 1H), 8.66 (s, 1H), 7.78-7.71 (m, 1H), 7.60 (m, 2H), 7.45 (s, 2H), 7.29-7.24 (m, 5H), 6.89 (s, 1H), 4.75 (s, 1H), 4.56 (m, 3H), 4.40 (s, 1H), 4.27 (d, *J* = 11.0 Hz, 1H), 3.94 (d, *J* = 6.9 Hz, 1H), 3.67-3.55 (m, 5H), 3.44 (s, 1H), 2.62-2.27 (m, 16H), 2.16 (s, 1H), 2.05 (s, 1H), 1.87 (s, 1H), 1.28 (m, 3H), 1.02-0.90 (m, 14H), 0.62 (s, 1H), 0.37 (s, 2H), -0.05 (s, 2H). ^{13}C-NMR (151 MHz, CHLOROFORM-D) δ 195.6, 172.2, 171.9, 171.5, 168.0, 162.8, 150.8, 148.7, 144.7, 141.0, 138.4, 131.9, 131.1, 130.3, 129.7, 128.6, 128.2, 128.0, 122.8, 119.6, 119.1, 70.3, 70.0, 67.1, 59.4, 57.9, 57.3, 54.6, 53.3, 43.3, 40.5, 37.2, 37.1, 36.7, 36.0, 35.5, 32.4, 31.1, 30.0, 28.8, 28.7, 26.8, 16.4, 11.9, 10.8, 5.0, 4.8. HRMS (ESI) calcd. for $C_{53}H_{68}N_8O_9SNa$ $[M+Na]^+$ 1015.4728, found 1015.4714.

2. Biology

Cell Culture. MCF-7 human breast cancer cells, supplied by RIKEN BRC through the National Bio-Resource Project of MEXT, Japan, were grown in Dulbecco's modified Eagle's medium (DMEM) enriched with 10% heat-inactivated fetal bovine serum (FBS), penicillin, and streptomycin, without phenol red. The cells were incubated at 37°C in a humidified 5% CO2 atmosphere. The mouse Neuro-2a (N2a) cell line, sourced from the Japanese Collection of Research Bioresources (JCRB) Cell Bank, was cultured in DMEM supplemented with 10% FBS, 1% sodium pyruvate, 100 U/mL penicillin, 100 μg/mL streptomycin, and 2 mM L-glutamine at 37°C in 5% CO2.

Western Blot Analysis. MCF-7 cells (5 × 105 cells/2 mL/dish) were treated with the test compounds at the indicated concentrations in the culture medium. The cells were collected and extracted with SDS buffer, and the protein concentrations of the lysates were determined using a BCA protein assay. Equivalent amounts of protein from each lysate were resolved in 7.5 % SDS-polyacrylamide gels for G9a and GLP and 12.5% SDS-polyacrylamide gels for H3K9Me2 and HP1γ and transferred onto PVDF membranes. After blocking, the transblotted

membranes were probed with primary antibodies. The probed membranes were washed four times with TBS-T (5 min/wash), incubated with HRP-linked secondary antibody, and again washed four times with TBS-T (5 min/wash). The immunoblots were visualized by enhanced chemiluminescence with ImmobilonTM Western Chemiluminescent HRP Substrate (Millipore, P90718). The conditions of the blocking and antibody reactions are included in the Table 1 listing the reagents and antibodies.

Table 1. List of reagents and antibodies for western blotting analysis

Reagents	Supplier	Code	Blocking and probing conditions	Dilution for probing
Primary antibody				
Rabbit polyclonal anti-G9a antibody	Merck	07-551	[a]Method A	1:500
Rabbit monoclonal anti- G9a antibody	Cell Signaling Technology	3306	[a]Method A	1:500
Mouse monoclonal anti-histone H3K9Me2 antibody	Abcam	Ab1220	[a]Method A	1:1000
Mouse monoclonal anti-α-tubulin antibody	Sigma Aldrich	T8203	[a]Method A	1:1000
Rabbit monoclonal anti-EHMT1(GLP) antibody	Cell Signaling Technology	35005	[a]Method A	1:500
HP1γ antibody	Cell Signaling Technology	2619	[a]Method A	1:1000
Mouse monoclonal β-actin	Santa Cruz Biotechnology	sc-47778	[a]Method A	1:2000

Secondary antibody				
ECL rabbit IgG, HRP-linked whole antibody	GE Healthcare Life Sciences	NA934	[a]Method A	1:2500
ECL mouse IgG, HRP-linked whole antibody	GE Healthcare Life Sciences	NA931	[a]Method A	1:2500

[a]Methods for blocking and probing conditions: *Method A*, TBS-T containing 5% skimmed milk for blocking buffer and TBS-T containing 5% skimmed milk for antibody dilution.

Neurite Outgrowth Assay. Initially, N2a cells were seeded at a density of 1×10^4 cells/mL DMEM with high glucose, 10% FBS, 100 U/mL penicillin, and 100 µg/mL streptomycin, and cultured at 37°C in a 5% CO2 humidified atmosphere. For the neurite outgrowth assay, the medium was switched to DMEM supplemented with 2% FBS. After treatment with the indicated compounds respectively for 48 h and 72 h, cell morphology was assessed using an Olympus CKX41 microscope. Cells with at least one neurite exceeding twice the cell body diameter were considered differentiated. The differentiation percentage was calculated based on the number of differentiated cells.

Cell Migration Assay. The experiment employed a CytoSelect™ 24-well cell migration assay kit (catalog no. CBA-101-C). To begin, the 24-well migration plate was warmed at room temperature for 10 minutes under sterile conditions. A cell suspension containing 500,000 cells/mL was prepared in serum-free media, and specific compound concentrations were added and thoroughly mixed. For the migration setup, 500 µL of media with 10% FBS was added to the lower chamber, while 300 µL of the cell suspension with compounds was added to each insert. The plate was then incubated for 24 hours at 37°C in a humidified atmosphere containing 5% CO_2. After the incubation, the media was carefully removed from each insert, and the inserts were transferred to clean wells containing 225 µL of the cell detachment

solution provided in the kit. The plate was incubated for 30 minutes at 37°C in a 5% CO_2 atmosphere. Following this, cells were released from the underside of the membrane, and the inserts were discarded. The lysis buffer/CYQuant® GR solution was then prepared by diluting the provided dye at a 1:75 ratio with the lysis buffer. Subsequently, 75 µL of this dye mixture was added to each well containing 225 µL of cell detachment solution and incubated for 20 minutes at room temperature. Finally, 200 µL of the resulting solution was transferred to a 96-well plate, and fluorescence intensity was measured.

In Vitro G9a Methyltransferase Assay. Recombinant G9a proteins (BPS Bioscience) were incubated with 15 µM SAM (Sigma) and 50 nM biotinylated-histone H3 (1−21; AnaSpec) in assay buffer (50 mM Tris-HCl [pH 9.0], 50 mM NaCl, 0.01% Tween-20, 0.3 % BSA and 1 mM DTT). After incubation at room temperature for 1 hour, AlphaLISA anti-H3K9me2 acceptor beads (final concentration 10 µg/mL) and AlphaScreen streptavidin donor beads (final concentration 10 µg/mL) were added and incubated for an additional hour before detection of the Alpha signal with an EnSpire Alpha plate reader (PerkinElmer).

siRNA Knockdown of G9a. Pre-designed siRNA targeting G9a was purchased from QIAGEN (target sequence: CACCATGAACATCGATCGCAA, cat. no. SI00091203). Lipofectamine™ RNAiMAX Transfection Reagent (Thermo Fisher Scientific) was used as the transfection reagent. To prepare the siRNA solution, 10 µM of siRNA stock was made by resuspending the lyophilized siRNA in nuclease-free water. The siRNA was then diluted in Opti-MEM™ I Reduced Serum Medium (Opti-MEM; Thermo Fisher Scientific) to the desired concentration. In a separate tube, the transfection reagent was also diluted in Opti-MEM. The diluted siRNA and transfection reagent were then combined and incubated at room temperature for 5 minutes to allow complex formation. The resulting mixture was subsequently added to MCF-7 cells, and the cells were incubated for 36 hours.

Table 2. Primers for RT-qPCR.

Genes	Forward primer	Reverse primer
EHMT2	GGTGAACAACCACCTGGAGGTA	AGGCTGACCATCTCCAAGTTC
GAPDH	CCGGGAAACTGTGGCGTGATGG	AGGTGGAGGAGTGGGTGTCGCTGTT

RNA Extraction and Reverse Transcription-Quantitative Polymerase Chain Reaction (RT-qPCR). Total RNA was isolated using TRI Reagent (MRC, Cincinnati, OH, USA) according to the manufacturer's instructions. For mRNA detection, total RNA was reverse-transcribed using Oligo(dT)$_{15}$ Primer (Takara Bio), Random 6 mers (Takara Bio) and PrimeScript™ Reverse Transcriptase (Takara Bio). The expression levels of mRNAs were then determined using TB Green Premix Ex Taq II (Takara Bio) according to the manufacturer's protocol. The sequences of the primers have been provided in Table S1. *Gapdh* was used as internal controls. RT-qPCR was performed using Thermal Cycler Dice Real Time System II TP950 (Takara Bio). Relative expression levels were calculated using the ΔΔCt method.

***Cell Viability Assay*.** MCF-7 were plated in 96-well plates at the initial density of 5000 cells/well (50 μL/well) and incubated (37 °C) for 24 hours. Test compound solutions of varying concentrations in DMEM enriched with 10% FBS, penicillin, and streptomycin, without phenol red were added (50 μL/well) and incubation was continued (37 °C; 3 days; humidified atmosphere of 5% CO2 in air), then 10 μL of alamar Blue™ was added to each well. The cells were further incubated (37 °C, 3 hr), and the fluorescence in each well was measured on a Ensight™ multilabel reader (PerkinElmer, Inc.; excitation: 540 nm; detection: 590 nm). From these data, the inhibition of cell viability (% viability) at each concentration of a test inhibitor were calculated according to the following equations: % viability = 100×T/C.

List of Abbreviations

AdoHcy, *S*-adenosyl-L-homocysteine; AML, Acute myeloid leukemia; AD, Alzheimer's disease; AUC, area under the curve; A*β*, β-amyloid; BBB, blood brain barrier; BEI, binding efficiency index; C. *elegans* CL2006, *Caenorhabditis elegans* CL2006; CL_{int}, clearance; C_{max}, maximum concentration; CLOT, chemiluminescence-based oxygen tunneling; CRBN, cereblon; DNMT1, DNA methyltransferase 1; ECSD, enzyme-coupled SAH detection; GLP, G9a-like protein; HKMT, histone lysine methyl transferase; H3K9, Histone H3 lysine 9; H3K9me2, H3K9 dimethylation; HTS, high throughput screening; HPLC, high performance liquid chromatography; HDAC, histone deacetylase; HCC, Hepatocellular carcinoma; hERG, ether-a-go-go-related gene; HbF, fetal hemoglobin; PWS, Prader–Willi syndrome; SCD, sickle cell disease; PAMPA, parallel artificial membrane permeability assay; PRMT1, protein arginine methyltransferase 1; PWWP, proline-tryptophan-tryptophan-proline; PROTAC, proteolysis targeting chimera; Pf, *Plasmodium falciparum*; PRC2, polycomb repressive complex 2; RMSD, root mean square deviation; SAM, *S*-adenosyl-L-methionine; SPR, surface plasmon resonance; SAR, structure−activity relationship; TRAIL, tumor necrosis factor-related apoptosis-inducing ligand; $T_{1/2}$, half-life; VHL1, Von-Hippel-Lindau 1; 5mC, 5-mehylcytocine.

References

[1] Waddington C. H. The epigenotype. *Endeavour* **1942**, *1*, 18–20.

[2] International Human Genome Sequencing Consortium. Finishing the euchromatic sequence of the human genome. *Nature* **2004**, *431*, 931–945.

[3] Kouzarides, T. Chromatin Modifications and Their Function. *Cell* **2007**, *128* (4), 693–705.

[4] Fei, L.; Shi, Y. Epigenetic Regulation: Methylation of Histone and Non-Histone Proteins. *Sci. China Ser. C-Life Sci.* **2009**, *52*, 311–322.

[5] Dai, W.; Qiao, X.; Fang, Y.; Guo, R.; Bai, P.; Liu, S.; Li, T.; Jiang, Y.; Wei, S.; Na, Z.; Xiao, X.; Li, D. Epigenetics-Targeted Drugs: Current Paradigms and Future Challenges. *Signal Transduct. Target. Ther.* **2024**, *9*, 98.

[6] Wang, Y.; Wang, Y.; Patel, H.; Chen, J.; Wang, J.; Chen, Z.-S.; Wang, H. Epigenetic Modification of m6A Regulator Proteins in Cancer. *Mol. Cancer* **2023**, *22*, 102.

[7] Liu, R.; Zhao, E.; Yu, H.; Yuan, C.; Abbas, M. N.; Cui, H. Methylation across the Central Dogma in Health and Diseases: New Therapeutic Strategies. *Signal Transduct. Target. Ther.* **2023**, *8*, 46.

[8] Gourisankar, S.; Krokhotin, A.; Wenderski, W.; Crabtree, G. R. Context-Specific Functions of Chromatin Remodellers in Development and Disease. *Nat. Rev. Genet.* **2024**, *25*, 340–361.

[9] Wang, Y.; Zhou, Q.; Huang, M.; Wu, L.; Liu, Z.; Zhang, Y. Targeting Tumor Endothelial Cells with Methyltransferase Inhibitors: Mechanisms of Action and the Potential of Combination Therapy. *Pharmacol. Ther.* **2023**, *247*, 108434.

[10] Müller, S.; Muir, T. W. Targeting Histone Methylation in Cancer Therapy. *Nature Reviews Cancer* **2023**, *23* (1), 1-15.

[11] Zhang, X.; Zhang, Y.; Wang, C.; Wang, X. TET (Ten-eleven Translocation) Family Proteins: Structure, Biological Functions, and Applications. *Signal Transduct. Target. Ther.* **2023**, *8*, 297.

[12] de Ruijter, A. J. M.; Gennip, A. H.; Caron, H. N.; Kemp, S.; vanKuilenburg, A. B. P. Histone deacetylases (HDACs): Characterizationof the classical HDAC family. *Biochem. J.* **2003**, *370*, 737−749.

[13] Lin, T.-C.; Engelhard, L.; Söldner, B.; Linser, R.; Summerer, D. Light-Activatable MBD-Readers of 5-Methylcytosine Reveal Domain-Dependent Chromatin Association Kinetics In Vivo. *Adv. Sci.* **2024**, *11*, 2307930.

[14] Martin, B. J. E.; Ablondi, E. F.; Goglia, C.; Mimoso, C. A.; Espinel-Cabrera, P. R.; Adelman, K. Global identification of direct SWI/SNF targets reveals compensation by EP400. *Cell* **2023**, *247*, 108434.

[15] Nemeth, K.; Bayraktar, R.; Ferracin, M.; Calin, G. A. Non-coding RNAs in Disease: From Mechanisms to Therapeutics. *Nat. Rev. Genet.* **2024**, *25*, 211–232.

[16] Rea, S.; Eisenhaber, F.; O'Carroll, D.; Strahl, B. D.; Sun, Z. W.; Schmid, M.; et al. Regulation of Chromatin Structure by Site-Specific Histone H3 Methyltransferases. *Nature* **2000**, *406*, 593-599.

[17] Bennett, R. L.; Licht, J. D. Targeting Epigenetics in Cancer. *Annu. Rev. Pharmacol. Toxicol.* **2018**, *58*, 187–207.

[18] Ribich, S.; Harvey, D.; Copeland, R. A. Drug Discovery and Chemical Biology of Epigenetics. *Cell Chem. Biol.* **2017**, *24*, 1120–1147.

[19] Tachibana, M.; Sugimoto, K.; Fukushima, T.; Shinkai, Y. Set domain-containing protein, G9a, is a novel lysine-preferring mammalian histone methyltransferase with hyperactivity and specific selectivity to lysine 9 and 27 of histone H3. *J. Biol. Chem.* **2001**, *276*, 25309-25317.

[20] Tachibana, M.; Ueda, J.; Fukuda, M.; Takeda, N.; Ohta, T.; Iwanari, H.; et al. Histone methyltransferases G9a and GLP form heteromeric complexes and are both crucial for methylation of euchromatin at H3-K9. *Genes. Dev.* **2005**, *19*, 815-826.

[21] Rice, J. C.; Briggs, S. D.; Ueberheide, B.; Barber, C. M.; Shabanowitz, J.; Hunt, D. F.; et al. *Mol. Cell*. **2003**, *12*, 1591-1598.

[22] Bannister, A. J.; Zegerman, P.; Partridge, J. F.; Miska, E. A.; Thomas, J. O.; Allshire, R. C.; et al. Selective recognition of methylated lysine 9 on Histone H3 by the HP1 chromo domain. *Nature*, **2001**, *410*, 120-124.

[23] Allali-Hassani, A.; Wasney, G. A.; Siarheyeva, A.; Hajian, T.; Arrowsmith C. H.; Vedadi, M. Fluorescence-based methods for screening writers and readers of histone methyl marks. *J. Biomol. Screen.* **2012**, *17*, 71-84.

[24] Estève, P. O.; Chin, H. G.; Smallwood, A.; Feehery, G. R.; Gangisetty, O.; Karpf, A. R.; et al. Direct interaction between DNMT1 and G9a coordinates DNA and histone methylation during replication. *Genes. Dev.* **2006**, *20*, 3089-3103.

[25] Cho, H. S.; Kelly, J. D.; Hayami, S.; Toyokawa, G.; Takawa, M.; Yoshimatsu, M.; Tsunoda, T.; Field, H. I.; Neal, D. E.; Ponder, B. A.; et al. Enhanced expression of EHMT2 is involved in the proliferation of cancer cells through negative regulation of SIAH1. *Neoplasia*. **2011**, *13* 676–84.

[26] Hua. K. T.; Wang, M. Y.; Chen, M. W.; Wei, L. H.; Chen, C. K.; Ko. C. H.; Jeng. Y. M.; Sung, P. L.; Jan, Y. H.; Hsiao, M.; et al. The H3K9 methyltransferase G9a is a marker of aggressive ovarian cancer that promotes peritoneal metastasis. *Mol. Cancer.* **2014**, *13*, 189.

[27] Wozniak, R. J.; Klimecki, W. T.; Lau, S. S.; Feinstein, Y.; Futscher, B. W. 5-Aza-2′-deoxycytidine-mediated reductions in G9A histone methyltransferase and histone H3 K9 di-methylation levels are linked to tumor suppressor gene reactivation. *Oncogene.* **2007**, *26*, 77–90.

[28] Huang, J.; Dorsey. J.; Chuikov, S.; Perez-Burgos, L.; Zhang, X.; Jenuwein, T.; Reinberg, D.; Berger, S. L. G9a and Glp methylate lysine 373 in the tumor suppressor p53. *J Biol Chem.* **2010**, *285*, 9636–9641.

[29] Lee, J. S.; Kim, Y.; Bhin, J.; Shin, H. J.; Nam, H. J.; Lee. S. H.; Yoon. J. B.; Binda, O.; Gozani. O.; Hwang, D.; et al. Hypoxia-induced methylation of a pontin chromatin remodeling factor. *Proc Natl Acad Sci U S A.* **2011**, *108*, 13510–13515.

[30] Bachman, K. E.; Park, B. H.; Rhee, I.; Rajagopalan, H.; Herman, J. G.; Baylin, S. B.; Kinzler, K. W.; Vogelstein, B.; Histone modifications and silencing prior to DNA methylation of a tumor suppressor gene. *Cancer Cell.* **2003**, *3*, 89–95.

[31] Casciello, F.; Windloch, K.; Gannon, F.; Lee. J. S. Functional role of G9a histone methyltransferase in Cancer. *Front Immunol.* **2015**, *6*, 487.

[32] Egger, G.; Liang, G.; Aparicio, A.; Jones, P. A.; Epigenetics in human disease and prospects for epigenetic therapy. *Nature.* **2004**, 429, 457–463.

[33] Tachibana, M.; Sugimoto, K.; Nozaki, M.; Ueda, J.; Ohta, T.; Ohki, M.; Fukuda, M.; Takeda, N.; Niida, H.; Kato, H.; et al. G9a histone methyltransferase plays a dominant role in

euchromatic histone H3 lysine 9 methylation and is essential for early embryogenesis. *Genes Dev.* **2002**, *16*, 1779–1791.

[34] Laumet, G.; Garriga, J.; Chen, S.-R.; Zhang, Y.; Li, D.-P.; Smith, T. M.; Dong, Y.; Jelinek, J.; Cesaroni, M.; Issa, J.-P.; Pan, H.-L. G9a is essential for epigenetic silencing of K(+) channel genes in acute-to-chronic pain transition. *Nat. Neurosci.* **2015**, *18*, 1746−1755.

[35] Ligresti, G.; Caporarello, N.; Meridew, J. A.; Jones, D. L.; Tan, Q.; Choi, K. M.; Haak, A. J.; Aravamudhan, A.; Roden, A. C.; Prakash, Y. S.; Lomberk, G.; Urrutia, R. A.; Tschumperlin, D. J. CBX5/G9a/ H3K9me-mediated gene repression is essential to fibroblast activation during lung fibrosis. *JCI Insight* **2019**, *4*, No. e127111.

[36] Irifuku, T.; Doi, S.; Sasaki, K.; Doi, T.; Nakashima, A.; Ueno, T.; Yamada, K.; Arihiro, K.; Kohno, N.; Masaki, T. Inhibition of H3K9 histone methyltransferase G9a attenuates renal fibrosis and retains klotho expression. *Kidney Int.* **2016**, *89*, 147−157.

[37] Singh, N.; Ramĩrez-Carvajal, L.; de Los Santos, T.; Golding, M. C.; Long, C. R. Inhibition of EHMT2 Induces a Robust Antiviral Response Against Foot-and-Mouth Disease and Vesicular Stomatitis Virus Infections in Bovine Cells. *J. Interferon Cytokine Res.* **2016**, *36*, 37−47.

[38] Kim, Y.; Lee, H.-M.; Xiong, Y.; Sciaky, N.; Hulbert, S. W.; Cao, X.; Everitt, J. I.; Jin, J.; Roth, B. L.; Jiang, Y.-H. Targeting the histone methyltransferase G9a activates imprinted genes and improves survival of a mouse model of Prader-Willi syndrome. *Nat. Med.* **2017**, *23*, 213−222.

[39] Ow, J. R.; Palanichamy Kala, M.; Rao, V. K.; Choi, M. H.; Bharathy, N.; Taneja, R. G9a inhibits MEF2C activity to control sarcomere assembly. *Sci. Rep.* **2016**, *6*, No. 34163.

[40] Krivega, I.; Byrnes, C.; de Vasconcellos, J. F.; Lee, Y. T.; Kaushal, M.; Dean, A.; Miller, J. L. Inhibition of G9a methyltransferase stimulates fetal hemoglobin production by facilitating LCR/γ-globin looping. *Blood* **2015**, *126*, 665−672.

[41] Griñán-Ferré, C.; Marsal-García, L.; Bellver-Sanchis, A.; Kondengaden, S. M.; Turga, R. C.; Vázquez, S.; & Pallàs, M. Pharmacological inhibition of G9a/GLP restores cognition and reduces oxidative stress, neuroinflammation and β-Amyloid plaques in an early-onset Alzheimer's disease mouse model. *Aging* **2019**, *11*, 11591–11608.

[42] Jana, A.; Bellver-Sanchis, A.; Griñán-Ferré, C.; Banerjee, D. R. Repurposing of Raltitrexed as an effective G9a/EHMT2 inhibitor and promising anti-Alzheimer's agent. *ACS Med. Chem. Lett* **2023**, *14*, 1531–1536.

[43] Mai, A. *Chemical Epigenetics*; Springer International Publishing, 2020; ISBN 9783030429812.

[44] Watanabe, J.; Clutter, M. R.; Gullette, M. J.; Sasaki, T.; Uchida, E.; Kaur, S.; Mo, Y.; Abe, K.; Ishi, Y.; Takata, N.; Natsumeda, M.; Gadd, S.; Zhang, Z.; Becher, O. J.; Hashizume, R. BET Bromodomain Inhibition Potentiates Radiosensitivity in Models of H3K27-Altered Diffuse Midline Glioma. *J. Clin. Investig.* **2024**, *134*, e174794.

[45] Tang, F.; Choy, E.; Tu, C.; Hornicek, F.; Duan, Z. Therapeutic Applications of Histone Deacetylase Inhibitors in Sarcoma. *Cancer Treat. Rev.* **2017**, *59*, 33–45.

[46] Issa, J. P.; Kantarjian, H. Azacitidine. *Nat. Rev. Drug Discov.* **2005**, *Suppl.*, S6–S7.

[47] Issa, J. P.; Kantarjian, H. Decitabine. *Oncologist* **2006**, *11*, 279–290.

[48] Korman, A. J.; Weaver, D.; Dronca, R.; Kharbanda, S. The Development of Romidepsin in the Treatment of Cutaneous T-Cell Lymphoma: A Review of the Clinical Data. *J. Oncol. Pharm. Pract.* **2017**, *23*, 3–10.

[49] O'Connor, O. A.; Pro, B.; Pinter-Brown, L.; et al. Vorinostat in Patients with Cutaneous T-Cell Lymphoma: Results of a Phase II Multicenter Study. *J. Clin. Oncol.* **2009**, *27*, 2624–2632.

[50] Duvic, M.; Talpur, R.; Thomas, S. H.; et al. Belinostat in the Treatment of Cutaneous T-Cell Lymphoma. *J. Clin. Oncol.* **2015**, *33*, 3396–3404.

[51] Pession, A.; Ferrari, A.; Tassi, G.; et al. Givinostat in Juvenile Myelomonocytic Leukemia: A Phase I Study. *Blood* **2015**, *126*, 2777–2786.

[52] Deren, G.; Duvic, M.; Kim, D.; et al. Tazemetostat in Advanced Epithelioid Sarcoma: Results from an Ongoing Phase II Trial. *Lancet Oncol.* **2020**, *21*, 1397–1406.

[53] Kubicek, S.; O'Sullivan, R.J.; August, E. M.; Hickey, E. R.; Zhang, Q.; Teodoro, M. L.; Rea, S.; Mechtler, K.; Kowalski, J. A.; Homon, C. A.; Kelly, T. A.; Jenuwein, T. Reversal of H3K9me2 by a small-molecule inhibitor for the G9a histone methyltransferase. *Mol. Cell.* **2007**, *25*, 473−481.

[54] Xiong, Y.; Li, F.; Babault, N.; Dong, A.; Zeng, H.; Wu, H.;Chen, X.; Arrowsmith, C. H.; Brown, P. J.; Liu, J.; Vedadi, M.; Jin, J. Discovery of potent and selective inhibitors for G9a-like protein(GLP) lysine methyltransferase. *J. Med. Chem.* **2017**, *60*, 1876−1891.

[55] Chang, Y.; Zhang, X.; Horton, J. R.; Upadhyay, A. K.; Spannhoff, A.; Liu, J.; et al. (2009). Structural basis for G9a-like protein lysine methyltransferase inhibition by BIX-01294. *Nat. Struct. Mol. Biol.* **2009**, *16*, 312–317.

[56] Kim, K.; Son, M. Y.; Jung, C. R.; Kim, D. S.; Cho, H. S. EHMT2 is a metastasis regulator in breast cancer. *Biochem. Biophys. Res. Commun.* **2018**, *496*, 758−762.

[57] Savickiene, J.; Treigyte, G.; Stirblyte, I.; Valiuliene, G.; Navakauskiene, R. Euchromatic histone methyltransferase 2 inhibitor, BIX-01294, sensitizes human promyelocytic leukemia HL-60 and NB4 cells to growth inhibition and differentiation. *Leuk. Res.* **2014**, *38*, 822−829.

[58] Vitkeviciene, A.; Baksiene, S.; Borutinskaite, V.; Navakauskiene, R. Epigallocatechin-3-gallate and BIX-01294 have different impact on epigenetics and senescence modulation in acute and chronic myeloid leukemia cells. *Eur. J. Pharmacol.* **2018**, *838*, 32−40.

[59] Wu, X. X.; Ogawa, O.; Kakehi, Y. TRAIL and chemotherapeutic drugs in cancer therapy. *Vitam Horm.* **2004**, *67*, 365–383.

[60] Rahman, M.; Davis, S. R.; Pumphrey, J. G.; et al. TRAIL induces apoptosis in triple-negative breast cancer cells with a mesenchymal phenotype. *Breast Cancer Res Treat.* **2009**, *113*, 217–230.

[61] Wiley, S.R.; Schooley, K.; Smolak, P. J.; et al. Identification and characterization of a new member of the TNF family that induces apoptosis. *Immunity.* **1995**, *3*, 673–682.

[62] Liu, F.; Chen, X.; Allali-Hassani, A.; Quinn, A. M.; Wasney, G. A.; Dong, A.; et al. (2009). Discovery of a 2,4-Diamino-7-aminoalkoxyquinazoline as a potent and selective inhibitor of histone lysine methyltransferase G9a. *J. Med. Chem.* **2009**, *52*, 7950–7953.

[63] Liu, F.; Chen, X.; Allali-Hassani, A.; Quinn, A. M.; Wigle, T. J.; Wasney, G. A.; Dong, A.; Senisterra, G.; Chau, I.; Siarheyeva, A.; Norris, J. L.; Kireev, D. B.; Jadhav, A.; Herold, J. M.; Janzen, W. P.; Arrowsmith, C. H.; Frye, S. V.; Brown, P. J.; Simeonov, A.; Vedadi, M.; Jin, J. Protein Lysine Methyltransferase G9a Inhibitors: Design, Synthesis, and Structure Activity Relationships of 2,4-Diamino-7-aminoalkoxy-quinazolines. *J. Med. Chem.* **2010**, *53*, 5844–5857.

[64] Chang, Y.; Ganesh, T.; Horton, J. R.; Spannhoff, A.; Liu, J.; Sun,A.; Zhang, X.; Bedford, M. T.; Shinkai, Y.; Snyder, J. P.; Cheng, X. Adding a lysine mimic in the design of potent inhibitors of histonelysine methyltransferases. *J. Mol. Biol.* **2010**, *400*, 1−7.

[65] Vedadi, M.; Barsyte-Lovejoy, D.; Liu, F.; Rival-Gervier, S.; Allali-Hassani, A.; Labrie, V.; Wigle, T. J.; DiMaggio, P. A.; Wasney, G. A.; Siarheyeva, A.; Dong, A. P.; Tempel, W.; Wang, S. C.; Chen, X.; Chau, I.; Mangano, T. J.; Huang, X. P.; Simpson, C. D.; Pattenden, S. G.; Norris, J. L.; Kireev, D. B.; Tripathy, A.; Edwards, A.; Roth, B. L.; Janzen, W. P.; Garcia, B. A.; Petronis, A.; Ellis, J.; Brown, P. J.; Frye, S. V.; Arrowsmith, C. H.; Jin, J. A chemical probe selectively inhibits G9a and GLP methyltransferase activity in cells. *Nat. Chem. Biol.* **2011**, *7*, 566−574.

[66] Liu, F.; Barsyte-Lovejoy, D.; Allali-Hassani, A.; He, Y. L.; Herold, J. M.; Chen, X.; Yates, C. M.; Frye, S. V.; Brown, P. J.; Huang, J.; Vedadi, M.; Arrowsmith, C. H.; Jin, J. Optimization of cellular activity of G9a inhibitors 7-aminoalkoxy-quinazolines. *J. Med. Chem.* **2011**, *54*, 6139−6150.

[67] Liu, F.; Barsyte-Lovejoy, D.; Li, F. L.; Xiong, Y.; Korboukh, V.; Huang, X. P.; Allali-Hassani, A.; Janzen, W. P.; Roth, B. L.; Frye, S. V.; Arrowsmith, C. H.; Brown, P. J.; Vedadi, M.; Jin, J. Discovery of an in vivo chemical probe of the lysine methyltransferases G9a and GLP. *J. Med. Chem.* **2013**, *56*, 8931−8942.

[68] Sweis, R. F.; Pliushchev, M.; Brown, P. J.; Guo, J.; Li, F.; Maag,D.; Petros, A. M.; Soni, N. B.; Tse, C.; Vedadi, M.; Michaelides, M.R.; Chiang, G. G.; Pappano, W. N. Discovery and development ofpotent and selective inhibitors of histone methyltransferase G9a. *ACS Med. Chem. Lett.* **2014**, *5*, 205−209.

[69] Katayama, K.; Ishii, K.; Tsuda, E.; Yotsumoto, K.; Hiramoto, K.; Suzuki, M.; Yasumatsu, I.; Igarashi, W.; Torihata, M.; Ishiyama, T.; Katagiri, T. Discovery of Novel Histone Lysine Methyltransferase G9a/ GLP (EHMT2/1) Inhibitors: Design, Synthesis, and Structure-Activity Relationships of 2,4-Diamino-6-Methylpyrimidines. *Bioorg. Med. Chem. Lett.* **2020**, *30*, 127475.

[70] Katayama, K.; Ishii, K.; Terashima, H.; Tsuda, E.; Suzuki, M.;Yotsumoto, K.; Hiramoto, K.; Yasumatsu, I.; Torihata, M.; Ishiyama,T.; Muto, T.; Katagiri, T. Discovery of DS79932728: A Potent, OrallyAvailable G9a/GLP Inhibitor for Treating β-Thalassemia and Sickle Cell Disease. *ACS Med. Chem. Lett.* **2021**, *12*, 121−128.

[71] Nishigaya, Y.; Takase, S.; Sumiya, T.; Kikuzato, K.; Sato, T.;Niwa, H.; Sato, S.; Nakata, A.; Sonoda, T.; Hashimoto, N.; et al. Discovery of Novel Substrate-Competitive Lysine MethyltransferaseG9a Inhibitors as Anticancer Agents. *J. Med. Chem.* **2023**, *66*, 4059−4085.

[72] Takase, S.; Hiroyama, T.; Shirai, F.; Maemoto, Y.; Nakata, A.; Arata, M.; Matsuoka, S.; Sonoda, T.; Niwa, H.; Sato, S.; Umehara, T.; Shirouzu, M.; Nishigaya, Y.; Sumiya, T.; Hashimoto, N.; Namie, R.; Usui, M.; Ohishi, T.; Ohba, S.; Kawada, M.; Hayashi, Y.; Harada, H.; Yamaguchi, T.; Shinkai, Y.; Nakamura, Y.; Yoshida, M.; Ito, A. A specific G9a inhibitor unveils BGLT3 lncRNA as a universal mediator of chemically induced fetal globin gene expression. *Nat. Commun.* **2023**, *14*, No. 23.

[73] Srimongkolpithak, N.; Sundriyal, S.; Li, F.; Vedadi, M.; Fuchter,M. J. Identification of 2,4-Diamino-6,7-Dimethoxyquinoline Derivatives as G9a Inhibitors. *MedChemComm* **2014**, *5*, 1821−1828.

[74] Chen, W.-L.; Wang, Z.-H.; Feng, T.-T.; Li, D.-D.; Wang, C.-H.; Xu, X.-L.; Zhang, X.-J.; You, Q.-D.; Guo, X.-K. Discovery, design and synthesis of 6H-anthra[1,9-cd]isoxazol-6-one scaffold as G9a inhibitor through a combination of shape-based virtual screening and structure based molecular modification. *Bioorg. Med. Chem.* **2016**, *24*, 6102− 6108.

[75] Milite, C.; Feoli, A.; Horton, J. R.; Rescigno, D.; Cipriano, A.;Pisapia, V.; Viviano, M.; Pepe, G.; Amendola, G.; Novellino, E.;Cosconati, S.; Cheng, X.; Castellano, S.; Sbardella, G. Discovery of anovel chemotype of histone lysine methyltransferase EHMT1/2 (GLP/G9a)

inhibitors: rational design, synthesis, biological evaluation, and co-crystal structure. *J. Med. Chem.* **2019**, *62*, 2666−2689.

[76] Kondengaden, S. M.; Luo, L.-F.; Huang, K.; Zhu, M.; Zang, L.;Bataba, E.; Wang, R.; Luo, C.; Wang, B.; Li, K. K.; Wang, P. G.Discovery of novel small molecule inhibitors of lysine methyltransferaseG9a and their mechanism in leukemia cell lines. *Eur. J. Med. Chem* .**2016**, *122*, 382−393.

[77] Jana, A.; Bellver-Sanchis, A.; Griñán-Ferré, C.; Banerjee, D. R. Repurposing of Raltitrexed as an effective G9a/EHMT2 inhibitor and promising anti-Alzheimer's agent. *ACS Med. Chem. Lett* **2023**, *14*, 1531–1536.

[78] Rabal, O.; San José-Enériz, E.; Agirre, X.; Sánchez-Arias, J. A.;Vilas-Zornoza, A.; Ugarte, A.; de Miguel, I.; Miranda, E.; Garate, L.;Fraga, M.; Santamarina, P.; Fernandez, P. R.; Ordoñez, R.; Sáez, E.;Roa, S.; García-Barchino, M. J.; Martínez-Climent, J. A.; Liu, Y.; Wu,W.; Xu, M.; Prosper, F.; Oyarzabal, J. Discovery of reversible DNA methyltransferase and lysine methyltransferase G9a inhibitors with antitumoral in vivo efficacy. *J. Med. Chem.* **2018**, *61*, 6518−6545.

[79] Rabal, O.; San José-Enériz, E.; Agirre, X.; Sánchez-Arias, J. A.; de Miguel, I.; Ordoñez, R.; Garate, L.; Miranda, E.; Sáez, E.; Vilas-Zornoza, A.; Pineda-Lucena, A.; Estella, A.; Zhang, F.; Wu, W.; Xu, M.; Prosper, F.; Oyarzabal, J. Design and Synthesis of Novel Epigenetic Inhibitors Targeting Histone Deacetylases, DNA Methyltransferase 1, and Lysine Methyltransferase G9a with In Vivo Efficacy in Multiple Myeloma. *J. Med. Chem.* **2021**, *64*, 3392-3426.

[80] Curry, E.; Green, I.; Chapman-Rothe, N.; Shamsaei, E.; Kandil, S.; Cherblanc, F. L.; Payne, L.; Bell, E.; Ganesh, T.; Srimongkolpithak, N.; et al. Dual EZH2 and EHMT2histone

methyltransferase inhibition increases biological efficacy in breast cancer cells. *Clin. Epigenet.* **2015**, *7*, 84.

[81] Shi, Y.; Zhang, Q.; Zhang, M.; Chen, Y.; Sun, J.; Chen, L.; Liu, S.; Liu, Z.; Yang, J.; Wu, C.; Zheng, Z.; Wang, L.; Chen, G. Discovery of dual lysine methyltransferase G9a and EZH2 inhibitors with in vivo efficacy against malignant rhabdoid tumor. *J. Med. Chem.* **2023**, *66*, 5685−5702.

[82] Yang, C.; et al. Discovery of a Highly Potent Lysine Methyltransferases G9a/NSD2 Dual Inhibitor to Treat Solid Tumors. *J. Med. Chem. **2024**, 67, 16072–16087*.

[83] uan, Y.; Wang, Q.; Paulk, J.; Kubicek, S.; Kemp, M. M.; Adams,D. J.; Shamji, A. F.; Wagner, B. K.; Schreiber, S. L. A small-moleculeprobe of the histone methyltransferase G9a induces cellular senescencein pancreatic adenocarcinoma. *ACS Chem. Biol.* **2012**, *7*, 1152−1157.

[84] Iwasa, E.; Hamashima, Y.; Fujishiro, S.; Higuchi, E.; Ito, A.;Yoshida, M.; Sodeoka, M. Total synthesis of (+)-chaetocin and itsanalogues: their histone methyltransferase G9a inhibitory activity. *J.Am. Chem. Soc.* **2010**, *132*, 4078−4079.

[85] Devkota, K.; Lohse, B.; Liu, Q.; Wang, M. W.; Staerk, D.; Berthelsen, J.; and Clausen, R. P. Analogues of the Natural Product Sinefungin as Inhibitors of EHMT1 and EHMT2. *ACS Med. Chem. Lett.* **2014**, *5*, 293−297

[86] Park, K. S.; Xiong, Y.; Yim, H.; Velez, J.; Babault, N.; Kumar, P.; Liu, J.; Jin, J. Discovery of the first-in-class G9a/GLP covalent inhibitors. *J. Med. Chem.* **2022**, *65*, 10506−10522.

[87] Feng, Z.; Yang, C.; Zhang, Y.; Li, H.; Fang, W.; Wang, J.; Nie, Y.; Wang, C. Y.; Liu, Z.; Jiang, Z.; Wang, J.; Wang, Y. Structure-based design and characterization of the highly potent

and selective covalent inhibitors targeting the lysine methyltransferases G9a/GLP. *J. Med. Chem.* **2023**, *66*, 8086−8102.

[88] Dale, B.; Cheng, M.; Park, K. S.; Kaniskan, H. U.; Xiong, Y.; Jin, J. Advancing targeted protein degradation for cancer therapy. *Nat. Rev. Cancer* **2021**, *21*, 638−654.

[89] Békés, M.; Langley, D. R.; Crews, C. M. PROTAC targeted protein degraders: the past is prologue. *Nat. Rev. Drug Discovery* **2022**, *21*, 181−200.

[90] Itoh, Y.; Ishikawa, M.; Naito, M.; Hashimoto, Y. Protein Knockdown Using Methyl Bestatin-Ligand Hybrid Molecules: Design and Synthesis of Inducers of Ubiquitination-Mediated Degradation of Cellular Retinoic Acid-Binding Proteins. *J. Am. Chem. Soc.* **2010**, 132,5820−5826.

[91] Chotitumnavee, J.; Yamashita, Y.; Takahashi, Y.; Takada, Y.; Iida, T.; Oba, M.; Itoh, Y.; Suzuki, T. Selective Degradation of Histone Deacetylase 8 Mediated by a Proteolysis Targeting Chimera (PROTAC). *Chem. Commun.* **2022**, *58*, 4635−4638.

[92] Gadd, M., Testa, A., Lucas, X. *et al.* Structural basis of PROTAC cooperative recognition for selective protein degradation. *Nat Chem Biol* **2017**, *13*, 514–521 (2017).

[93] Mukherjee, A.; Suzuki, T. G9a/GLP Modulators: Inhibitors to Degraders. *J. Med. Chem.* **2025**, https://doi.org/10.1021/acs.jmedchem.4c02474.

[94] Adams, J.; & Kauffman, M. Development of the Proteasome Inhibitor Velcade™ (Bortezomib). *Cancer Investigation*, **2004**, *22*, 304–311.

[95] Collins, R.; & Cheng, X. A case study in cross-talk: the histone lysine methyltransferases G9a and GLP, *Nucleic Acids Research* **2010**, *38*, 3503–3511.

[96] Jin, Y.; Park, S.; Park, S-Y.; Lee, C-Y.; Eum, D.Y.; Shim, J-W.; Choi, S-H.; Choi, Y-J.; Park S-J.; Heo, K. G9a Knockdown Suppresses Cancer Aggressiveness by Facilitating Smad

Protein Phosphorylation through Increasing BMP5 Expression in Luminal A Type Breast Cancer. *Int J Mol Sci.* **2022**, *23*, 589.

[97] Lee, J-Y.; Lee, S-H.; Heo, S-H.; Kim, K-S.; Kim, C.; Kim, D-K.; Ko, J-J.; Park, K-S. Novel Function of Lysine Methyltransferase G9a in the Regulation of Sox2 Protein Stability. *PLoS One* **2015**, *10*, No. e0141118.

List of Publications

[1] Yosuke Ota, Yukihiro Itoh, Takashi Kurohara, Ritesh Singh, Elghareeb E. Elboray, Chenliang Hu, Farzad Zamani, **Anirban Mukherjee**, Yuri Takada, Yasunobu Yamashita, Mie Morita, Mano Horinaka, Yoshihiro Sowa, Mitsuharu Masuda, Toshiyuki Sakai, and Takayoshi Suzuki. Cancer-Cell-Selective Targeting by Arylcyclopropylamine−Vorinostat Conjugates. *ACS Med. Chem. Lett.,* **2022**, *13*, 1568-1573.

[2] **Anirban Mukherjee**, Farzad Zamani, and Takayoshi Suzuki; Evolution of Slow-Binding Inhibitors Targeting Histone Deacetylase Isoforms. *J. Med. Chem.*, **2023**, *66*, 11672-11700.

[3] **Anirban Mukherjee***, and Takayoshi Suzuki*; G9a/GLP Modulators: Inhibitors to Degraders. *J. Med. Chem.*, **2025**, *https://doi.org/10.1021/acs.jmedchem.4c02474*.

List of Conferences

1. Poster Presentation in the *14th AFMC International Medicinal Chemistry Symposium (**AIMECS 2023**)*; June 25-28, **2023**, Organized by-**Asian Federation for Medicinal Chemistry** (AFMC), Seoul, South Korea.
2. Poster Presentation in the ***17th Annual Meeting of the Japanese Society for Epigenetics***; June 13-14, **2024**, Osaka City Central Public Hall in Kita Ward, Japan.

Summary of the Thesis

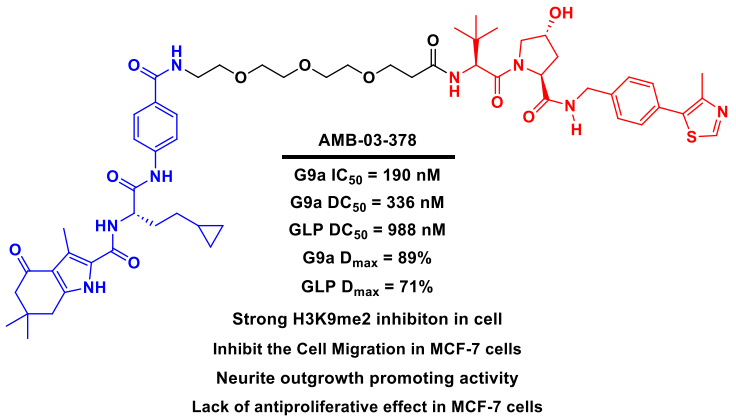

This thesis presents the design, synthesis, and biological evaluation of several novel G9a/GLP-PROTAC degraders. Two different classes of PROTAC candidates were developed using UNC0638 and RK-701 as G9a/GLP binding ligand. The UNC0638-based class I PROTACs failed to induce significant degradation of G9a protein under the tested conditions. However, an evaluation of their antiproliferative activity revealed that certain candidates were capable of inhibiting MCF-7 cell growth. These observations underscore the critical role of linker optimization and efficient ternary complex formation in facilitating effective targeted protein degradation. Notably, the observed antiproliferative effects raise the possibility of off-target interactions, which may contribute to the anticancer activity observed, independent of G9a degradation. To overcome the existing challenges, advancements in PROTAC design were implemented by utilizing RK-701, a norleucine-based selective G9a/GLP inhibitor, as the targeting ligand to develop class II PROTACs. Assessment of the degradation efficacy of these newly synthesized candidates identified AMB-03-378 as the most potent PROTAC in the series. that degrades G9a/GLP in a dose- and time-dependent manner via the UPS and reduces H3K9me2 levels in cells. Furthermore, AMB-03-378 downregulates HP1γ expression, highlighting G9a's scaffolding function. It also demonstrates potential in promoting neurite outgrowth in the mouse neural crest-derived N2a cell line, suggesting therapeutic implications for neural development and repair. Although AMB-03-378 inhibits the migration of MCF-7 breast cancer cells, it does not exhibit antiproliferative effects in these cells, indicating the need to reevaluate the role of G9a in breast cancer development.

ACKNOWLEDGEMENT

First of all, I am deeply grateful to Prof. Dr. Takayoshi Suzuki for his invaluable guidance, unwavering support, and heartfelt encouragement throughout my journey. Above all, I admire his patience and the opportunities he provided me as a member of his remarkable research group. His trust in allowing me the flexibility to explore diverse research topics, combined with his insightful feedback, has been instrumental in my growth as a scientist. Being part of his team has been an extraordinary privilege, and delving into the fascinating world of medicinal chemistry and chemical biology under his mentorship has been both a profoundly enriching and truly unforgettable experience. One of his most memorable and encouraging remarks, "I am sure you can do it," played a key role in boosting my confidence and empowering me to present and discuss own ideas openly within the scientific community.

I am sincerely thankful to Associate Prof. Dr. Yukihiro Itoh for his insightful advice and invaluable guidance in the field of medicinal chemistry and chemical biology. His mentorship has been pivotal in helping me cultivate essential research skills and instil a commitment to integrity in my work. He encouraged me to rigorously question my findings and analyze data with the utmost scrutiny, urging me to approach my research as though I were its most critical reviewer. This perspective has profoundly shaped my approach to scientific inquiry.

I wish to express gratitude to my immediate mentor, Assistant Prof. Dr. Yasunobu Yamashita, for his continued support throughout this journey. His one-on-one discussions were helpful in overcoming challenges and resolving complex research problems. What I particularly appreciated was his ability to generate ideas and foster collaborative discussions within a group of students. This approach not only encouraged the exploration of multiple perspectives but also broadened my understanding of the diverse facets of this research field.

I am thankful to Assistant Prof. Dr. Yuri Takada for her expert guidance in mastering the operation of instruments like analytical and preparative HPLC, as well as LCMS. Her support has been instrumental in enhancing my technical proficiency.

I am also thankful to Dr. Farzad Zamani for his true mentorship and guidance. Adjusting to a new environment and immersing myself in chemical biology research was made much smoother with his invaluable support. He played a key role in helping me settle efficiently in the lab, and I greatly appreciate the insightful scientific discussions and advice he shared, which have significantly contributed to my development as a researcher.

I have been fortunate to collaborate with scientists beyond our group, and I sincerely thank Prof. Dr. Makoto Tachibana and Dr. Ryo Maeda from the Laboratory of Epigenome Dynamics at the Graduate School of Frontier Biosciences, Osaka University, for their support and engaging discussions.

I would also like to extend my heartfelt thanks to all the past and present lab members of Suzuki group that I have had the pleasure to work with. In particular, I am grateful to Dr. Jiranan Chotitumnavee, Dr. Yutaro Hanatani, Dr. Atika Nurani, Dr. Ryan Hubbal, Dr. Katsunori Endo, Dr. Toshiki Akiyama, Mr. Shengwang Yu, Ms. Chenliang Hu, Mr. Mitsuhiro Terao, Mr. Hirokazu Takeshima, and Mr. Paddy Melsen for their assistance with experimental setups and their contributions to the insightful discussions.

I sincerely thank Prof. Dr. Kazuhiko Nakatani and Prof. Dr. Taki Nishimura for their valuable suggestions and guidance as members of my thesis committee.

I sincerely appreciate the efforts of Ms. Miho Sawada, Ms. Yukiko Moriyama, and Ms. Kazumi Nakano, whose guidance was instrumental in helping me learn and master various biological assays.

I am grateful to Ms. Kaya Yoshino, the secretary of the Suzuki group, for her invaluable assistance with administrative matters.

I extend my heartfelt gratitude to my previous supervisors, Prof. Gourab Kanti Das, Dr. Ritesh Singh, and Dr. Pradip Maity, for their invaluable contributions to my growth as both a scientist and an individual. Their unwavering encouragement and dedication to research have profoundly shaped my perspective and instilled in me a resilient research mindset.

I am grateful for the MEXT scholarship from the Ministry of Education, Culture, Sports, Science and Technology of Japan for financial support and to Osaka University for providing an unforgettable research atmosphere.

Finally, I want to express my heartfelt gratitude to my family members, Ms. Papiya Mukherjee, Mr. Ashoke Kr. Mukherjee, Mr. Anupam Mukherjee, Ms. Sutapa Debnath Mukherjee, Ms. Tanwi, Ms. Rakhi Das, Mr. Gautam Das, Ms. Shreejita Das and my friend Mr. Sayan Mukherjee. Their unwavering emotional support and constant presence have been a source of strength.

March 2025

Anirban Mukherjee


OSAKA UNIVERSITY
SANKEN
OSAKA UNIVERSITY
文部科学省
MEXT Scholarships